VILNIUS UNIVERSITY
CENTER FOR PHYSICAL SCIENCES AND TECHNOLOGY

BRONIUS ŠAULYS

QUALITY DIAGNOSTICS OF NITRIDE BASED LIGHT EMITTING DIODES VIA LOW FREQUENCY NOISE CHARACTERISTICS

Doctoral dissertation
Physical science, Physics (02P)

Vilnius 2017

The thesis was prepared at Vilnius University in 2007 – 2013 during PhD studies and is defended extramurally.

Scientific consultant:

Prof. dr. Jonas Matukas (Vilnius University, physical sciences, physics – 02 P).

VILNIAUS UNIVERSITETAS
FIZINIŲ IR TECHNOLOGIJOS MOKSLŲ CENTRAS

BRONIUS ŠAULYS

TRIUKŠMINĖ ŠVIESOS DIODŲ SU NITRIDINIAIS SLUOKSNIAIS KOKYBĖS DIAGNOSTIKA

Daktaro disertacija
Fiziniai mokslai, fizika (02P)

Vilnius 2017

Disertacija rengta 2007 – 2013 Vilniaus universitete studijuojant doktorantūroje ir ginama eksternu.

Mokslinis konsultantas:

Prof. dr. Jonas Matukas (Vilniaus universitetas, fiziniai mokslai, fizika – 02 P).

Acknowledgements

The author is sincerely grateful:

To the scientific consultant Prof. Jonas Matukas for the excellent leadership.

To dr. Sandra Pralgauskaitė for valuable advices and support;

To prof. Vilius Palenskis for valuable advices;

To other colleagues of the Noise research laboratory for collaboration in experimental work;

To all employees of the Department of Radiophysics;

To my family for the understanding and moral support.

Content

1 Introduction

Light emitting diode (LED) is heavily doped *p*-*n* junction diode which emits noncoherent light once direct current (DC) bias is applied in a forward direction. The first commercial LEDs available for mass production was developed in 1968 using gallium arsenide phosphide [1]. These LEDs were emitting red light. Due to their poor efficiency and brightness they were suitable for use as indicator lamps and in seven-segment displays only. The first commercially available blue light emitting diodes based on SiC appeared on 1989 [2]. However, these LEDs didn't distinguish with high brightness. The high brightness blue light emitting diodes based on InGaN first time were demonstrated in 1994 [3]. Availability of high brightness blue light emitting diodes led to the development of white LED which was based on the blue LED covered with YAG phosphor coating. Thus, part of blue light converted to the yellow in conjunction with the blue appears white light. The invention and development of the high-power white-light emitting diodes led to use it for illumination, and is replacing incandescent and fluorescent lighting slowly. LEDs distinguish by many advantages over other light sources:

- Efficiency: emits more lumens per watt than incandesced light bulbs;
- Color: traditional light sources usually have broad emission spectrum and in applications demanding single color illumination, need special filters. While LEDs can emit light of intended color and efficiency is not reduced due filtering;
- Dimensions: LEDs have very small dimensions and can be used in applications where light source size is critical;
- Shock resistant: fluorescent and incandesce bulbs are fragile and easily can be damaged by external shock while LEDs are solid state components;
- Life time: LEDs distinguishes by relatively long life time (up to 20 000 – 70 000 hours) compared to fluorescent tubes (10 000 – 15 000 hours) and incandesce bulbs (1000 – 2000 hours). The life time for LEDs is described as 70% (most often) light emission decrease from the initial level.

- Number of cycling's: LEDs suits for the applications requiring often on – off switching without degrading the life time. Incandesce bulbs and fluorescent light life time shortens in such applications where often on – off switching occurs.

LEDs have some disadvantages also:

- High initial cost: LEDs still are more expensive in initial capital costs. However, the long life time and efficiency of LED pays off if counting the maintenance and energy consumptions;
- Light quality: Most of cool-white LEDs have spectra that differ significantly from a black body radiator. The spike at 460 nm and dip at 500 nm causes the color of objects to be perceived differently under cool-white LED illumination than sunlight or incandescent sources. However, the color-rendering properties of common fluorescent lamps are often inferior to what is now available in state-of-art white LEDs.
- Temperature dependency: LED performance largely depends on the ambient temperature of the operating environment. Over-driving an LED in high ambient temperatures may result in overheating the LED package, eventually leading to device failure. An adequate heat sink is needed to maintain long life.
- Voltage and current sensitivity: LEDs must be powered with the appropriate voltage and current values: voltage above their threshold voltage and a current below their rating. Current and lifetime change greatly with a small change in applied voltage. To keep voltage and current within LED operation range, is necessary to use a current-regulated power supply.
- Use in winter conditions: In some applications in particular conditions the high efficiency of LED could be a disadvantage. For example, in traffic lights used LEDs due very low IR heat radiation couldn't heat up the snow or ice covered the lamp thus leading to the accidents.

Regardless of the disadvantages of the LEDs, they are used almost everywhere and the application of LED is huge (automotive, motocycle and

bicycle lights, traffic lights and signals, information displaying boards, light bulbs, etc.). LED applications can be classified in some types:

- Indicators and signs: mostly used for traffic signals, exit signs, light weight message, displaying box etc.;
- Lighting: LED lamps have become highly popular because energy consumption is very low. Also, LEDs are used as backlight for the TV and computer/laptop displaying.
- Non visual application: Communication (optical fiber and free space communication), sensor system (computer mouse) are the main area of non-visual application of LEDs. Because LEDs can cycle on and off in microseconds, very high data bandwidth can be achieved. Infrared LEDs have lower current density in the junction thus has a longer life time than laser diodes used in optical communication systems. Due to simpler LED construction, they are economically more attractive for short distance moderate speed optical communications than laser diodes.

Despite the LEDs are characterized as light sources with long life time the operational time can highly degrade under unfavorable operation conditions. Also, life time is statistical value, and doesn't ensure, that the output of LED will not decrease to specified level earlier or even worse – initial LED failure appear. In many of applications, where LEDs are used, it is important to have reliable light source. Also for LEDs used in communications it is important to have low noise, as it impacts the system sensitivity. The degradation of LED traditionally is seen via changes of its characteristics (emitted light intensity decrease and leakage current increase). However the change of these characteristics is small if compared to its absolute value. When measuring low frequency noise DC component is filtered out and counted only the voltage fluctuations. The degradation of LED could cause a small change in its IV characteristics and emitted light intensity while noticeable changes in noise level. For this reason, analysis of low frequency noise of LED provides not only evaluation of its noise level, but also gives valuable information about the physical processes in the structure. Thus, analysis of low frequency noise characteristics of LED is

sensitive, nondestructive method giving information about its quality and reliability.

The aim and task of the work

The aim of the dissertation was to investigate quality and reasons of degradation of modern InGaN high brightness light emitting diodes via low frequency noise characteristics investigation.

The tasks of the dissertation were:

1. Investigate low frequency noise characteristics of InGaN LED and compare it with the ones of phosphide based LEDs;
2. Evaluate influence of secondary optics and phosphor layer to quality of LEDs;
3. Due to fact that LEDs are used as replacement of LD in optical communications, was decided to compare noise characteristics of LED and laser diode;
4. Evaluate leakage current relationship to noise characteristics of LED;
5. Investigate the reasons of degradation of InGaN LED during long term aging;
6. Investigate degradation of phosphor layer of white LED;
7. Compare degradation mechanisms of InGaN and AlInGaP based LEDs;
8. To analyze low frequency noise characteristics of LEDs by correlation method;

Scientific novelty

1. Investigated influence of secondary optics to low frequency noise characteristics of nitride based LEDs.
2. Evaluated influence of phosphor layer to noise characteristics of white LEDs.
3. Analyzed InGaN LED noise spectrum by decomposing different type noise components and correlation between them.

Statements presented for defence

1. Origin of LED degradation is increase of non-radiative generation and recombination centers in LED structure.

2. The main influence in the LED quality and reliability is by the active region (not by the additional optics or phosphor layer).
3. The first signs of LED degradation appear at el noise and cross-correlation characteristics, IV at small current (Not at LI characteristics).
4. At low frequency electrical and optical noise of investigated InGaN blue LED comprises from partly (d_1=0.64) correlated 1/f and completely (d_2=1) correlated 1/$f^{1,5}$ spectra. In higher frequency shot noise component dominates and additionally in electrical noise – poorly (d_3=0.03) correlated Lorentzian noise.

1.1 List of Publications on the theme of the thesis

Scientific publications having impact factor in the Thomson Reuters Web of Knowledge database:

P1 S. Pralgauskaitė, V. Palenskis, J. Matukas, J. Glemža, G. Muliuk, B. Šaulys, A. Trinkūnas, Reliability investigation of light-emitting diodes via low frequency noise characteristics, Microelectronics reliability. Vol. 55, iss. 1. p. 52-61 (2015), http://dx.doi:10.1016/j.microrel.2014.09.027

P2 S. Pralgauskaitė, V. Palenskis, J. Matukas, B. Šaulys, V. Kornijčuk, V. Verdingovas, Analysis of mode-hopping effect in Fabry-Pérot multiple-quantum well laser diodes via low frequency noise investigation, Solid-State Electronics, V. 79, 104-110, (2013) http://dx.doi: 10.1016/j.sse.2012.07.021.

P3 B. Šaulys, V. Kornijčuk, J. Matukas, V. Palenskis, S. Pralgauskaitė, K. Glemža, Optical and electrical noise characteristics of side emitting LEDs, Acta Physica Polonica A, V. 119, No. 2, 244-246 (2011), http://przyrbwn.icm.edu.pl/APP/PDF/119/a119z2p47.pdf.

P4 B. Šaulys, J. Matukas, V. Palenskis, S. Pralgauskaitė, G. Kulikauskas, Light-Emitting Diode Degradation and Low-Frequency Noise Characteristics, Acta Physica Polonica A, V. 119, No. 4, p. 514-520 (2011), http://przyrbwn.icm.edu.pl/APP/PDF/119/a119z4p10.pdf

P5 V. Palenskis, J. Matukas, S. Pralgauskaitė, B. Šaulys, A detail analysis of electrical and optical fluctuations of green light-emitting diodes by correlation method, Fluctuations and Noise Lett. 9, No. 2, p. 179-192 (2010), http://dx.doi: 10.1142/S0219477510000149

P6 V. Palenskis, J. Matukas, B. Šaulys. Analysis of electrical and optical fluctuations of light-emitting diodes by correlation method. Lithuanian Journal of Physics/ Lithuanian Physical Society, Lithuanian Academy of Science, vol. 49, no. 4 p. 453-460, (2009), http://dx.doi: 10.3952/lithjphys.49408

Articles in peer reviewed papers of international conferences:

O1 B. Saulys, V. Palenskis, J. Matukas, S. Pralgauskaitė, E. Tylaitė, Characterization of degradation process in white light nitride-based LEDs by low-frequency noise, Proc. of 21st International Conference on Noise and Fluctuations, IEEE Conf. Proc. CD-R, softboard, Toronto, Canada, Catalog No. CFP1192N-CDR, ISBN 978-1-4577-0192-4, pp. 448-451, (2011), http://dx.doi.org/10.1109/ICNF.2011.5994366

O2 S. Pralgauskaitė, V. Palenskis, B. Saulys, J. Matukas, V. Kornijcuk, S. Smetona, Noise characteristics and radiation spectra of multimode MQW laser diodes during mode-hopping effect, Proc. of 21st International Conference on Noise and Fluctuations, IEEE Conf. Proc. CD-R, softboard, Toronto, Canada, Catalog No. CFP1192N-CDR, ISBN 978-1-4577-0192-4, pp. 301-304, (2011), http://dx.doi.org/10.1109/ICNF.2011.5994327.

O3 B. Šaulys, J. Matukas, V. Palenskis, S. Pralgauskaitė, J. Vyšniauskas, Analysis of mode-hopping effect in fabry-perot diodes, In: Proc. of 18th international conference on microwave radar and wireless communication (MIKON), p. 1-4, (2010). (ISBN: 978-1-4244-5288-0). http://ieeexplore.ieee.org.

O4 B. Šaulys, J. Matukas, V. Palenskis, S. Pralgauskaitė, Red light-emitting diode degradation and low-frequency noise characteristics, In: Proc. of 18th international conference on microwave radar and wireless communication (MIKON), p. 1-4, (2010). (ISBN: 978-1-4244-5288-0). http://ieeexplore.ieee.org.

O5 V. Palenskis, J. Matukas, B. Šaulys, S. Pralgauskaitė, V. Jonkus, Low frequency noise characteristics and aging processes of high power white light emitting diodes, AIP conference proceedings of 20th International Conference on Noise and Fluctuations. Ed. Massimo Macucci and Giovanni Basso, p. 399 – 402, Melville, New York (2009). (ISBN 978-0-7354-06665-0, ISSN 0094- 243X), http://dx.doi.org/10.1063/1.3140483

O6 V. Palenskis, J. Matukas, S. Pralgauskaitė, B. Šaulys, J. Laučius, Advanced materials for light emitting diodes: noise characterization, Physica Status Solidi (c): Current topics in solid state physics. vol. 6, no. 12. p. 2870-2872, (2009), http://onlinelibrary.wiley.com/doi/10.1002/pssc.v6:12/issuetoc

O7 J. Matukas, V. Palenskis, J. Vyšniauskas, B. Šaulys, S. Pralgauskaitė, A. Pincevičius, Noise characteristics and reliability of high power white light emitting diodes based on nitrides, Proc. of SPIE, vol. 7142, 71420H (2008), http://dx.doi.org/10.1117/12.816513

1.2 Results presented at scientific conferences

C1 J. Glemža, J. Matukas, S. Pralgauskaitė, B. Šaulys, V. Palenskis, Koreliacijos tarp elektrinių ir optinių fliuktuacijų analizė didelės galios šviesos diodų kokybės ir patikimumo įvertinimui, 41-oji Lietuvos nacionalinė fizikos konferencija. 2015.

C2 S. Pralgauskaitė, V. Kornijčuk, B. Šaulys, V. Palenskis, J. Matukas, J. Vyšniauskas, Daugiamodžių lazerinių diodų triukšmo ir spinduliuotės charakteristikų analizė modų šuolių metu, 39-osios Lietuvos nacionalinės fizikos konferencija. 2011.

C3 B. Šaulys, A. Trinkūnas, J. Matukas, S. Pralgauskaitė, V. Palenskis, Noise spectroscopy of high power white nitride-based light emitting diodes, 39-oji Lietuvos nacionalinės fizikos konferencija. 2011.

C4 B. Šaulys, J. Matukas, V. Kornijčuk, I. Stasevičius, Optical and electrical noise characteristics of side emitting LEDs, 14th international symposium on ultrafast phenomena in semiconductors, Vilnius, 2010

C5 B. Šaulys, J. Matukas, V. Palenskis, S. Pralgauskaitė, J. Vyšniauskas, Analysis of mode-hopping effect in fabry-perot laser diodes, MIKON 2010:18th international conference on microwaves, radar and wireless communications, Vilnius, 2010.

C6 B. Šaulys, J. Matukas, V. Palenskis, S. Pralgauskaitė, Red light-emitting diode degradation and low-frequency noise characteristics, MIKON 2010:18th international conference on microwaves, radar and wireless communications, Vilnius, 2010.

C7 V. Palenskis, J. Matukas, B. Šaulys, S. Pralgauskaitė, V. Jonkus, Low frequency noise characteristics and aging processes of high power white light emitting diodes, 20th International Conference on Noise and Fluctuations, Pisa, Italy, 2009.

C8 V. Palenskis, J. Matukas, S. Pralgauskaitė, B. Šaulys, J. Laučius, Noise characterization of advanced materials for light emitting diodes, 15 th

semiconducting and insulating materials conference, Vilnius, Lithuania, 2009.

C9 J. Matukas, V. Palenskis, S. Pralgauskaitė, B. Šaulys, Triukšminė didelės galios InGaN šviesos diodų diagnostika juos sendinant, (Characterization of high power InGaN light emitting diodes during aging by noise investigation), 38 – oji Lietuvos nacionalinė fizikos konferencija, Vilnius, 2009.

C10 J. Matukas, V. Palenskis, J. Vyšniauskas, B. Šaulys, Noise characteristics and reliability of high power light emitting diode based on nitrides, 6 th International conf. "Advanced optical materials and devices AOMD-6", Riga, Latvia, 2008.

2 Overview of LED

2.1 Materials used for the LED fabrication

In the last forty years, technical progress of development of light emitting diodes has been breathtaking [4, 5]. Nowadays LEDs are small, reliable and efficient. Light emitting diodes as reliable light sources are used widely and after improving their brightness, effectiveness and color spectrum, it still finds new applications.

Electroluminescence phenomenon as a light emission from solid state material caused by electrical power was discovered in 1907 by H. J. Round investigating silicon carbide (SiC) [6]. Due to the indirect bandgap, the efficiency of SiC light emitting diode was only 0.005% [7]. The era of III-V compound semiconductors has started in 1950th. These compounds proved to be optically very active, what proposed to apply them for development of the more efficient light emitting diodes. Infrared LED based on GaAs first time was reported in 1962 [8]. The first LEDs of visible light spectrum based on GaAsP were reported on the same year [9]. GaAsP materials are used for the emission of red, orange, yellow and green wavelength ranges. GaAsP system has a large lattice mismatch to GaAs substrates (about 3.6 %), what results in occurrence of dislocations misfit when critical thickness of GaAsP on GaAs is exceeded [10]. For this reason, internal quantum efficiency substantially decreases when increasing phosphor content in GaAsP [11]. This makes GaAsP materials suitable only for low brightness LEDs. To increase the brightness of LEDs there was necessary to find other materials which lattice could match with the one of the substrates. Such candidate was AlGaAs materials which lattice matches with GaAs. This allowed growing AlGaAs alloy directly onto substrate, without using transition layer, creating abrupt heterojunctions. Such heterojunctions added one very important property not available for GaAsP based LEDs: carrier containment, which reduces the movement of injected carriers in perpendicular to the junction direction. That allowed increase of carrier density beyond the diffusion limited levels, what caused increase of internal quantum efficiency.

AlGaAs material direct-indirect crossover occurs at 621 nm. At this wavelength, radiative efficiency becomes quite low due to direct-indirect transition. Thus, for high brightness visible spectrum applications LEDs based on AlGaAs can be used only in the red wavelength range. AlInGaP materials have most of the advantages of AlGaAs systems: it can be lattice matched to GaAs substrates; ratio of Al to Ga can be changed without affecting the lattice match. Also, the AlInGaP has a higher energy of direct energy band gap (2,33 eV), which corresponds to the 532 nm green light emission [12]. Thus, this material is suitable for the LEDs of high brightness visible spectrum emitting in the red, orange, amber and yellow wavelengths.

For the short wavelength applications promising candidates are GaN, AlN, InN materials and their alloys. Their direct bandgap extends from ultraviolet to near-infrared [13, 14]. For high brightness, blue and green light emitting diodes are primary based on InGaN. Unlike GaAs and InP based semiconductors, InGaN based materials have very high concentration of threading dislocations in InGaN/GaN epitaxial films [1]. These dislocations are caused by the lattice mismatch between commonly used SiC substrates, GaN and InGaN epitaxial films. Typical densities of such threading dislocations are in the range of (10^7 – 10^9) cm^{-2} [1, 15]. Although there is a high density of threading dislocations, InGaN materials has high radiative efficiency. It is believed that small diffusion length of holes and low electrical activity of dislocations in InGaN and GaN allows high radiative efficiency [16]. It has also been postulated that In content fluctuations in InGaN cause carrier to be localized in potential minima, what prevents them from reaching dislocations. Such localized carriers will recombine radiatively. Threading dislocations effect is much lower for optical properties of III-V nitrides than those of arsenide or phosphide based materials.

Although InGaN-based LEDs are already commercially available, further improvement of the light output power and efficiency are investigated by improving internal quantum efficiency and light extraction efficiency with using patterned sapphire substrates or inverted hexagonal pyramid dielectric LEO masks [17-21].

2.2 Generation of white light using LEDs

As the efficiency of light emitting diodes are continuously improving, the new applications of LEDs are founded as well. One of the high interest applications with a very large potential market is general daylight illumination. In this application illumination sources are expected to have high efficiency and power capability, good color reendering capability, high reliability and low cost of manufacturing. Light emitting diode inherently generates monochromatical light which is not acceptable for that application. However, there are several ways to generate a white light by LEDs. One of the ways to have a white light from LEDs is combining several (from 2 up to 4) light emitting diodes (or single diode with several active layers) with different wavelength together so, that the mix of colors creates a white light [1]. For example, dichromatic white source can be achieved by combining blue and yellow LEDs with appropriate power ratios. Getting of high color rendering is complicated with additive mixing of two complementary colors. High quality white light can be achieved by mixing three or more primary colors. The weakness of mixing monochromatic lights from several LEDs has a drawback of biasing and controlling complexity. Such drawback is reduced with monolithic dichromatic and trichromatic LEDs having separate active layers for different wavelengths. White light sources based on mixing emission from different wavelengths LEDs (or active layers) has drawback due to emission power, peak wavelength and spectral width characteristics unequal dependency on temperature for different wavelengths [22]. The chromaticity dependency on temperature can be eliminated by adjusting power ratio of each color component. This can be implemented by constantly measuring the emission spectrum and via feedback control adjusting the power for each component, but it increases the complexity of the system [1]. A simpler method is monitoring of LED temperature, and according known temperature dependency for individual wavelengths to adjust the power for each component [1]. However, such simpler method doesn’t consider LED aging process. Although this method of white light emission is not the most suitable

for general daylight lighting in offices or houses, due to color flexibility it is well accepted for some niche applications like stage lighting, architectural lighting, and surgical lighting. In some specific applications, there is required lighting with some forbidden wavelengths, for example in photolithography workspace with photosensitive materials [23]. By utilizing narrow peaks of individual colors from several LEDs custom spectra can be designed where light emission at unwanted wavelengths are eliminated, while maintaining an acceptable white chromaticity and high efficiency.

A highly publicized example is the illumination of the painting of Mona Lisa by Leonardo da Vinci. In this instance, a system consisting of seven color channels is used to compensate discoloration from the bulletproof glass of the display case, as well as compensate the age depreciation of paint pigments [16, 24, 25].

Another method to generate white light is by utilizing the Stokes shift. By using wavelength converting material the short wavelength light can be converted to longer wavelength resulting in broad-spectrum white light obtainment [16]. Phosphor material placed on the top of blue or UV LED absorbs portion of blue light emitted by the diode and converts it to the yellow light. Usually yttrium aluminum garnet (YAG) doped with Ce^{3+} ions is used as a wavelength converting material [26]. The peak of excitation spectrum (around 460 nm) coincides with the peak spectrum of the most efficient blue AlInGaN LED. Also, the emission spectrum of phosphor coincides yellow light wavelengths (570 - 590 nm) required for white light obtainment. Due to inherent losses in the wavelength conversion process, the efficiency of such white LEDs is reduced ~20%. Such white LEDs with a single phosphor material has a drawback of poor color rendering index due to lack of Yellowish – Green and Reddish – Purple color. To improve the color rendering index two different phosphor materials are used. For example, $SrGa_2S_4:Eu^{2+}$ used for conversion of blue light to the green emission (~535 nm) and $SrS:Eu^{2+}$ for conversion to orange – red emission (~615 nm). Since high color rendering requires costly conversion from short to long wavelengths, phosphor based white light sources must be

made with a tradeoff between high efficiency and high color rendering [28]. Due to priority for better color rendering such white LEDs are more suitable for general lighting in houses and offices. White LEDs based on phosphor layer also has a drawback of their color rendering changes during aging, caused by intensity ratio change of blue and yellow lights due to active layer or phosphor layer degradation [27].

2.3 Reliability of LED

Reliability is defined as the probability, that a system or individual component remains functional during a timeframe *t* under normal operating and environmental conditions and can be expressed as follows:

$$\boldsymbol{Reliability\ (t)} = \frac{\boldsymbol{N_0 - N_f(t)}}{\boldsymbol{N_0}}; \qquad (2.3.1)$$

where N_0 is total number of samples under test; N_f (t) is number of failed samples during time *t*.

Failure rate distribution over time for semiconductor devices generally can be expressed using bathtub curve as shown in Fig. 2.1. The curve can be divided into three regions:

- Initial failure (or early failure);
- Random failure;
- Wear out failure.

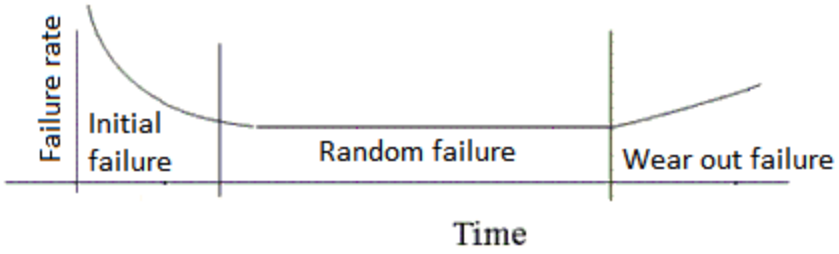

Fig. 2.1. Failure rate distribution in time.

Initial and random failures are mainly caused by the problems (e.g. defects in the structure) in manufacturing process or by improper usage or operation of the device (e.g. exceeding current, voltage, or temperature limits). Most of the

initial failure appears during the installation process (for example soldering) or within the first couple hours of operation [29]. Random failure ratio for semiconductor devices is very small compared to the initial failure ratio. Wear out failure region corresponds to the end of life time of the LED. The failure rate increases during the time due to aging and wear out of LED materials. For an incandescent bulb, a failure is the catastrophic flash experienced when the filament fuses open. However, for LEDs to have a catastrophic failure is unusual. More commonly, there appears lumen decrease over the time. When lumen decrease reaches some value described by its manufacturer, for example by 30% of its initial value, the LED is considered as failed to meet specification [29]. As LED failure is statistical process, its life time also has statistical distribution. Manufacturers of LEDs usually specifies life time as typical median life time, in which 50% of samples has failed. High quality LED life time varies from 20 000 to 70 000 hours considering the terms of use (temperature, bias current and voltage, etc.).

Direct measurement of such a long life time of LED is far too long to use it in practice. Instead of direct aging measurement there are used so called accelerated aging testing [30-32]. The main idea is to test at high levels of the accelerating variable(s) to speed up failure processes and extrapolate to lower levels of the accelerating variable(s). During the test LEDs are stressed by increasing one or more of the operating parameters, which influence their life time (temperature, humidity …). Interpretation of accelerated test data requires models that relate accelerating variables to time acceleration. Temperature is one of the most commonly used accelerating variable [33]. Thermally activated degradation process can be represented by the Arrhenius model that uses the Arrhenius reaction rate equation:

$$rr = Ae^{-(\frac{E}{kT})}; \tag{2.3.2}$$

where *rr* is reaction rate, *A* is total acceleration factor, *E* is activation energy of the process expressed in eV, *k* – Boltzmann constant, *T* – temperature in Kelvins.

Acceleration factor between accelerated stress and usual environment conditions, can be expressed as following:

$$AF = e^{\frac{E}{k}(\frac{1}{T_U} - \frac{1}{T_A})}; \quad (2.3.3)$$

where *AF* is acceleration factor, T_A – temperature during accelerated stress, T_U – temperature of usual environment conditions. Light output degradation is the major failure mode of LEDs, and it results from hygro-mechanical and electrical stresses in addition to thermal stresses [34]. A more realistic method of LED lifetime estimation, that reflects total consideration of temperature, the level of forward current, relative humidity, mechanical stress, and materials is required. The Eyring model improves the Arrhenius model by taking into effect environmental stresses such as thermo-mechanical phenomena [35]. The median life of a device is given by the equation:

$$t_{50\%} = Ae^{\frac{E}{kT} * F(V) * F(RH)}; \quad (2.3.4)$$

where A is total acceleration factor, *F(V)* – stress factor for applied voltage, *F(RH)* – stress factor for relative humidity.

Peck model accounts for temperature and humidity stresses separately, and it assumes normalized humidity and temperature stresses of 85 ° C and 85 % RH, respectively [36]. Then these factors are used to obtain the overall acceleration factor. The following equation describes the model:

$$AF = \frac{(RH_u)^n}{(RH_A)^n} * e^{\frac{E}{k}(\frac{1}{T_u} - \frac{1}{T_A})}; \quad (2.3.5)$$

where RH_u is relative humidity during normal operation, RH_A – relative humidity during accelerated aging, *n*- an arbitrary determined constant. Life time prediction based on accelerated testing requires deep physical/chemical knowledge of the effect of accelerating variable on the failure mechanism. Accelerated aging must generate the same failure mode occurring in the normal operation. If there is more than one failure mode, it could be that the different failure mechanisms will have different acceleration rates. In such cases life time estimation could be incorrect [33]. Accelerated aging test by using low

frequency noise analysis considers all the failure mechanisms of LED providing more accurate estimation.

Life time and reliability of LEDs are affected by some issues in materials used. Research focuses on the following GaN based LEDs issues:

- In the active layer interaction between hydrogen and Mg dopant limits the density of hole, affecting the internal quantum efficiency [37];
- Due to the large internal electrical field and the defects generation caused by the large lattice mismatch between GaN and InGaN layer, efficiency of green LEDs is still insufficient for white light emitting LEDs [1].
- Ohmic contacts degradation, which causes increase of the operating voltage [38];
- Non-radiative defects generation and propagation to active layer of the devices [39-41].

Phosphide based LEDs faces the following issues [42-44]:

- Dislocation growth in the active layer;
- Metal diffusion in AlGaInP;
- Heating effects of AlGaInP active region resulting in enhanced current injection.

LED reliability and its life time is also affected by the packaging processes [45]:

- Interdifusion of metal contacts;
- Bond wire failures caused by electro-migration or burn-out due to excessive current;
- Heat sink delamination;
- Plastic encapsulation failure such as discoloration, carbonization or polymer degradation.

These causes can influence LED performance by decreasing the optical output or occurrence of abrupt LED failure (for example bond wire failure).

2.4 Noise sources in Light Emitting Diode

In real devices, there is always present electrical noise. Very often this noise limits the performance of the devices, for example receiver sensitivity. Electrical noise is a consequence of fluctuation of macroscopic parameters (resistance, voltage, etc.). Bellow there are discussed different types of noise, found in light emitting diodes.

Thermal noise is caused by Brownian motion of charge carriers. Thermal noise spectral density depends on absolute temperature and ohmic resistance of the device and can be expressed by Nyquist formula [51]:

$$S_u = 4kTR; \tag{2.4.1}$$

where *k*, *T* and *R* are Boltzmann constant, absolute temperature and ohmic resistance of the light emitting diode respectively. Thermal noise doesn't depend on frequency, so the spectrum is constant. Thermal noise of known resistor is very often used as a reference for noise measurement system calibration.

Shot noise is a second type of noise always present on diode type devices. The origin of shot noise is random current fluctuations across potential barrier due to a fact that current consists of discrete charge carriers. The spectrum of shot noise is white and can be expressed by Shotkey formula [52]:

$$S_I = 2eI; \tag{2.4.2}$$

where *e* and *I* correspond to elementary charge and average current, respectively. Shot noise with applied very low current levels is very useful tool detecting parasitic shunt resistors across photodiodes [52]. Device analysis based on shot noise also can be used by applying higher currents for example to detect the beginning of multiplication where S_I is no more linear to the current. For this reason, shot noise can be used for quality evaluation in zener diodes and avalanche diodes [53]. In low current range shot noise for light emitting diodes appears as leakage current.

Generation and recombination noise as its name implies is caused by statistical processes of charge carrier generation and recombination. Some electrons gets enough energy from thermal lattice vibration to get released from

valence band – charge carrier is generated. On the same time reverse process occurs: electron from conduction band jumps to the valence band by releasing some energy. As the generation and recombination processes occur randomly, the quantity of charge carriers is statistical value. Spectral density of generation and recombination noise can be expressed as:

$$S_I(f) = 4I_0^2 \frac{\overline{\Delta N_0^2}}{N_0^2} \frac{\tau_0}{1+(\omega\tau_0)^2}; \qquad (2.4.3)$$

where I_0 is averaged current, $\overline{\Delta N_0^2}$ – variance of fluctuating number of charge carrier, N_0^2 – number of charge carriers in conductance band, τ_0 – relaxation time of carriers. In low frequencies ($w\tau_0 \ll 1$) this type of noise has constant spectrum, while in high frequencies ($w\tau_0 \gg 1$) is inversionally proportional to f^2. Generation and recombination noise is often negligible in high quality silicon devices, while due to lattice defects it is noticeable in heterostructure and compound semiconductors [53].

1/*f* noise (or often called flicker noise) is present in many physical (e.g. in hourglass flow of sand), biological (e.g. in heart beat rhythms) and economy (e.g. in stock markets) systems. In electronic systems, this type of noise is a consequence of random current or voltage fluctuation due to instability of electrical resistance or other characteristics of system [56]. Power spectral density is inverse proportional to current powered in square and inverse proportional to the number of mobile charge carrier:

$$\frac{S_U}{U^2} = \frac{S_i}{I^2} = \frac{S_R}{R^2} \sim \frac{1}{N}. \qquad (2.4.4)$$

This type of noise is usually dominant in very low frequencies and decreases inverse proportional to the frequency.

In higher frequencies (above 100 or 1000 Hz) usually it is grooved over by other type noise like thermal noise or generation and recombination noise. The

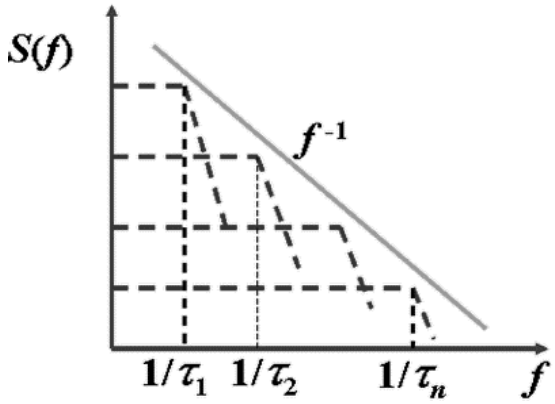

Fig. 2.2. 1/*f* spectrum as superposition of generation and recombination noise.

proportionality of spectrum is not always exactly 1/*f*. Very often it can be found what spectrum is inverse proportional to the frequency in ψ power ($S \sim 1/f^{\psi}$), where ψ varies from 0.8 to 1.3. The 1/*f* noise can be explained as superposition of generation and recombination noises with relaxation times distributed very widely [52]:

$$\frac{S_u}{U^2} = \sum_i \frac{a_i \tau_i}{1 + \omega^2 \tau_i^2}; \tag{2.4.5}$$

where a_i is dimensionless value which describes the intensity of relaxation noise with τ_i relaxation time. Selecting appropriate relaxation times τ_i, their intensity values a_i and the quantity i appropriate proportion of $S_u / U^2 \sim 1/f^{\gamma}$ can be achieved as shown in Fig. 2.2.

Typically, all the previously discussed types of noise contribute to the total noise spectrum of light emitting diode. But as already mentioned earlier, in low frequencies dominates 1/*f* type noise. As this type of noise is related to the defects which cause distortion of energy band, centers of charge carrier trapping and non-radiative recombination, the level of noise varies depending on quality of light emitting diode [53].

2.5 Noise and reliability

It is well known that electrical noise is a sensitive indicator of quality and reliability of electrical devices [57-60]. Increased electrical noise of a device used in low noise system will reduce its quality, impacting all the system sensitivity. Increased noise level indicates non-ideal processes occurring in the device, which can degrade its operation. But direct relationship of high level electrical noise of device with its reliability and its lifetime is not very often used. Experiments on many electrical systems have shown that their noise level increases as device degrades [57]. Also, if device at its initial use shows high level of noise it has a short lifetime [53-57]. During the noise measurement, no stress is applied to the device. Also, it is much more sensitive than DC or AC measurements. During the stress, the DC or AC values may vary by 1%, while noise level may increase by order of magnitude [57]. However, noise measurement requires special very sensitive equipment, electrically quiet environment and very good knowledge and care of measurement itself. Also, due to the low frequency (between 0.1 and 100 kHz) the measurement time is relatively long. For this reason, such measurements are not well suited for the high volume manufacturing test, which prefer very short measurement time per device (Typically in microseconds). Measurement of noise level could be used in research and development of products in order to improve the quality of the device.

LED quality and reliability investigations are mostly based on the analysis of light intensity decrease and current-voltage as well as capacitance-voltage characteristic changes during accelerated aging [61-64]. It is known that LED degradation is caused by defect formation or migration in the active region. As in previous paragraph explained $1/f$ noise intensity is related to the defects in LED structure. Small changes of LED structure could cause hardly noticeable changes of current-voltage characteristics, while noise level changes could be significant. However, there are only some publications on the low frequency noise in LEDs, where it is used for noise level evaluation [63, 65-67]. Optoelectronic device noise characteristic measurement is valuable not only for

noise level evaluation but also it is highly sensitive and informative method for clearing up physical processes in device structure and for predicting LED quality and reliability [53-56, 68]. Measuring electrical fluctuations all the noise sources of the device are considered. While measured optical fluctuations are caused by electrical fluctuations in the active region of LED. Analysis of cross-correlation between electrical and optical fluctuation allows to distinguish processes taking place in active and peripherial regions. Method based on noise characteristic analysis doesn't need long and expensive ageing experiments and is non-destructive.

3 Measurement and Calculation method of LED characteristics

In this work the following measurements of light emitting diodes were performed:

- Low frequency noise (electrical noise, optical noise, cross-correlation factor) in frequency range from 10 Hz to 20 kHz;
- Optical spectrum
- Current-Voltage and LI (light intensity dependency on LED current) characteristics.

3.1 Noise measurement

As noise itself is very weak signal, the measurement system must have appropriate gain factor in order it could detect and measure noise signal. Gain factor of low noise amplifier, used in the noise measurement system, can be expressed as:

$$K = \frac{U_{out}(t)}{U_{in}(t)}; \tag{3.1}$$

where U_{in} and U_{out} are signal amplitude in amplifier input and output, respectively. Amplifier itself has its own noise. If we add it to the previous equation we get:

$$K = \frac{U_{out}(t) - U_{sist}(t)}{U_{in}(t)}; \tag{3.2}$$

where U_{sist} is noise voltage of amlifier its own. As in our case the measured signal is a noise, we can rewrite this equation by using spectral densities of voltage fluctuations:

$$K^2(\omega) = \frac{(S_{out}(\omega) - S_{sist}(\omega))}{S_{in}(\omega)}; \tag{3.3}$$

from (3.3) we can express the noise voltage spectral density in the input of the measurement system:

$$S_{in}(\omega) = \frac{(S_{out}(\omega) - S_{sist}(\omega))}{K^2(\omega)}. \tag{3.4}$$

As already discussed in Chapter 2 thermal noise of resistor is proportional to its resistance value and can be expressed by (2.4.1). This expression we can use to find the gain factor in eq. (3.3):

$$K^2(\omega) = \frac{(S_R(\omega) - S_{sist}(\omega))}{4kTR}. \tag{3.5}$$

Now we can use this expression and rewrite eq. (3.4) as follows:

$$S_{in}(\omega) = \frac{(S_{out}(\omega) - S_{sist}(\omega))}{(S_R(\omega) - S_{sist}(\omega))} 4kTR. \tag{3.6}$$

And can rewrite it for the voltage fluctuations:

$$S_U = \frac{U_D^2 - U_S^2}{U_R^2 - U_S^2} 4kTR; \tag{3.7}$$

where U_D is voltage fluctuation of light emitting diode; U_S – measurement system added voltage fluctuations; U_R – thermal noise voltage of resistor of known value (R); k – Bolcman konstant; T – resistor temperature. Based on eq. (3.7) LED noise spectrum can be calculated if there are known LED voltage fluctuations, voltage fluctuations caused by known resistance, and measurement system own noise. Similarly we can use equation for the LED optical noise:

$$S_U = \frac{U_{ph}^2 - U_S^2}{U_R^2 - U_S^2} 4kTR; \tag{3.8}$$

where U_{ph} is photo voltage fluctuations (voltage fluctuations of photodiode illuminated by the LED under test). All the LED parts (active and peripherial region, contacts, and etc.) contribute to the electrical noise spectral density. While optical noise spectral density is created by light which is emited in the active region of LED only. Cross-correlation factor shows how strongly electrical and optical noise spectral densities are related. It can be expressed as follows:

$$r = \frac{\overline{\Delta U_{el}(t) \Delta U_{opt}(t)}}{[\overline{\Delta U_{el}^2(t)} \cdot \overline{\Delta U_{opt}^2(t)}]^{1/2}} \cdot 100\%; \tag{3.9}$$

where $\Delta U_{el}(t)\Delta U_{opt}(t) = \frac{1}{T}\int_0^T \Delta U_{el}(t)\cdot\Delta U_{opt}(t)dt$; $\overline{\Delta U_{el}^2(t)} = \frac{1}{T}\int_0^T \Delta U_{el}^2(t)dt$;

$\overline{\Delta U_{opt}^2(t)} = \frac{1}{T}\int_0^T \Delta U_{opt}^2(t)dt$; T – measurement time; $\Delta U_{el}(t) = U_{el}(t) - \overline{U_{el}}$ - LED voltage fluctuations; $\Delta U_{opt}(t) = U_{opt}(t) - \overline{U_{opt}}$ - photodiode voltage fluctuations caused by LED light fluctuation; U_{el} and U_{opt} – electrical and optical noise voltages, respectivelly.

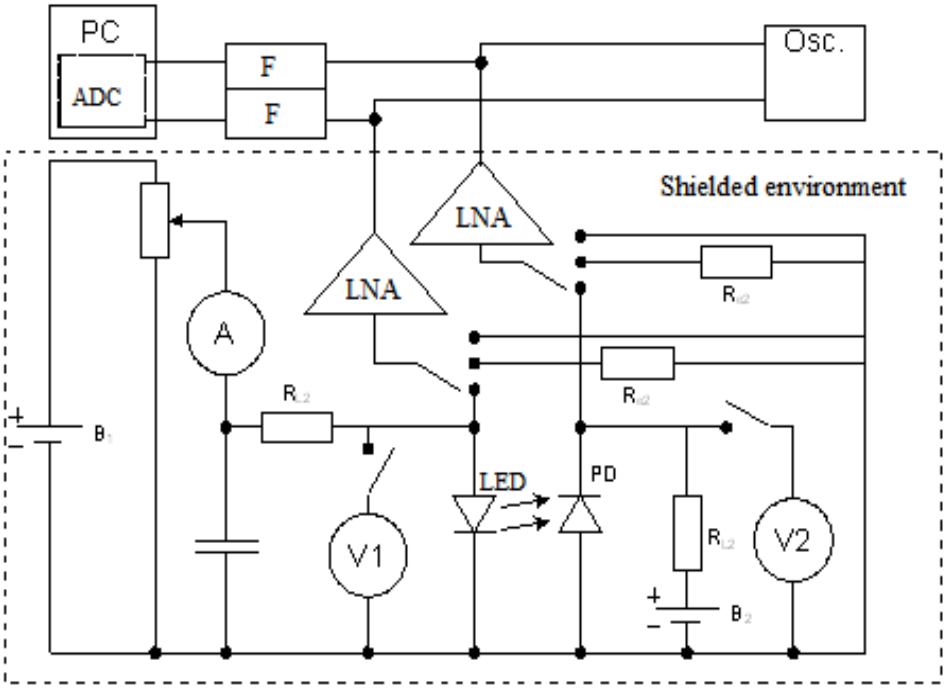

Fig. 3.1. Low frequency noise measurement setup.

Measurement setup used for low frequency noise measurement is shown in Fig. 3.1. Electrical noise of LED is measured by registering fluctuations of LED voltage. While optical noise – registering voltage fluctuations of photodiode illuminated by the LED under investigation. To avoid interference from mains power line separate batteries are used to power the LED under test, photodiode and low noise amplifiers. Curent of LED under test is changed by adjustable resistor and measured with ampermeter. Because the noise signals are very weak shielded environment is used in order to awoid interference from external radio transmitters. Only amplified noise signal is routed out of shielded

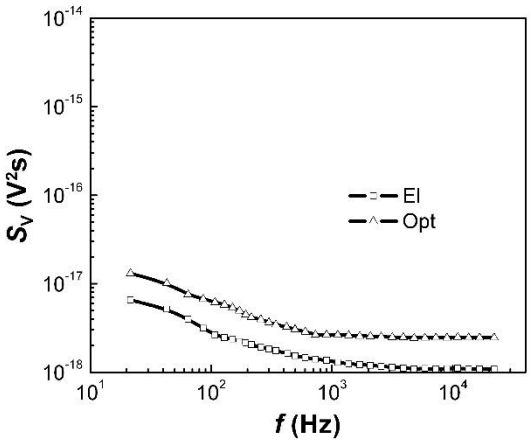

Fig. 3.2. Own noise spectral density of the system.

environment. Noise was measured within current range between 0,35 mA to 150 mA. As mentioned earlier in this paragraph in order to be able to evaluate the noise spectral density of LED using equation (3.8), it is necessary to measure own noise of the system. This is done by inputs of low noise amplifiers switching to the ground. The own noise spectral density of the system is displayed in Fig. 3.2. The same mechanical switches are used to

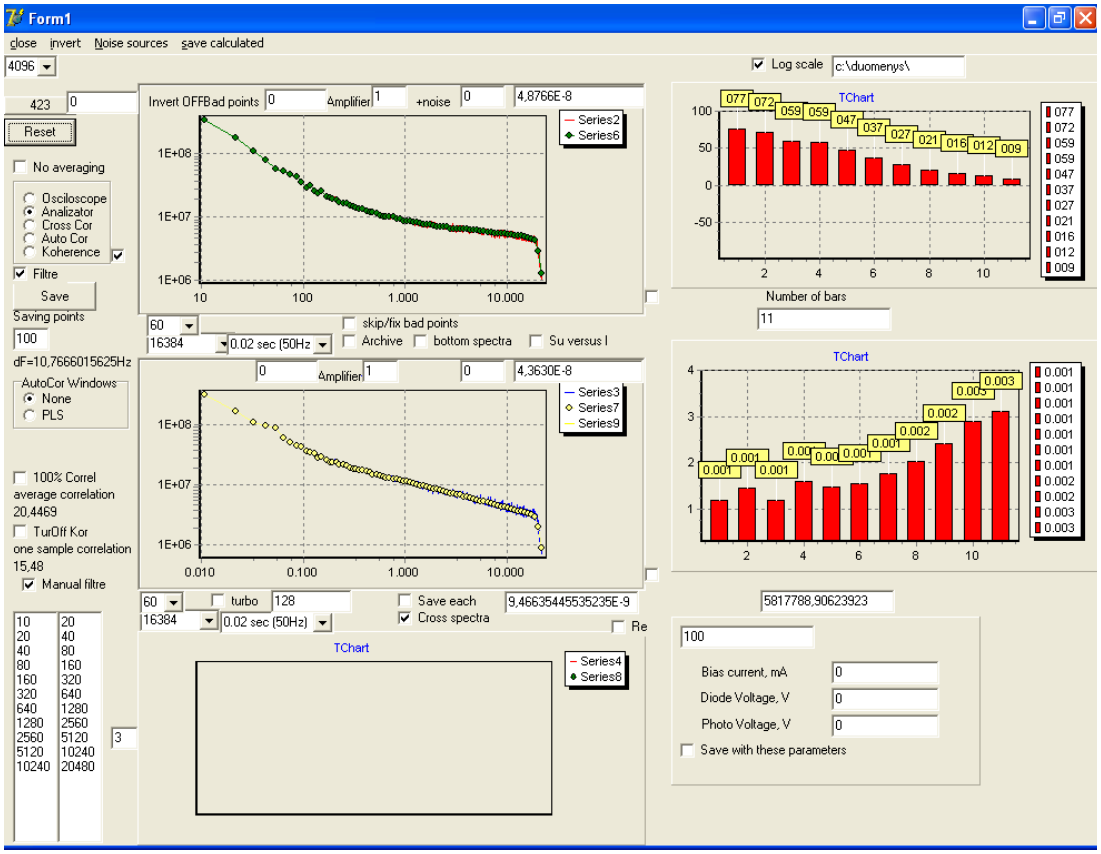

Fig. 3.3. Window of noise measurement software.

connect refference resistors of known value to the inputs of low noise amplifiers. Both electrical and optical noise measurement channels once amplified are routed to the two channel oscilloscope for live monitoring of the signal and to the simultanious sampling analog-digital converter via filters. National Instrument PCI 6115 board was used as analog-digital converter. Once digitized the signal is analysed in dedicated software on computer (Fig. 3.3). This software is capable to display the measured signal in time domain or in frequency domain. It is very convenient to check in time domain if the system gain is correct (noise signal not too weak for analog to digital converter and if its input is not overloaded due to too high gain). Once system gain is confirmed, the signal view is switched to the frequency domain and a number of samples are acquired and averaged, spectrum of noise is displayed. Average cross-correlation factor between electrical and optical noise is calculated and displayed. It is very convenient to evaluate the dependency of cross-correlation factor on frequency. For this reason, the software has digital filtering functionality. One-octave filters, what cover all measured frequency range ([10 – 20] Hz, [20 – 40] Hz, [40 – 80] Hz, [80 – 160] Hz, [160 – 320] Hz, [320 – 640] Hz, [640 – 1280] Hz, [1,28 – 2,56] kHz, [2,56 – 5,12] kHz [5,12 – 10,24] kHz, [10,24 – 20,48] kHz) are applied and the software can calculate the cross-correlation coefficient for every octave.

3.2 Measurement of optical spectrum

As investigated LEDs are optoelectronic devices, their optical spectrum measurements are very informative. Especially this is valid for white light emitting LEDs because of their optical spectrum complexity.

The optical spectrum of LED was measured with Advantest Q8341 Optical spectrum analyzer which is capable to measure optical spectrum within 350 nm and 1000 nm with accuracy up to ±0.05 nm.

Laser diode radiation spectrum and LD low frequency (10 Hz – 100 kHz) noise characteristics have been measured simultaneously: at the LD output the laser light beam was coupled into two fibers optical cable (Fig. 3.4). One fiber

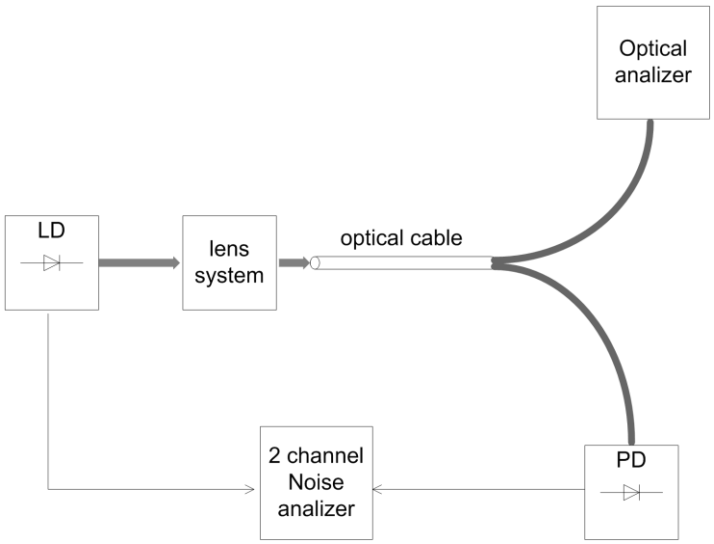

Fig. 3.4. The scheme for simultaneous measurement of LD radiation spectrum and noise characteristics.

was connected to the optical noise measurement equipment and the second - to the optical spectrum analyzer.

3.3 Measurement of current-voltage characteristic

Usually manufacturers of LEDs provide current-voltage characteristics within the current range where the diode outputs the light. However as mentioned in Chapter 2 the low current region can provide valuable information about the reliability of LED.

In this work, the current-voltage characteristics as well as light intensity dependency on current flowing through LED was measured in the same setup as noise measurement (Fig. 3.1). For this purpose, voltmeters were used. In order, these voltmeters couldn't impact very sensitive noise measurement results, their leads were disconnected from the setup during the noise measurement. However, this setup was not very accurate for very low current measurements. For this reason, dedicated Agilent Technologies B1500A Semiconductor device parameter analyzer was used which has integrated voltage and current source as well as voltage and current meter. It has voltage source and voltage measurement accuracy up to 150 μV and 120 μV, respectively, and current source as well as current measurement accuracy up to 0.3 pA and 0.2 pA, respectively. LED under test was in shielded environment during low current measurement. To eliminate the influence of cable resistance to the measurement results 4-wire connection

(also known as Kelvin connection) was used. The idea of such connection is to eliminate the resistive voltage drop caused by the current flow through the cable and measure only the resistive effects associated with the LED under test. In 4-wire connection technique there are used two separate lines for each terminal of the LED to be measured (Fig. 3.5). One pair of lines is used to

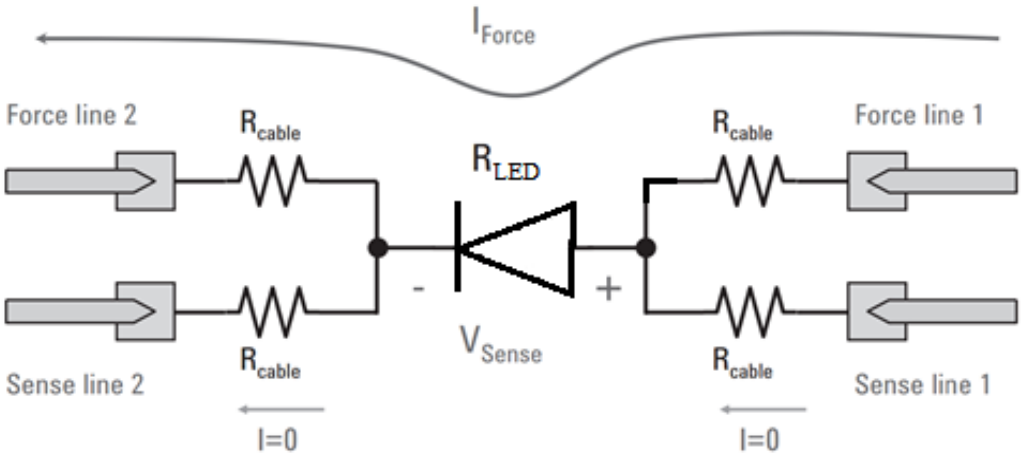

Fig. 3.5. 4-wire connection principle.

force current to the LED, and the other pair of lines - to measure the voltage. Since the voltage measurement lines are not conducting any current, there is no voltage drop due to cable resistance. Therefore, the cable resistance effects are eliminated [69]. Measurement results could be affected by leakage current of the coaxial cables, when very small currents are measured. Every coaxial cable uses insulating material between center conductor and shielding. If we assume that this insulating material has resistance of 1 GΩ and then 100 V is applied to the center conductor, then Ohms law gives the leakage current of 100 nA. Such leakage current can highly impact accuracy of small current measurements. To isolate the leakage current, triaxial cables were used instead of standard coaxial cables. Triaxial cable is a coaxial cable with additional conducting layer between center conductor and the shielding. The analyzer applies voltage to this additional Guard layer of the same level as voltage is forced (or measured) on the center conductor. Because the voltage difference between signal and guard lines are very close to zero, the leakage current is minimized [69]. The cut

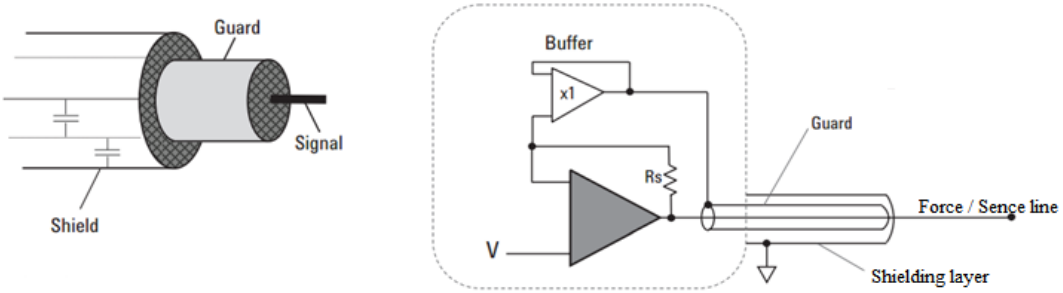

Fig. 3.6. Cut away view of triaxial cable (on the left) and its connection to the analyser (on the right).

away view of triaxial cable and its connection to the analyzer is shown in Fig. 3.6. Triaxial cables were used for all four 4-cable connections between the analyzer and the shielding enclosure.

3.4 **Investigated devices**

Nowadays light emitting diodes span all visible light spectrum and beyond. Different materials are used for the fabrication of different color LEDs: phosphide-based materials are used to cover infrared, red-yellow light spectrum regions, while for green-blue, ultraviolet regions, also white LEDs, nitride-based materials are common. There was investigated several samples of various

Table 3.1. Investigated LEDs.

No.	Colour	λ (nm)	Material	Notes
1.	Green	530	InGaN	LXHL – MM1D
2.	Blue	470	InGaN	LXHL-MB1D
3.	White	---	InGaN	LXHL-MW1D
4.	Red	625	AlInGaP	LXHL-MD1D
5.	Orange	590	AlInGaP	LXHL-ML1D
6.	Blue	470	InGaN	Radiation Pattern: Side emitting LXHL-FB1C
7.	Infrared	1330	InGaAsP/InP	Laser diode

LUXEON START HEX LEDs shown in Table 3.1. Most of the investigated LEDs has Lambertian radiation pattern (Fig. 3.7 on the left). Light emitted from LED with Lambertian radiation pattern has intensity peak at 0° from the LED

axis, and intensity decreases as angular displacement increases. At 80° angle the light intensity is almost negligible. LEDs with Lambertian type radiation well fits for the spotlight, floodlight, etc.

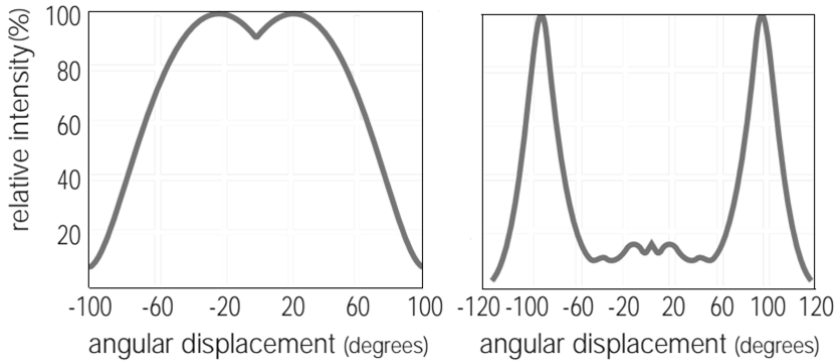

Fig. 3.7. Lambertian (on the left) and Side emitting (on the right) radiation

There was investigated nitride based blue (470 nm) LEDs with Side emitting radiation pattern (No 6 in Table 3.1). Radiation pattern of the diode has toroid form and intensity of the light has a peak at 75 – 85 degrees off the optical axis (Fig 3.7 on the right). Side emitting LEDs can illuminate a large surface located at near distance, for example to backlight LCD screen. Such light radiation of LED allowed to direct light into two photodetectors with identical measurement channels.

To compare LED noise with the one of laser diode, ridge-waveguide graded-index separated-confinement heterostructure InGaAsP/InP Fabry-Pérot laser diodes were investigated (No 7 in Table 3.1). The investigated LDs were grown on n–InP substrate using MOCVD technology. Their active region contains ten 4-nm-thick compressively strained (0.7%) InGaAsP quantum wells separated by 10 nm thick p-doped InGaAsP/InP barrier layers, the lattice of which was matched to InP. The cavity width of the samples is 2 μm. The devices were bonded p-side up onto SiC heat sinks mounted on copper blocks, which in turn were mounted onto ceramic subcarriers. The laser diode emission wavelength is about (1.33) μm, radiation spectrum is multimode and consists from 3-5 main modes. Barrier layer band-gap energy is 1.18 eV and cavity length is 250 μm.

4 Results and discussion

4.1 Noise characteristics of LED

In this chapter is presented comprehensive investigation of noise characteristics of un-aged nitride-based light emitting diodes and compared to phosphide based LEDs. Investigated InGaN based LEDs emitting different colour light: green (No. 1 in Table 3.1), blue (No. 2 in Table 3.1), white (No. 3 in Table 3.1) For comparison with phosphide based LEDs there was investigated several samples of AlInGaP LEDs emitting different color light: red (No. 4 in Table 3.1) and orange (No. 5 in Table 3.1) [O6, C8].

Investigated nitride based blue (470 nm) light side emitting LEDs (No. 6 in Table 3.1), which allowed to measure optical noise and cross-correlation factor from light emitting in two opposite directions of lenses. Such investigations allow to determine where the noise source comes from [P1, P3, C4].

To clarify phosphor layer influence on noise characteristics of white light emitting LED, there was used a photodiode matrix comprised from three photodiodes with different wavelength of sensitivity maximums. This allows to separate and investigate blue light from the active layer and the broadband yellow from phosphor one (Fig. 4.1) [O5, O1, P1].

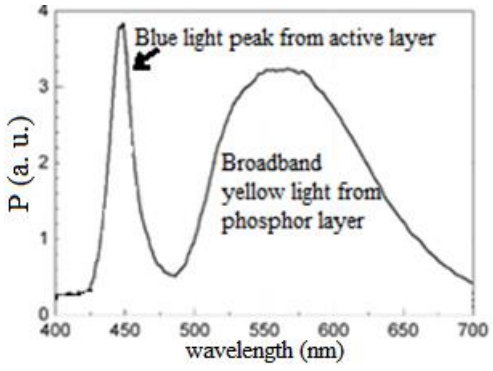

Fig. 4.1. Optical spectrum of white LED under test.

Non-coherent light emitting LEDs can be transferred into coherent light sources by inserting it into optical resonators. To clarify the optical resonator influence to the noise characteristics, Fabry-Perot laser diodes based on

InGaAsP/InP were investigated and compared its characteristics to the ones of LEDs [P2, O2, O3, C2, C5].

4.1.1 Comparison of noise characteristics of nitride based and phosphide based LEDs

The light power spectra, the electrical (LED terminal voltage) and optical (emitted light power) fluctuation spectra, cross-correlation factor between these fluctuations vs. current were measured for several groups of high power (1 W) LEDs irradiant at different wavelength and fabricated from different materials (Table 3.1): green, blue – from InGaN; red, orange – from AlInGaP [O6, C8]. The white LEDs were fabricated on the base of blue InGaN LEDs which surface was covered by YAG:Ce+3 phosphor layer emitting broadband yellow light.

The typical optical spectra of the investigated LEDs are presented in Fig. 4.2 (on the left). White LED results are shown by black curve, for the rest LEDs curve color corresponds to the diode light color (in this and all further figures unless otherwise stated). Here we note that some of spectra (blue and

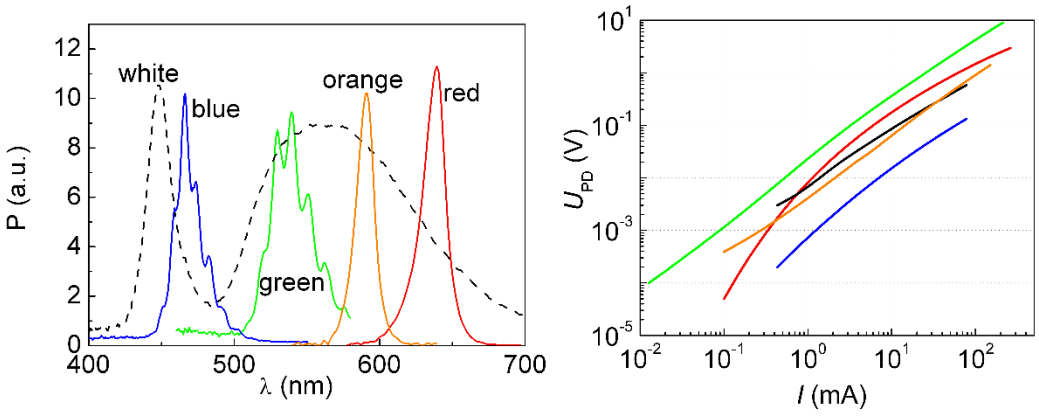

Fig. 4.2. The typical optical spectra of investigated LEDs (on the left) and their optical output power (proportional to the photodiode load resistance voltage) dependencies on forward current (on the right).

green) show Fabry-Pérot oscillations in the emission intensity [70]. Optical output power (proportional to the photodiode load resistance voltage) dependencies on forward current are close to linear (Fig. 4.2 on the right) for the most of investigated LEDs.

Typical electrical and optical noise characteristics for the investigated LEDs are presented in Fig. 4.3. Electrical noise of the investigated LEDs is

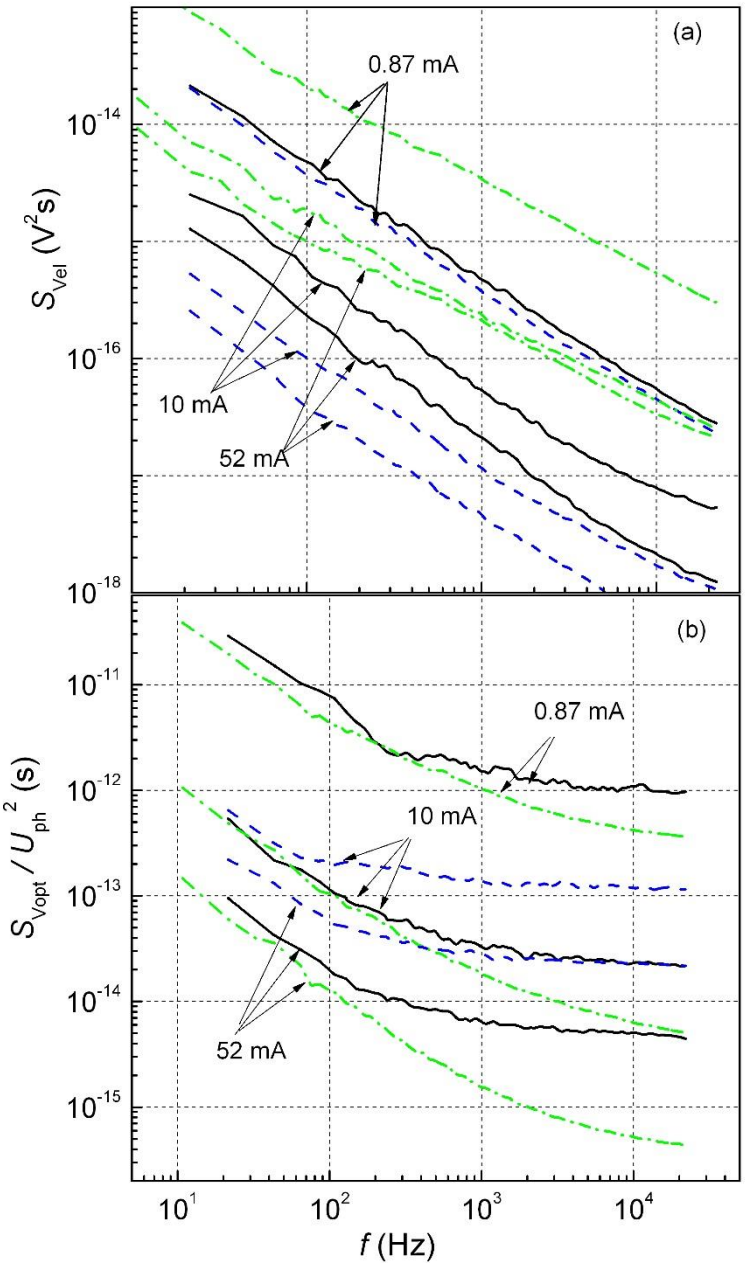

Fig. 4.3. Electrical (a) and optical (b) noise spectra at different forward currents for InGaN-based LEDs: solid line – white, dashed line – blue, and dash dot line – green LEDs.

mainly characterised by $1/f^{\alpha}$-type fluctuations (graph (a) in Fig. 4.3). The source of $1/f^{\alpha}$-type noise in semiconductor devices generally is caused by the superposition of charge carrier generation and recombination (GR) and capture

processes through GR and capture centers with widely distributed relaxation times. These centers are formed by different defects, dislocations and imperfections in the device structure, and can be in the active area or other layers and interfaces of the LED. Electrical noise decreases with forward current increasing (graph (a) in Fig. 4.3) can be explained by defects in LED structure: at small current conditions, current flows through the narrow channels formed by the defects, and the electron capture or release events in these defects lead to the large random modulation of flowing current. As forward current increases, it starts flowing through whole device cross-section and the influence of the defect decreases due to shunting effect. The experimental results have shown that nitride-based blue and white LEDs demonstrate quite low $1/f^{\alpha}$-type electrical and optical noise levels (Fig. 4.3), what indicates on high quality of these investigated LEDs. Not all the light of LED is registered in photodiode. To normalize the measured optical noise, the spectral density is divided by the photovoltage powered in square. Optical fluctuations distinguish by $1/f^{\alpha}$-type spectrum at low frequencies and "white" noise that prevails at frequencies above 1 kHz (Fig. 4.3 graph (b)). Optical fluctuations with "white" spectrum are caused by the shot noise due to discreteness of emitted photons from the LED. The green LEDs show the larger electrical noise level, what indicates on larger defect and imperfection density in these structures comparing with ones of blue LEDs.

Cross-correlation factor between electrical and optical noises (Fig. 4.4) reveals physical processes that take place in LED structure. Considering that light emission is produced in the active layer of LED the correlated electrical and optical low-frequency $1/f^{\alpha}$-type fluctuations at constant dc current can be related only with defects and imperfections in the active layer or near to its interfaces. On the other hand, the noise sources with different spectra are not correlated. So, 1/*f*-type fluctuations and noise with "white" spectrum (thermal or shot noises) never be correlated. High cross-correlation factor between flicker ($1/f^{\alpha}$) electrical and optical noises indicates that they are essentially related with the defects and imperfections in the active region or on its interfaces. The

presence of defects and imperfections in the active region not only changes the level of electrical and optical noises, but also increases non-radiative recombination, and therefore, decreases LED efficiency. Different samples distinguish by different cross-correlation factor value: close to zero (for blue LED), moderate value (for white LED) and independent on forward current or high cross-correlation factor strongly dependent on current for green LED (Fig. 4.4) [68, 71, 72].

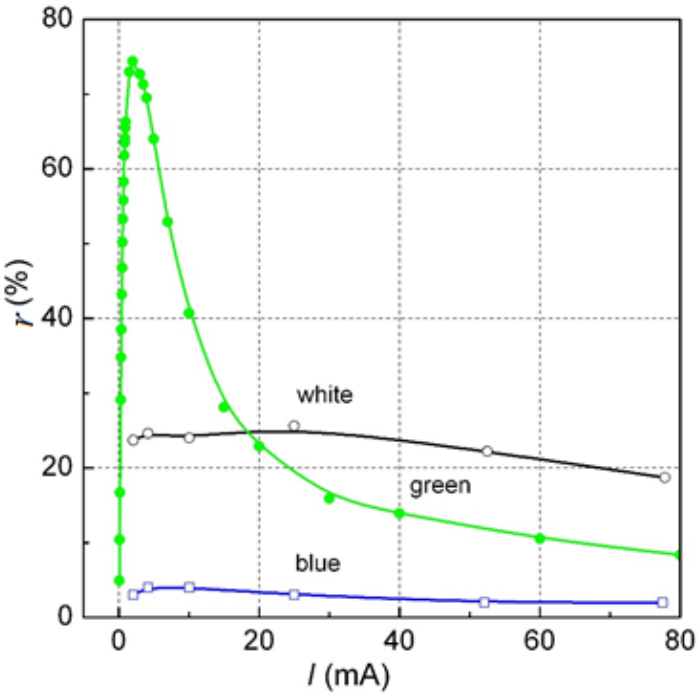

Fig. 4.4. The Cross-correlation factor between optical and electrical fluctuations (frequency range from 10 Hz to 22 kHz) dependency on forward current for InGaN-based LEDs.

Close to zero cross-correlation factor shows, from one hand, that there are defects in other than active layers or interfaces of LED structure that cause only the electrical noise characteristics (for example, a metal-semiconductor interface), on the other hand, it can take place in such a case when optical flicker noise level is small comparing with one of "white" noise, e.g. when the variance of $1/f^{\alpha}$ -type noise is many times smaller than that of shot noise.

In the case of green LED, highly correlated $1/f^{\alpha}$ -type optical and electrical noises take place at dc current smaller than 10 mA while at larger current not

correlated noise sources are more intensive. This could be explained by the decreased influence of defects due to shunting effect at higher current.

Noise characteristics and cross-correlation factors of AlInGaP-based LEDs are presented in Fig. 4.5 and Fig. 4.6 accordingly. Optical and electrical noise

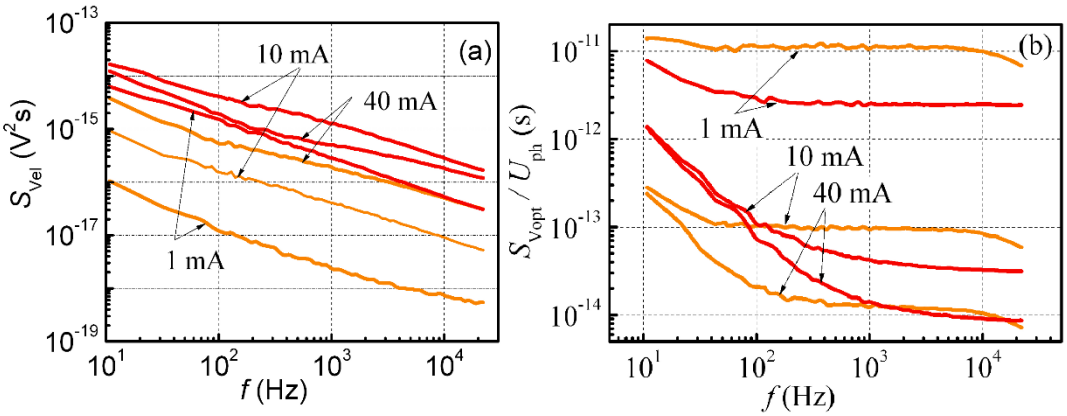

Fig. 4.5. Electrical (a) and optical (b) noise spectra at different forward currents for AlInGaP-based LEDs: solid line – red and dashed line – orange LEDs.

intensities are similar to those of blue and white InGaN-based LEDs. As for nitride based LEDs, there also in electrical noise dominates $1/f^{\alpha}$ type component. Electrical noise level is higher for the red LED when compared with the orange one. $1/f^{\alpha}$ optical noise component is much higher for the red LED than compared to the orange one. The cross-correlation factor between optical and electrical fluctuations for the red and orange LEDs is small which indicate that electrical noise essentially is related not with the active layer of the investigated LED structure.

It was shown that $1/f^{\alpha}$-type electrical and optical noise levels for green nitride-based LEDs are many times larger than ones for blue LEDs, and that is caused by larger defect and imperfection density in the active LED layer. To emit longer wavelengths (i.e. green instead of blue), higher concentration of Indium is required in InGaN layer of LED. Due to lattice mismatch between

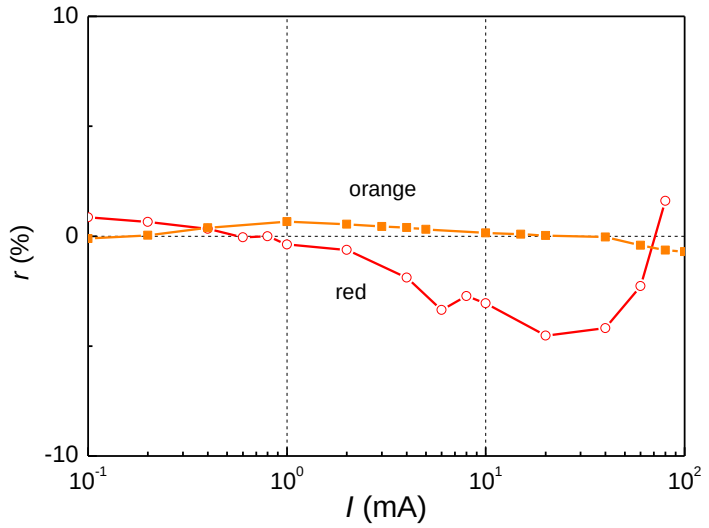

Fig. 4.6. The cross-correlation factor between optical and electrical fluctuations (frequency range from 10 Hz to 22 kHz) dependency on forward current for AlInGaP-based LEDs.

InGaN and GaN, in green LEDs higher number of defects appears which causes higher noise levels of green nitride-based LEDs [73].

Analogical analysis of investigated AlInGaP-based LEDs noises show that electrical noise is essentially related not with the active region of the LED structure.

4.1.2 Influence of the secondary optics to the LED noise characteristics

Side emitting LEDs were investigated in order to evaluate secondary optics influence to the noise characteristics of light emitting diode [P1, P3, C4]. In the side emitting diode the light goes upwards and is collimated and redirected 90° by a conical reflector to exit in the horizontal plane (Fig. 4.7 (a)). Investigated devices were nitride-based side emitting diodes radiating blue (470 nm) light. Radiation pattern of the diode has toroid form and intensity of the light has a peak at 75 – 85 degrees off the optical axis.

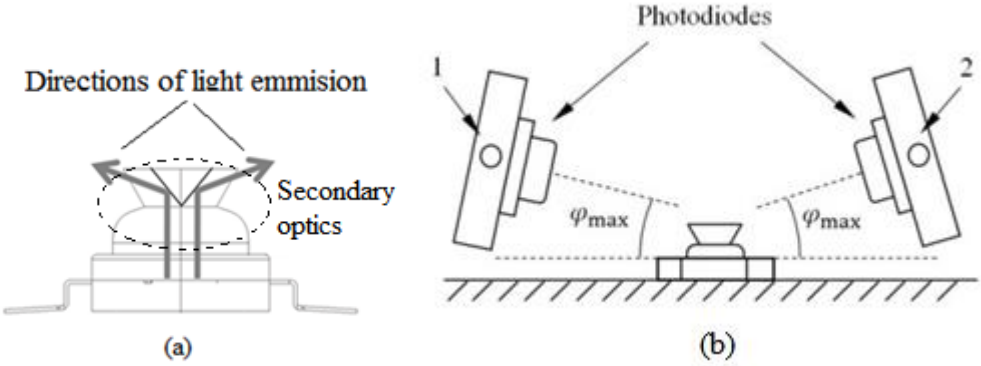

Fig. 4.7. Side emitting diode light emission directions (a) and its investigation scheme (b);1 and 2 are photodiodes rotation axis, φ_{max} is an angle of the peak intensity of the diode.

Optical and electrical noise characteristics, cross-correlation factor between optical and electrical fluctuations and cross-correlation factor between two optical signals detected at the opposite directions of the LED radiation pattern have been measured of the investigated LEDs. Therefore, for the side emitting diode optical noise investigation two identical photodiodes have been aimed precisely at the two opposite points of the peak intensity of the diode (Fig. 4.7 (b)). For both photodiodes, almost identical photodetector's voltage dependency on DC current were measured (Fig. 4.8), what shows that intensity

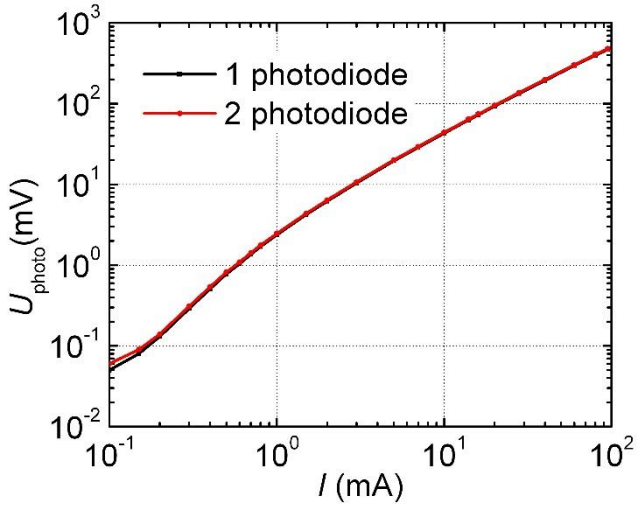

Fig. 4.8. Photodetectors voltage (proportional to the emitted light flow rate) dependence on d.c. current.

of the light incident upon PDs is the same and should not be difference due to different measurement channels.

Side-emitting LED demonstrates $1/f^{\alpha}$ optical and electrical noise spectra (Fig. 4.9) – the same type as the ones without secondary optics. The origin of noise sources is the same as described in Chapter 4.1.1. Fluctuations of output light power for investigated device show $1/f^{\alpha}$ -type spectrum at low frequencies and "white" noise at frequencies above 1 kHz (graph (b) in Fig. 4.9). $1/f^{\alpha}$ -type optical fluctuations are caused by the modulation of charge carrier number in the active region due to flowing current fluctuations. Optical fluctuations with "white" spectrum are attributable to the shot noise due to emitted photons as it was mentioned in Chapter 4.1.1. Optical noise spectral density increases with forward current increase (graph (b) in Fig. 4.9) as light output power increases.

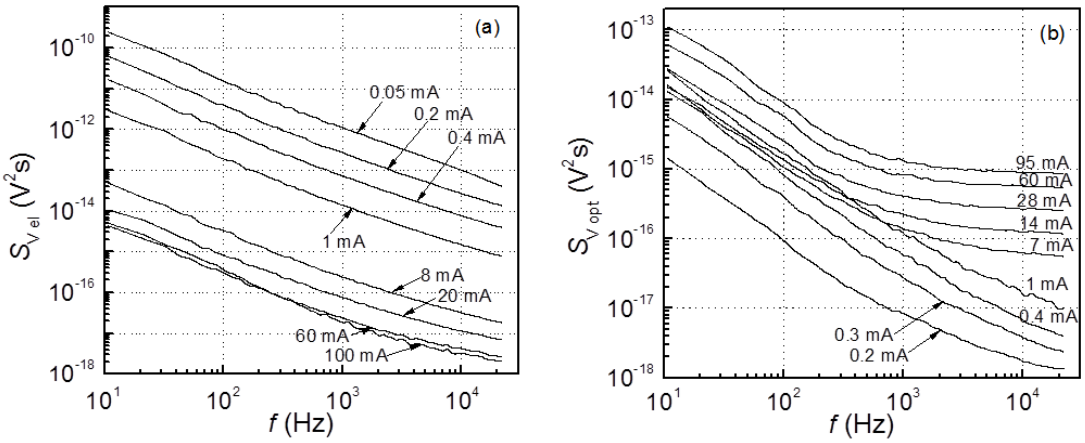

Fig. 4.9. Electrical (a) and optical (b) noise spectra of side emitting diode at different forward currents.

Cross-correlation factor between two optical signals detected at opposite sides of the side emitting diode radiation pattern have been measured in every one-octave frequency band (Fig. 4.10). Close to 100 % cross-correlation was observed and it is true to say that light emission from the active region goes from the single point and that lenses and secondary optics do not influence the pervasive light.

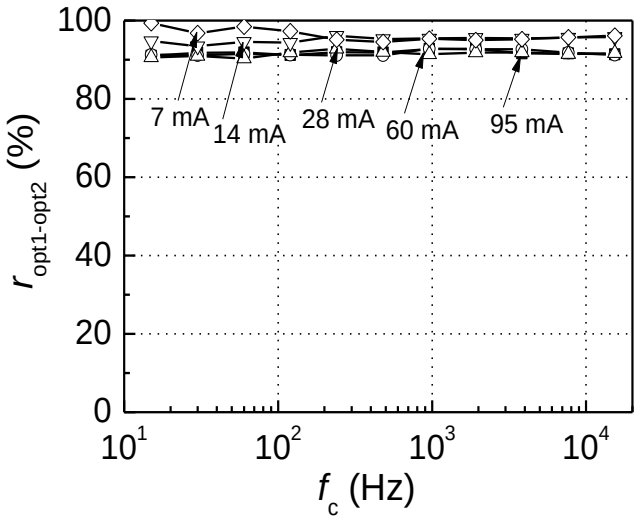

Fig. 4.10. Cross-correlation factor between two optical signals detected at the opposite points of the side emitting diode radiation pattern dependency on octave central frequency at different forward currents.

Optical and electrical $1/f^{\alpha}$-type fluctuations of the investigated side emitting light diodes (LEDs) at low frequencies are caused by the superposition of generation and recombination (GR) processes through defects created charge carrier GR and capture centers, the same as to the conventional LEDs. Secondary optics do not influence noise characteristics and LED operation. As has shown close to 100 % cross-correlation factor between optical signals detected at opposite points of the radiation pattern lenses and secondary optics do not influence the output light.

4.1.3 Influence of the phosphor layer to the noise characteristics of white light emitting diode

In order to investigate phosphor layer influence to the noise characteristics of white LED, noise characteristics of high power nitride-based white light-emitting diodes have been measured [P1, O5, O1]. LED output light power and optical noise signal was measured by photodiode matrix comprised from three photodiodes (PDs) that are sensitive to the different part of visible spectrum: the sensitivity maximum of the first PD coincides with the blue light peak (around

460 nm), peak sensitivity of the second PD is at 540 nm, and the third PD has maximum sensitivity around 620 nm. In Fig. 4.11, there is presented investigated white LED radiation spectrum, and lined areas represent spectral response range of each photodiode: “blue”, “green” and “red”. Using such photodiode matrix enables separation and investigation of

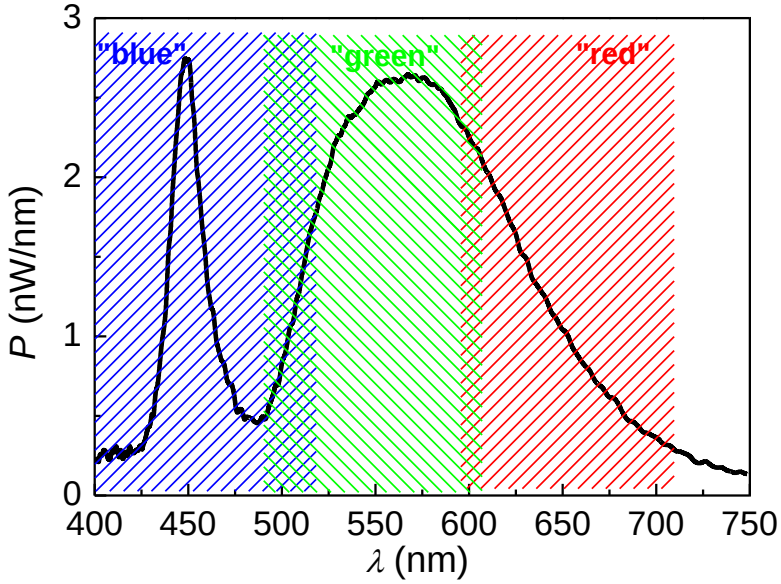

Fig. 4.11. Radiation spectrum of investigated white LED at 300 mA forward current. Lined areas show spectrum part that is covered by each of the photodetectors.

different parts of the white LED optical spectrum: blue spectrum range (BSR) photodiode is sensitive to the optical signal from the active region, green spectrum range (GSR) and red spectrum range (RSR) PDs are sensitive to the luminescence light from the phosphor layer. Such division of radiation spectrum enables to separate physical processes that take part in different parts of the white LED structure.

Optical and electrical noise and cross-correlation factor between optical and electrical fluctuations (also between two optical signals, i. e. detected by the BSR and RSR photodetectors) have been measured at room temperature. Both noise signals were processed simultaneously using two identical channels of noise measurement system. Cross-correlation factor was computed over the whole investigated frequency range: 10 Hz – 20 kHz, and in one-octave frequency bands by using digital filters.

Operation (current-voltage (IV) and light output power vs. current (LI)) and noise (optical and electrical fluctuations and cross-correlation factor between two noise signals) characteristics of investigated white LEDs have been carried out. The results are presented in Fig. 4.12 - Fig. 4.15.

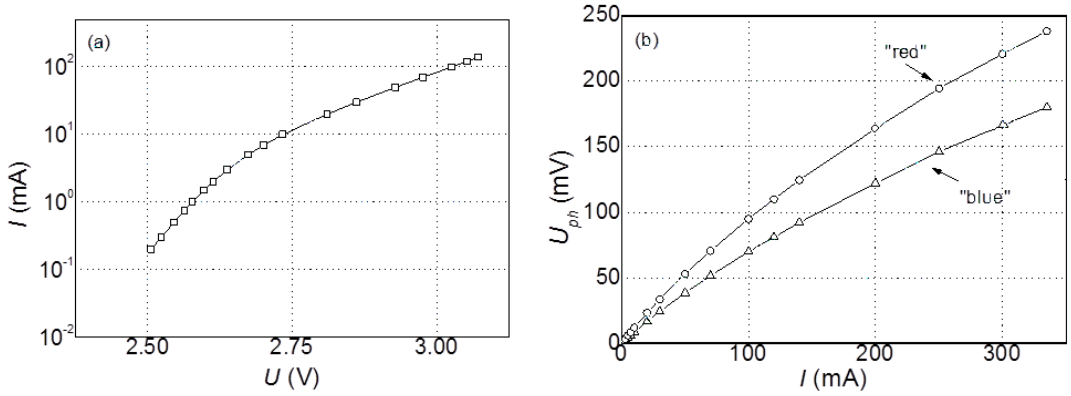

Fig. 4.12. Current-voltage (a) and output light power vs. current (b) characteristics of investigated LED ("red" is for the light output power measurements by RSR photodetector, "blue" – for the measurements by BSR photodetector).

In Fig. 4.12, there are presented typical IV and LI characteristics of investigated devices. Electrical fluctuations of investigated LEDs distinguish by $1/f^{\alpha}$ -type spectrum (graph (a) in Fig. 4.13).

Both – red and blue - optical noise spectrum characteristics of the investigated LEDs contain "white" noise part at higher frequencies, while at low frequencies (below 100 Hz) $1/f^{\alpha}$ -type fluctuation prevails "white" noise level (graphs (b) and (c) in Fig. 4.13).

Low frequency optical fluctuations are partly correlated with electrical noise (graphs (a) in Fig. 4.14 and graphs (a) and (b) in Fig. 4.15), and this is caused by $1/f^{\alpha}$ -type noise components. Optical fluctuations with "white" spectrum are caused by the shot noise due to random events of photon emission. Similar type of noise spectra is observed for both blue and red light intensity fluctuations (graphs (b) and (c) in Fig. 4.13). Optical noise intensity increases with forward current increasing mainly due to the light output power increase. Averaged over all investigated frequency range (10 Hz – 20 kHz)

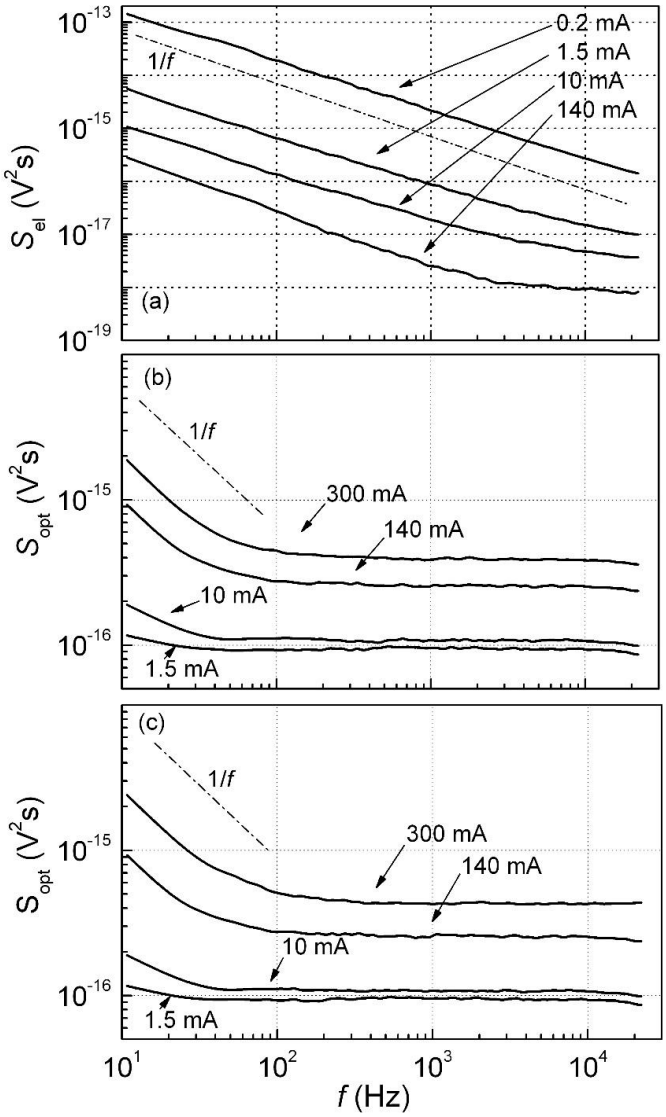

Fig. 4.13. Electrical (a) and optical ((b) - measurement by BSR photodetector, (c) - measurement by RSR photodetector) noise spectra at different forward current.

cross- correlation factor between electrical and optical fluctuations is small ((3-4) %; graph (a) in Fig. 4.14).

More informative are cross-correlation measurements in one-octave frequency bands (Fig. 4.15). It is seen that highly correlated are low-frequency noise components: looking into both electrical-optical ((30-50) % in (10-20) Hz band) and optical-optical (increases with current increasing) cross-

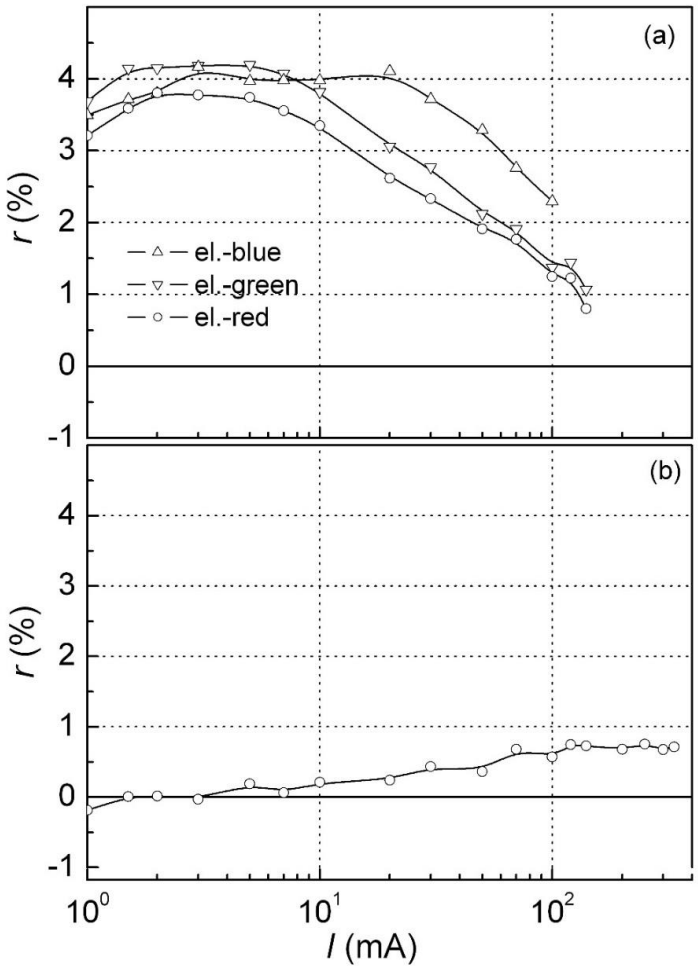

Fig. 4.14. Cross-correlation factor over 10 Hz – 20 kHz frequency range dependencies on current: (a) between electrical and optical blue signals measured by BSR (el.-blue), GSR (el.-green) or RSR (el.-red) photodetectors; (b) between two optical signals measured by BSR and RSR photodetectors.

correlation factors. It shows that only $1/f^{\alpha}$ -type optical and electrical fluctuation components are correlated.

Partial ((30-50) %) cross-correlation between electrical and optical fluctuations at low frequencies ((10-20) Hz) shows that not all injected current flows through the active region of the LED: part of it flows through the peripheral areas and does not participate in the light emission.

Similar values of cross-correlation factor between electrical and blue light intensity fluctuations and between electrical and red light intensity fluctuations,

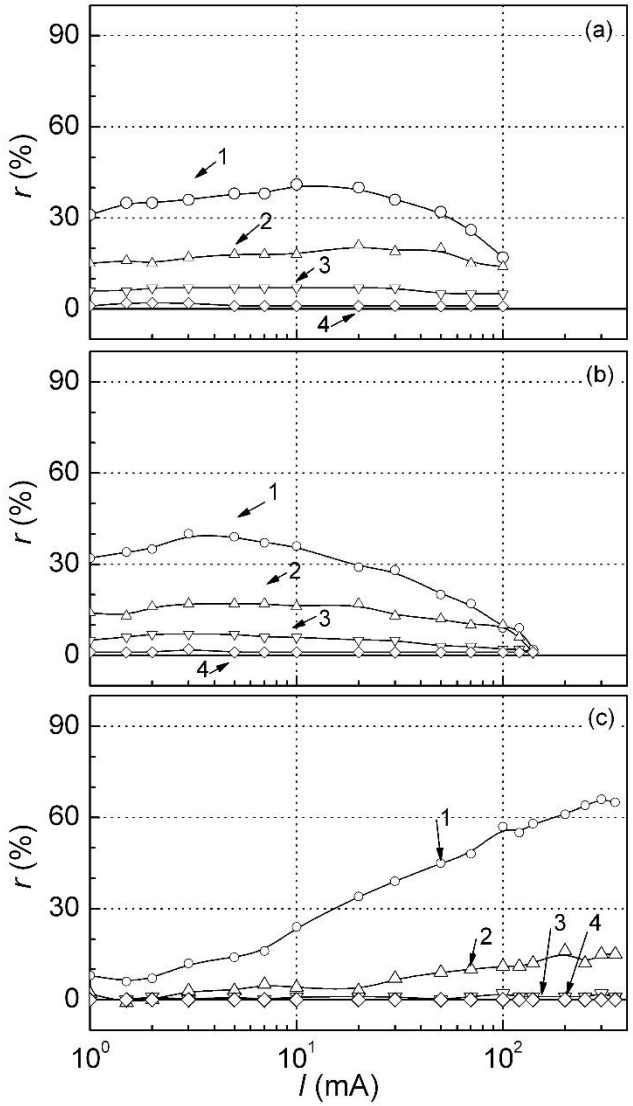

Fig. 4.15. Cross-correlation factor in one-octave frequency bands (1 – [10 – 20] Hz, 2 – [80 - 160] Hz, 3 – [0.64 – 1.28] kHz, 4 – [10.24 – 20.48] kHz) dependencies on current: (a) between electrical and optical signal measured by BSR photodetector, (b) - between electrical and optical signal measured by RSR photodetector; (c) between two optical signals measured by BSR and RSR photodetectors.

and also the high cross-correlation factor between blue and red light intensity fluctuations shows that phosphor layer does not have weighty impact to the $1/f^{\alpha}$ -type optical fluctuations observed in investigated LEDs – origin of this noise should be in the active region.

Investigation of white LED characteristics, dividing its optical spectrum into non-overlaping ranges has shown, that phosphor layer luminescence process has almost no influence to the noise characteristics of the investigated white LEDs.

4.1.4 Laser diode noise comparison to LED

One of the applications for the light emitting diode is a light source for short range optical communications, where laser diodes are replaced [74]. In this chapter, there are described the differences between LED and laser diode noise characteristics and their origin. The investigated lasers are ridge-waveguide graded-index separated-confinement heterostructure InGaAsP/InP multiple quantum well Fabry-Pérot laser diodes [P2, O2, O3, C2, C5]. The laser diode emission wavelength is about (1.33) μm, radiation spectrum is multimode and consists from 3-5 main modes. Laser diode optical peaks are very narrow when compared to the LED emission (Fig. 4.16).

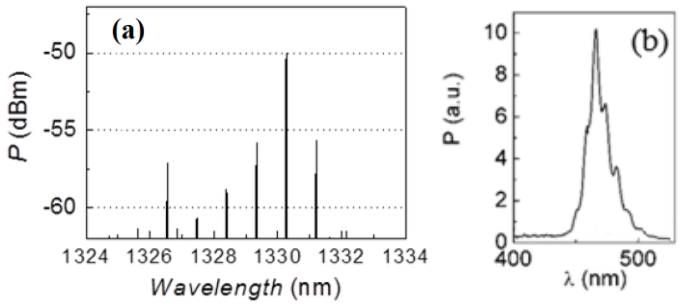

Fig. 4.16. FP LD radiant spectrum at the stable operation (injection current: 82.2 mA, temperature: 294.26 K (a) and typical Blue InGaN LED optical spectrum (injection current 200 mA, at room temperature).

Laser diode radiation spectrum and LD low frequency (10 Hz – 100 kHz) noise characteristics have been measured simultaneously: at the LD output the laser light beam was coupled into two fibers optical cable (Fig. 3.4). One fiber was connected to the optical noise measurement equipment and the second - to the optical spectrum analyzer.

Noise characteristics of the LDs involve optical noise, electrical noise and cross-correlation factor between optical and electrical fluctuations dependencies on injection current, temperature and frequency.

Noise characteristics of investigated Fabry-Pérot laser diodes at stable lasing (above threshold) operation ((a) and (b) in Fig. 4.17) are similar to the LEDs (Fig. 4.3): $1/f^{\alpha}$-type, where $0.95<\alpha<1.2$, fluctuations were observed in both optical and electrical noise signals at low frequencies. Optical and electrical noise intensity at the stable operation (where there is no sharp peaks of high

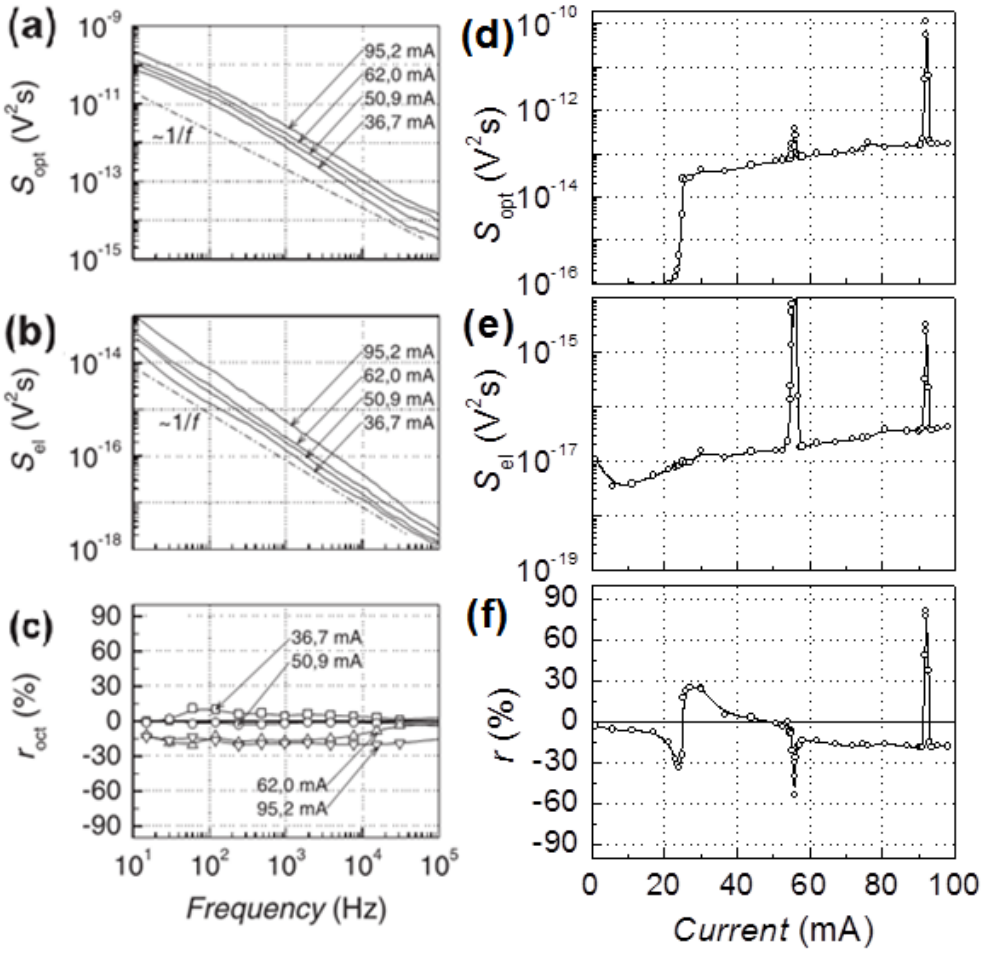

Fig. 4.17. Typical optical (a) and electrical (b) noise spectra and cross-correlation factor dependency on central frequency of octave (c) at different injection current at stable operation of FP LDs (at room temperature) and optical (d) and electrical (e) noise spectral density at 10 kHz and cross-correlation factor (f) in the frequency range from 10 Hz to 20 kHz dependencies on injection current (at room temperature).

intensity fluctuations) increases approximately proportional to the injection current ((d) and (e) in Fig. 4.17). As in LEDs, the origin of $1/f^{\alpha}$-type noise in laser diodes is superposition of many charge carriers generation and recombination (GR) processes through GR and capture centers with widely distributed relaxation times. $1/f^{\alpha}$- type optical and electrical fluctuations at stable lasing operation are weakly corelated: cros-corelation factor in the most cases does not exeed 30% and weakly depends on injection current and frequency (graph (c) in Fig. 4.17). Low cross-correlation between optical and electrical fluctuations indicates that defects formed centers that originate $1/f^{\alpha}$ – type noise at stable operation are located in peripherial LD regions (not in the active one). At certain operation conditions, sharp strongly correlated optical and electrical noise peaks are observed in operation of investigated LDs (graphs (d)-(f) in Fig. 4.17). These noise peaks are caused by the mode-hopping effect and are extremely sensitive to the injection current (graphs (d)-(f) in Fig. 4.17) and temperature (Fig. 4.18). During mode-hopping the peak longitudinal mode of the laser radiant spectrum hops to the next one (at longer wavelength side if temperature or injection current increases) due to laser diode optical gain spectrum (the quantum well band-gap energy determines its maximum) moving to the longer wavelength, when optical gain of the adjacent mode exceeds the gain of the radiant peak mode. Shift of the peak radiant mode covers narrow but finite range in the temperature and injection current region, where both peak modes are radiated: laser radiation spectrum randomly hops between two radiant mode sets and mode-hopping is observed. As a result LD radiant power spectrum is not stable in time during the mode-hopping (Fig. 4.19 (presented radiation spectra are taken at different time moments during one mode-hopping event at fixed injection current and temperature)): intensity of radiating longitudinal modes strongly fluctuates. Consequently, averaged LD radiation spectrum widens: it consists of 6-7 longitudinal modes of almost equal intensity, which intensity randomly fluctuates in time, instead of 3-5 peak intensity modes at the

stable operation (Fig. 4.16).

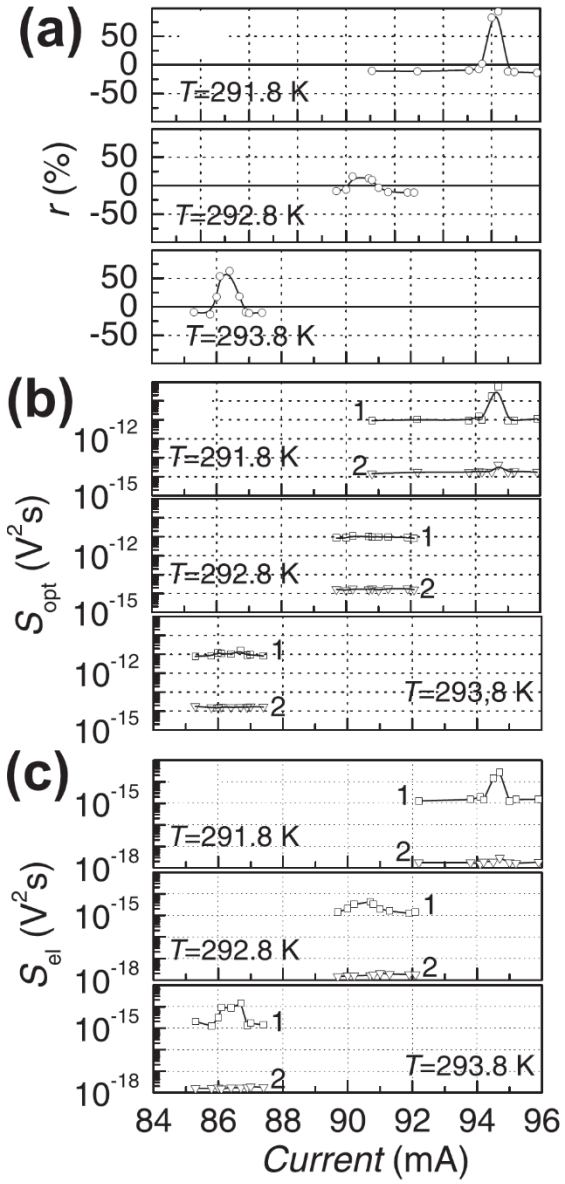

Fig. 4.18. Cross-correlation factor (a) in frequency range from 10 Hz to 20 kHz), optical (b) and electrical (c) noise spectral density (at different frequencies: 1- 0.312 kHz, 2- 1.04 kHz) dependencies on injection current at different temperatures at different mode-hopping peaks.

As presented in Fig. 4.17, mode-hoping effect leads to highly correlated intensive optical and electrical fluctuations. Noise spectral density at the mode-hopping is 1-3 orders larger comparing to the noise level at stable lasing operation. Cross-correlation factor between optical and electrical fluctuations increases up to (60-90) % during mode-hopping and could be positive or negative (noise intensity level and cross-correlation value vary for different

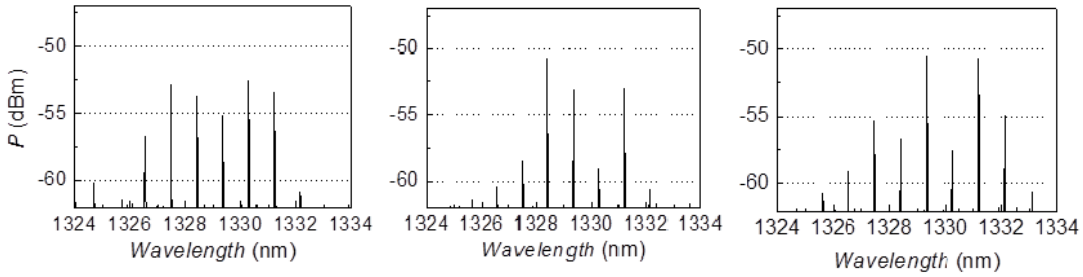

Fig. 4.19. FP LD radiant spectra at the mode-hopping peak at the fixed operation conditions (injection current: 83.0 mA, temperature: 294.26 K) at different time moments.

mode-hopping peaks (Fig. 4.17)). Optical and electrical noise spectra during the mode-hopping are Lorentzian-type with different cut-off frequency for various peaks (Fig. 4.20 (there are presented noise spectra at the very top of mode-hopping peak that moves in injection current scale with temperature change)): Lorentzian-type optical and electrical fluctuations at mode-hopping prevail $1/f^{\alpha}$ -type noise. Different cross-correlation sign and different cut-off frequency indicate that there are several different physical processes that are active in laser diode during distinct mode-hopping events and lead to the intensive optical and electrical fluctuations.

Occurrence of the mode-hopping effect is very sensitive on LD operation conditions (temperature and injection current): mode-hopping position moves to the larger injection current values, when temperature decreases (Fig. 4.18). Mode-hopping effect is present just in particular injection current and temperature ranges: out step of this range mode-hopping (and with it related intensive correlated Lorentzian-type optical and electrical noise) vanishes.

There is observed cross-correlation factor between optical and electrical fluctuations dependency on frequency (graphs (c) in Fig. 4.20): measurements in one-octave frequency band show that cross-correlation during mode-hopping is the largest at frequencies close to the cut-off frequency of measured Lorentzian-type noise spectra. At different temperature, different cut-off frequencies are observed (Fig. 4.20). Such Lorentzian-type spectra are characteristic for the generation and recombination process. Therefore optical

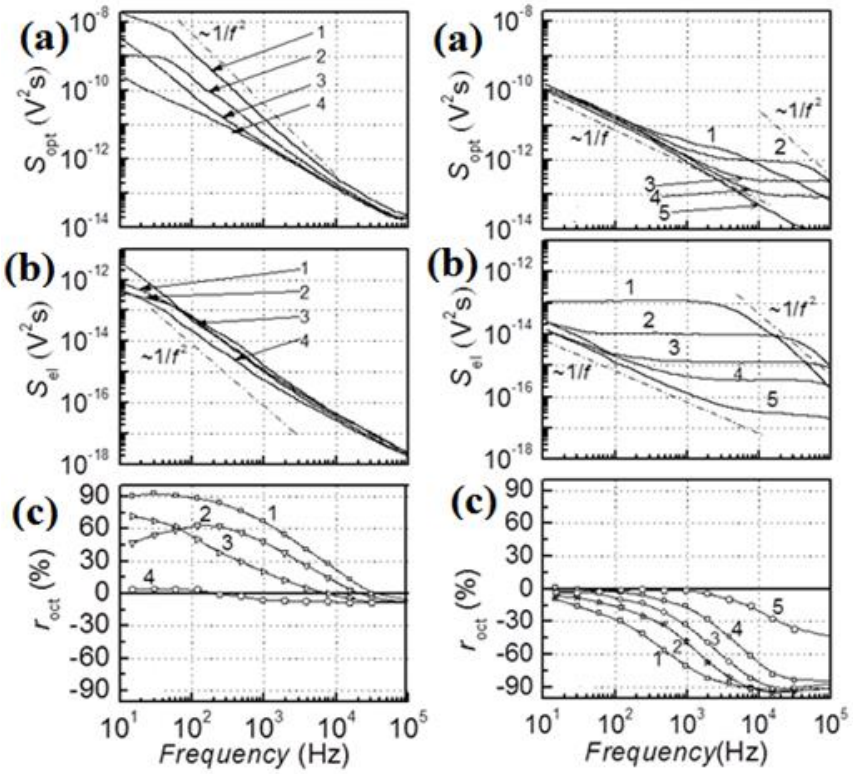

Fig. 4.20. Optical (a) and electrical (b) noise spectra and cross-correlation factor dependencies on central frequency of octave (c) at the mode-hopping peak maximum at different injection currents and temperatures: on the left (1- 96.5 mA, 291.3 K, 2- 91.3 mA, 292.3 K, 3- 88.2 mA, 293.3 K, 4- 85.8 mA, 294.0 K) and on the right (1- 61.1 mA, 288.8 K, 2- 54.4 mA, 291.0 K, 3- 50.70 mA, 291.5 K, 4- 49.3 mA, 292.3 K, 5- 43.1 mA, 293.3 K)

and electrical fluctuations with Lorentzian-type spectrum during mode-hopping are caused by the carrier capture and release processes in GR or capture centers that are formed by defects and imperfections in LD structure and creates localized states with different cross-section. Large cross-correlation factor between optical and electrical fluctuations shows that these centers are in the LD active region, where injected charge carriers recombine and produce photons.

As LD injection current (that determines Joule heating intensity) or temperature increase laser diode optical gain spectrum moves to the longer

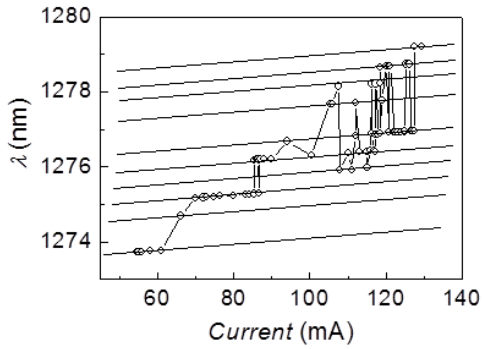

Fig. 4.21. Wavelength of the maximum peak radiant mode dependency on injection current (at room temperature).

wavelength (parallel lines in Fig. 4.21). However at particular temperature values the maximum peak mode salutatory hops to the next wavelength. There is some threshold that should be reached for the "next" mode set radiation. The state of the generation and recombination and carrier capture centers influences the threshold reaching conditions. Considering that radiative recombination of charge carriers can occur only in quantum wells, we can state that correlated electrical and light intensity fluctuations are related with the random potential height fluctuations of barrier layer due to charge carrier capture and recombination in defects in the barrier (in the quantum wells structure) layers. These potential fluctuations modulate that part of carriers which recombines in the quantum wells and produce photons. As a consequence fulfillment of longitudinal mode radiation threshold condition is randomly jumping between two mode sets during mode-hopping. Therefore there is strong correlation between optical and electrical fluctuations during mode-hopping.

Fabry-Pérot laser diodes at the stable lasing operation like light emitting diodes distinguish by $1/f^{\alpha}$-type optical and electrical fluctuations. And origin of this noise is a superposition of many generation – recombination processes through defects formed centers with widely distributed cross-sections.

Differently from LED investigated laser diodes because of resonators has a mode-hopping efect, that leads to the laser radiation spectrum widening and instability and causes intensive highly correlated Lorentzian-type optical and electrical fluctuations. High cross-correlation between mode-hopping optical

and electrical fluctuations enables to conclude that origin of LD operation instability during the mode-hopping is generation and recombination processes through defects formed centers in the barrier layers (of the active region).

4.1.5 Summary

There are presented comprehensive investigations of nitride-based and phosphide-based light-emitting diodes. Measured characteristics were electrical, optical and noise (electrical and optical) characteristics. Cross-correlation factor between electrical and optical fluctuations was measured too. There is shown that noise characteristics of nitride-based and phosphide-based LEDs are comparable.

LEDs with conical reflector in the lenses were investigated in order to evaluate lenses influence to the noise characteristics of light emitting diode. In adition to the electrical and optical fluctuation and cross-correlation factor between them there was also measured cross-correlation factor between two optical fluctuations from oposite sides of the reflector. Cross-correlation factor close to 100% between two optical noises from opposite sides of the reflector proved, that optical fluctuations measured with two different photodiodes are from the same source, i.e. from the active layer and not from the lenses.

In order to clarify phosphor layer influence to the noise characteristics of white light emitting diode, there was used a PD matrix comprised from three photodiodes with different wavelength of sensitivity maximums. This allowed us to separate and investigate blue light from the active layer and broadband yellow from the phosphor one. There was shown that phosphor layer does not influence the noise characteristics of white light emitting LED.

InGaAsP/InP Fabry-Perot LDs were investigated to compare LED noise characteristics with the laser diode ones. There was found that in stable LD operation noise characteristics are similar to the ones of LED. Because of resonator of LD at specific current and temperature conditions mode hopping effect appears. In this case noise characteristics and optical spectrum becames unstable. Generation and recombination processes in defects in the active layer

are sources of unstable characteristics during mode-hopping. Mode-hopping effect is not characteristic for LEDs.

4.2 LED reliability and quality investigation via noise characteristics

The applications where light emitting diodes are used demands for reliable and stable light sources with long time operation. There is high interest in the light sources behavior during long term operation. In this chapter there are presented results quality and reliability investigation of LEDs via optical and noise characteristics changes during accelerated aging [P1, P4, O2, O7, C6, C7, C9, C10]. Also, there were investigated aspects of the degradation of different parts of LED (lenses, phosphor layer) during accelerated aging [O7, C10].

4.2.1 Leakage current reflection on the LED noise characteristics

Several samples of LEDs of the same model of InGaN based blue light emitting diodes have been investigated to clarify leakage current relationship with noise level of light emitting diodes [P1].

Current-Voltage (*IV*) characteristics of investigated LEDs were measured not only in the operating range of the diode, but also in a very low current range (down to 1 pA). In Fig. 4.22 there are shown measured *IV* characteristics of investigated LEDs. In the LED operational range (above 10 mA) the IV characteristics of different samples overlaps. This is because the investigated LEDs are of the same material. At current just bellow 1 mA most

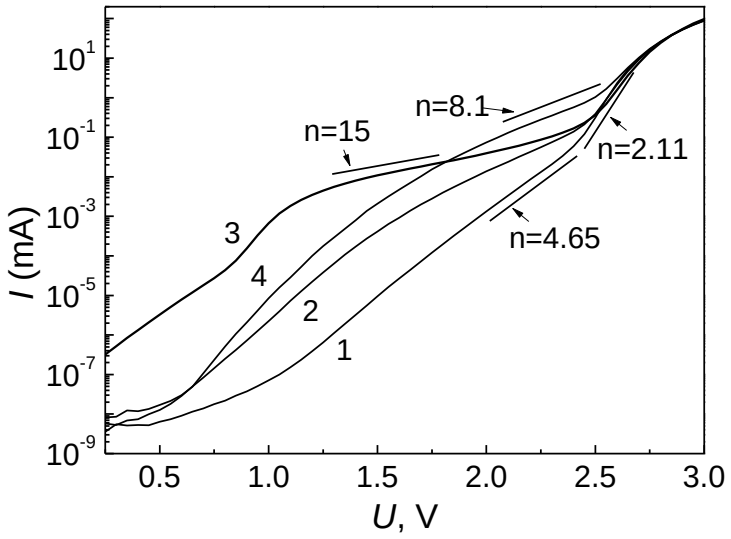

Fig. 4.22. Current versus voltage characteristics of investigated samples.

of the samples still have similar characteristics and non-ideality factor is small

(n = 2.11), which is caused by electron and hole recombination in p-n junction region [75]. Highest non-ideality factor at this curent is for Sample no. 4 (n = 8.1) (trace 4 in Fig. 4.22). Such high value shows formation of current leakage microchannels, and leakage current in these microchannels at low bias may be many times larger than electron and hole recombination component. At currents below 0.1 mA leakage current increases for the rest samples too. At 10 μA non-ideality factor varies from n = 4.65 to n = 15. In the current range from 2 mA down to 20 μA the largest leakage current has sample no. 4 and bellow this range for sample no. 3 leakage current starts dominate.

Within all the measured current range sample no. 1 has lowest leakage current compared with the rest samples. As leakage current level depends on the defectivness of the LED, sample no. 1 should have lowest noise level, what is proved by the electrical and optical noise measurement results (Fig. 4.23).

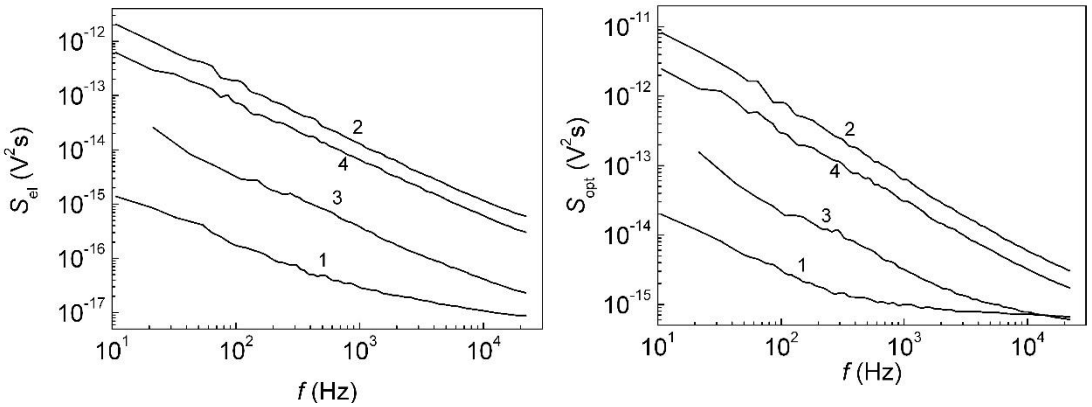

Fig. 4.23. Electrical (on the left) and optical (on the right) noise spectra of investigated LEDs (I= 8 mA).

This sample has low $1/f^{\alpha}$ optical noise, which at higher frequencies (at ~1 kHz) is outweighted by the white noise component. For the rest samples higher level $1/f$ noise dominates within all measured frequency range. In electrical noise spectrum at higher frequencies shot noise has noticable influence for sample no. 1. Although sample no. 2 has moderate leakage current, measured noise level is highest if compare with the rest samples. This could be caused by change of defect density due to nonsimultaneous IV and noise measurements. Existence of high number of deffects in the active layer is confirmed by highly

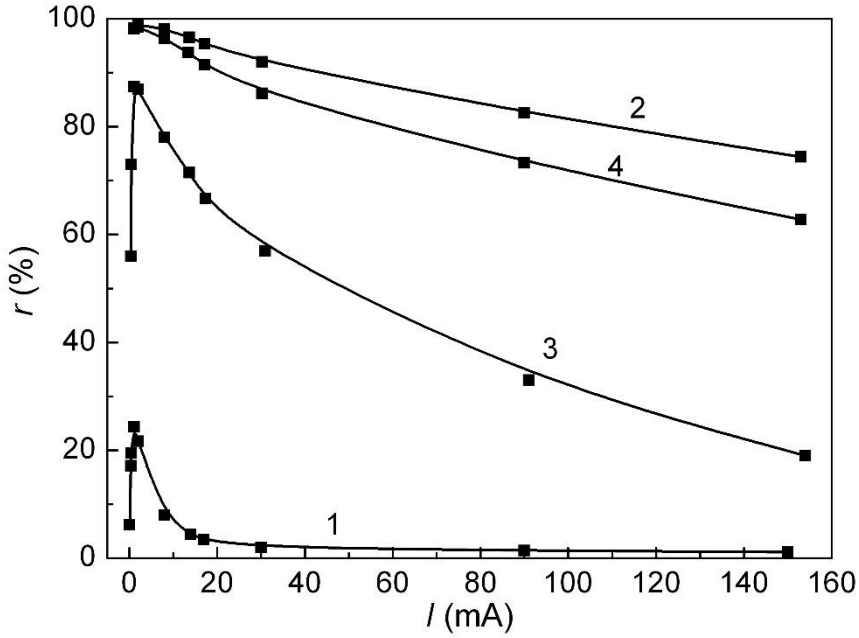

Fig. 4.24. Cross-correlation factor between electrical and optical fluctuations dependencies on LED current for different samples (10 Hz – 22 kHz).

correlated electrical and optical $1/f^{\alpha}$ noise. Cross-correlation factor for this sample is very high and at low current range it is close to 100% (Fig. 4.24). Due to shot noise dominance in optical noise spectrum at higher frequencies, cross-correlation factor for sample no. 1 is very low (10-20% in low current range).

4.2.2 Investigation of LED degradation during long term aging

High quality light emitting diodes are expected to have stable output characteristics during long term operation. To clarify the LED characteristics degradation during long term operation accelerated aging was applied. Aging experiments were performed at room temperature using 1 A forward current (maximum permissible current for these investigated LEDs). High power white light emitting diodes, that active region is grown from AlInGaN, have been investigated. Investigated samples are from the same batch as presented in the Chapter 4.1.1. All measurements have been carried out for initial samples and during their aging.

Noise characteristics of investigated light emitting diodes have been measured before their aging [P1, P4, O2, O7, C1, C6, C7, C9, C10]. The

observed optical and electrical fluctuations at low frequencies are the result of superposition of Lorentzian type fluctuations (Fig. 4.25). The $1/f^{\alpha}$ - type noise originates from various defects and imperfections in device structure due to charge carrier capture and emission processes in localized states with different capture cross-sections [52-57]. It was obtained that investigated LEDs distinguish by low level of $1/f^{\alpha}$ type noise for both electrical and optical fluctuations (Fig. 4.25), what shows on high quality of investigated LEDs.

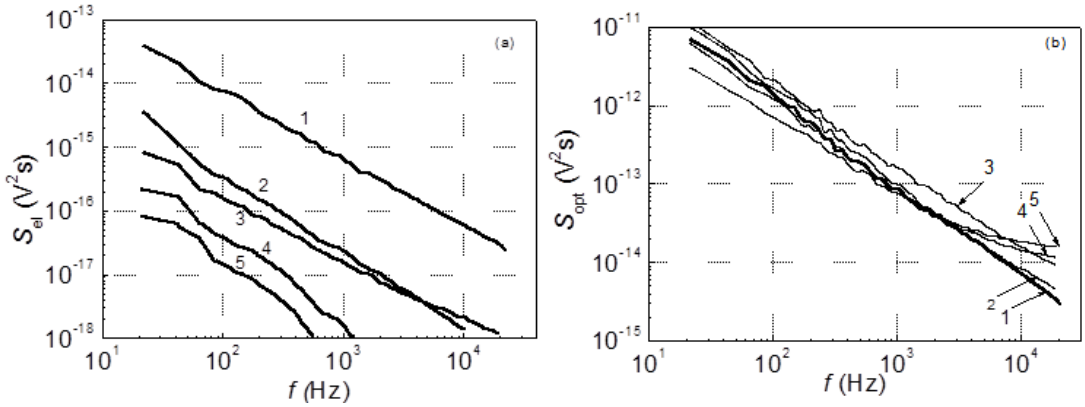

Fig. 4.25. Electrical (a) and optical (b) noise spectra at different forward currents: 1- 0.35 mA, 2- 8.0 mA, 3- 30.0 mA, 4- 90.0 mA, 5- 150.0 mA for not aged LED.

Electrical $1/f^{\alpha}$ noise intensity decreases with forward current increasing due to smaller role of individual defects at larger current density (graph (a) in Fig. 4.25, and graph (a) in Fig. 4.26), as explained in Chapter 4.1.

Optical noise is partly related with electrical fluctuations: charge carrier number in the active region changes lead to the photon number changes (i. e. output light power fluctuation). These processes lead to the positive cross-correlation factor between optical and electrical fluctuations (graph (c) in Fig. 4.26): presence of defects and imperfections in the LED structure not only changes electrical device characteristics, but also optical: increases non-radiative recombination, and therefore, decreases LED efficiency. So, there are some defects in the device structure that randomly modulate the emitted photon number.

Cross-correlation between optical and electrical fluctuations of investigated LEDs is determined by $1/f^{\alpha}$ type noise. Cross-correlation factor between optical and electrical fluctuations for initial samples (without aging) is positive and keeps value around 30 % (graph (c) in Fig. 4.26). That indicates

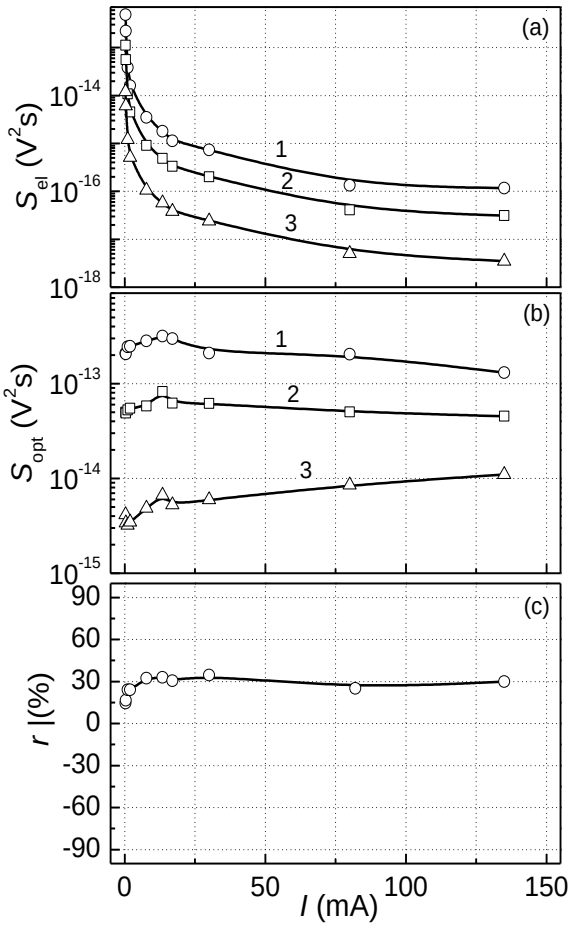

Fig. 4.26. Electrical (a) and optical (b) noise spectral density (1- 280 Hz frequency, 2- 970 Hz, 3- 10.3 kHz) and cross-correlation factor between optical and electrical fluctuations 10 Hz – 22 kHz (c) dependencies on forward current for not aged LED.

that optical and electrical processes in these devices are not completely related: there are physical processes in the active *p-n* region that cause both electrical and optical fluctuations, but there are some regions that cause only electrical (for example, a metal electrode interface at constant current) or light intensity fluctuations. Cross-correlation shows that there are some defects in the active region that change charge carrier number related to radiative and non-radiative

recombination. These charge carrier and photon number changes result to correlated $1/f^{\alpha}$ fluctuations of electrical and optical signals. LED characteristics presented in Fig. 4.25 and Fig. 4.26 are typical for initial samples – they were measured before any aging procedure.

To reveal physical processes that degrade investigated light emission diodes aging experiments have been performed and noise, optical and electrical characteristic changes during the aging have been studied.

Emitted light spectra of investigated LED (sample No. 3 in Table 3.1) before the aging and after 8000 h aging are shown in Fig. 4.27. Comparing these two graphs we can see a large difference: the intensity of the blue light peak in optical spectrum after long-time aging decreased more than twice while the intensity of wide-ranging yellow light peak decreased only about 30%. Considering that wide-ranging yellow light is caused due to phosphor layer luminescence induced by blue light transmission through the phosphor layer, such large blue light peak decrease in comparing with the yellow one is not related with LED's AlInGaN active layer, but it is caused by increased blue light absorption in phosphor layer.

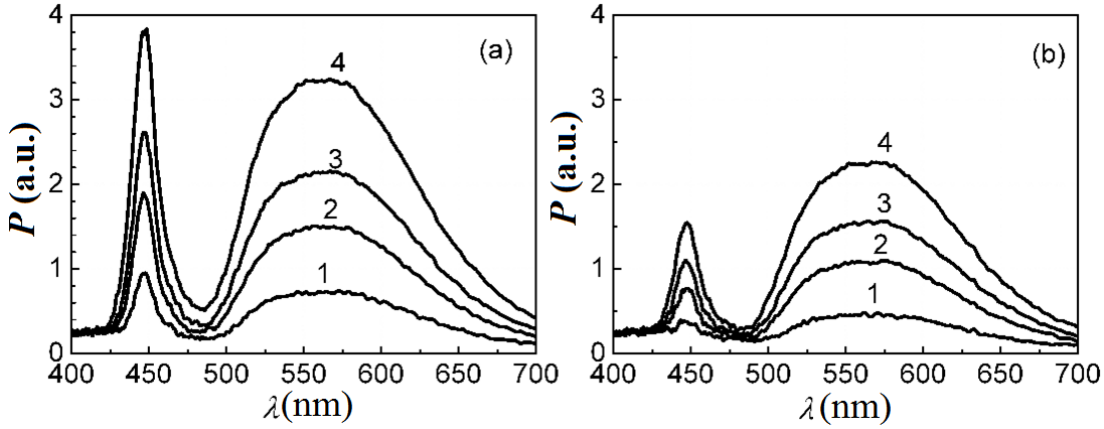

Fig. 4.27. Optical spectra of investigated device at different forward currents: 1- 20.9 mA, 2- 55.5 mA, 3- 86.4 mA, 4-141.3 mA, (a) – for initial sample (b) - after 8000 h aging; sample No. 5.

Optical output power very slowly decreases during all aging experiment, more rapidly after 2000 h of aging (graph (a) in Fig. 4.28). The emitted light

intensity after 8000 h aging decreased about 30%, which is in agreement with optical spectrum measurement results.

Noise characteristic (optical and electrical noise spectral density and cross-correlation factor) changes reflect degradation of LED operation characteristic (Fig. 4.28). In the initial phase of aging (up to 400 h) electrical noise intensity slightly decreases, while optical noise level decreases

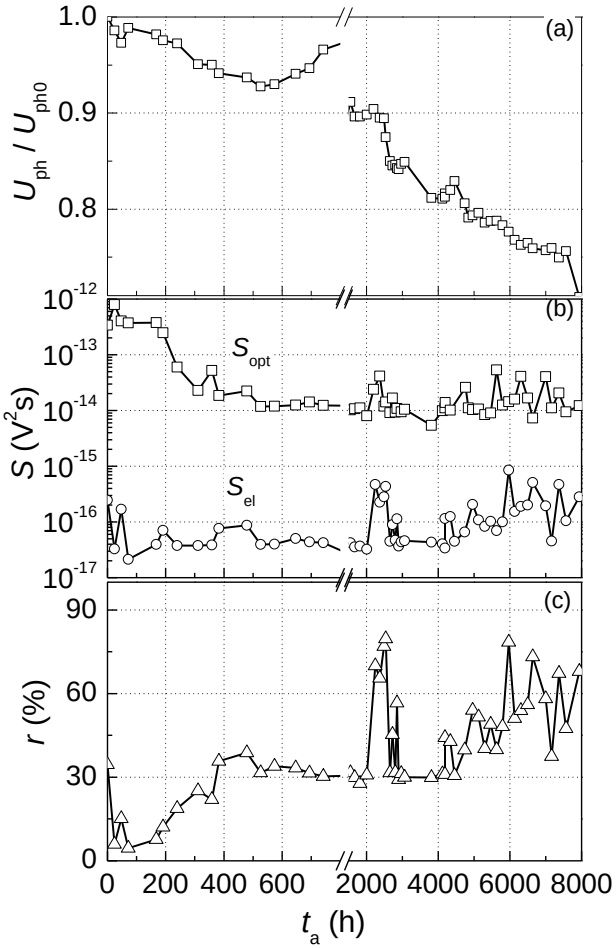

Fig. 4.28. Optical output power (proportional to the photodetector load resistor voltage) (a); electrical and optical noise spectral density (b) 280 Hz; and cross-correlation factor between optical and electrical fluctuations (c) 10 Hz – 22 kHz dependencies on aging time measured at 30 mA forward current.

about two orders. It shows that in initial stage of aging not stable defects and impurities in the active layer migrate to more stable position of ordered structure. Cross-correlation factor during the first 100 h decreases and then increases to

the value ~30 %. Thus, short-time aging by maximum permissible forward current does not degrade LED operation characteristics, conversely, improve them. During further 1500 h (to ~2000 h) of aging operation and noise characteristics of investigated LEDs do not change – stable LED operation is observed. During long-time aging process at particular time intervals (e. g. (2010-2500) h) steep increase of $1/f^{\alpha}$ type noise intensity was observed (graphs (b) and (c) in Fig. 4.28, Fig. 4.29). This noise peak appears both in optical and electrical fluctuations. These fluctuations are highly correlated: cross-correlation factor reaches value 80 % (graph (c) in Fig. 4.28). Such noise intensity peaks indicate microdefects formation or movement in the active layer or in adjacent layers. Large cross-correlation factor indicates that processes take place in the active region. After some aging time the noise intensity and cross-correlation factor returns to previous level (Fig. 4.28). This instable operation at this aging phase does not reflect in the LED output characteristics, because the formation of leakage microchannels by defects includes very small part of the total area of the active layer. During further ~2000 h aging of investigated LED demonstrate moderate stable noise behavior, when the optical output power starts to decrease more rapidly.

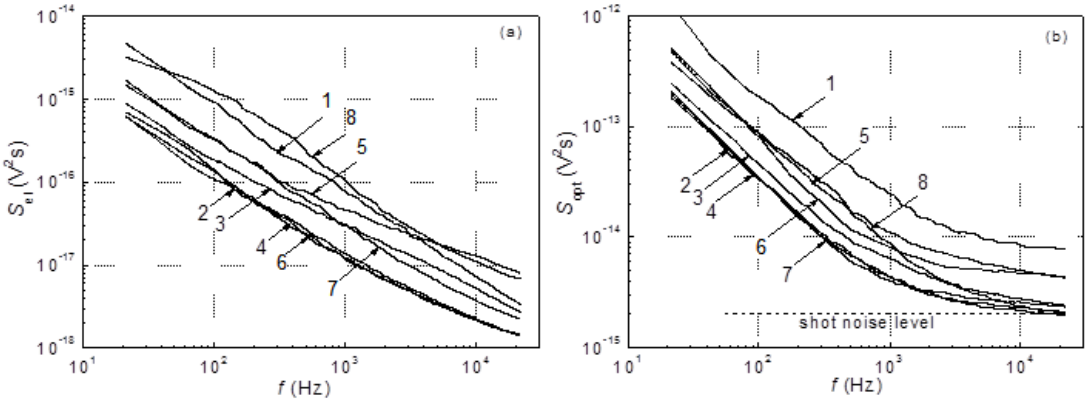

Fig. 4.29. Electrical (a) and optical (b) noise spectra after different aging time: 1– 2200 h, 2– 2500 h, 3– 2540 h, 4– 2660 h, 5– 2730 h, 6– 2800 h, 7– 4120 h, 8– 8000 h (30 mA forward current).

After 4000 h of aging till 8000 h the noise intensity and cross-correlation factor between optical and electrical fluctuations show instable behavior and

light intensity decreases more rapidly (Fig. 4.28). LED degradation is caused by formation of leakage microchannels due to generation of defects and migration of atoms at high aging current and at the elevated temperature of the active layer due to Joule heating. A rapid degradation starts, when some threshold defect density is reached in the structure. These defects form current leakage channels, increases density of non-radiative recombination and photon absorption centers. The most sensitive parameter to the LED degradation is cross-correlation factor between optical and electrical fluctuations: its value during aging changes in the range from 15 % to 80 % (graph (c) in Fig. 4.28).

Changes of spectrum type of electrical and optical fluctuation during aging are negligible (Fig. 4.29): electrical noise spectra consist of Lorentzian noise component superposition, while optical noise spectra at higher frequencies have additional shot noise component due to incident photon shot noise and it increases with current increase. The low frequency noise level depends on the LED structure defectiveness. That is also confirmed by

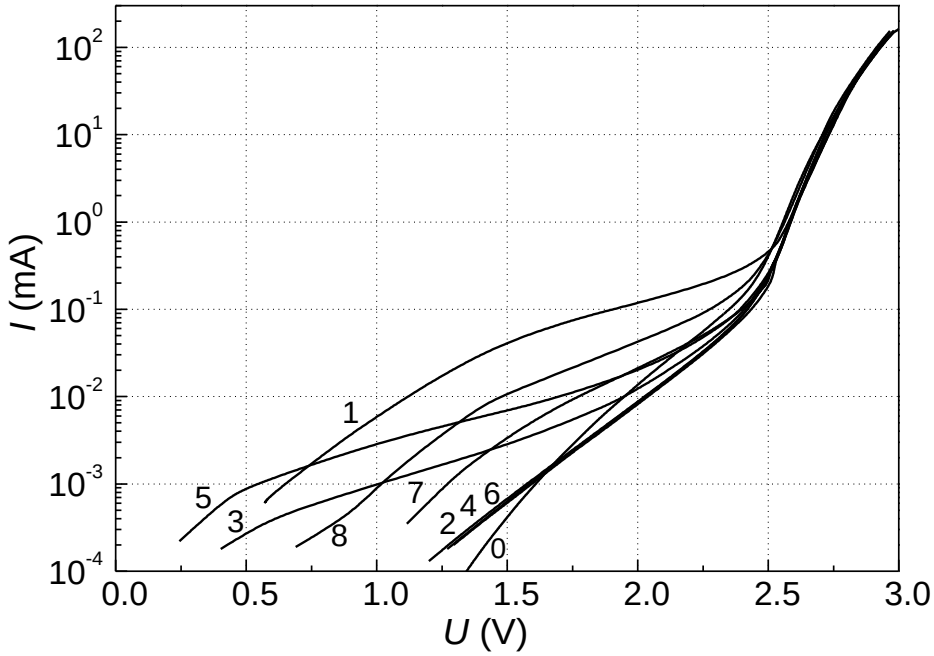

Fig. 4.30. Current-voltage characteristics of LED after different aging time: 0- before aging, 1– after 2200 h aging, 2– 2500 h, 3– 2540 h, 4– 2660 h, 5 – 2730 h, 6– 2800 h, 7– 4120 h, 8– 8000 h; sample no. 5.

measurements of current-voltage characteristics at low bias at different aging stages (compare Fig. 4.29 and Fig. 4.30).

After about over 2000 h aging we observed the large leakage current changes at different aging stages as ones of noise characteristics. So, there is a large correlation between the leakage current at low bias and noise characteristics in normal LED operation range. Such large changes of leakage current and noise characteristics show on kinetics of defects during aging at high currents. The cross-correlation factor between optical and electrical fluctuations increases, when device degrades. Cross-correlation factor was ascertained as parameter that is the most sensitive to the LED structure degradation.

The obtained results of aging of white high-power LEDs at maximum permissible current (1 A) have shown that at initial phase of aging during (400 – 600) h LED structure performs an ordering, and then during the next time interval about 1500 h the operation of LEDs is stable, and after (2000 – 4000) h of aging starts a more rapid degradation of LEDs characteristics. It was shown that during 8000 h aging the total light output power decreases about 30 %, while the primary blue light intensity decreases more than two times. The latter fact can be related only with decreased blue light transmission factor through the phosphor layer. These results show that investigation of electrical and optical noise characteristics of LED in normal forward current operation range and of current-voltage characteristics at low bias gives almost all information about device quality and reliability.

4.2.3 Phosphor layer influence on the white LED degradation

Noise characteristics of high power nitride-based white light-emitting diodes have been measured in frequency region from 10 Hz to 20 kHz for initial samples and after accelerated aging, using PD matrices described in chapter

4.1.3. Accelerated aging of investigated LEDs was performed at room temperature at maximum permissible forward current (350 mA) [P1, O7]. Current-voltage (IV), light output power vs. current (LI) and noise (optical and electrical fluctuations and cross-correlation factor between two noise signals) characteristics of investigated white LEDs have been carried out for initial samples and after 1344 h accelerated aging. The results are presented in Fig. 4.31 to Fig. 4.35.

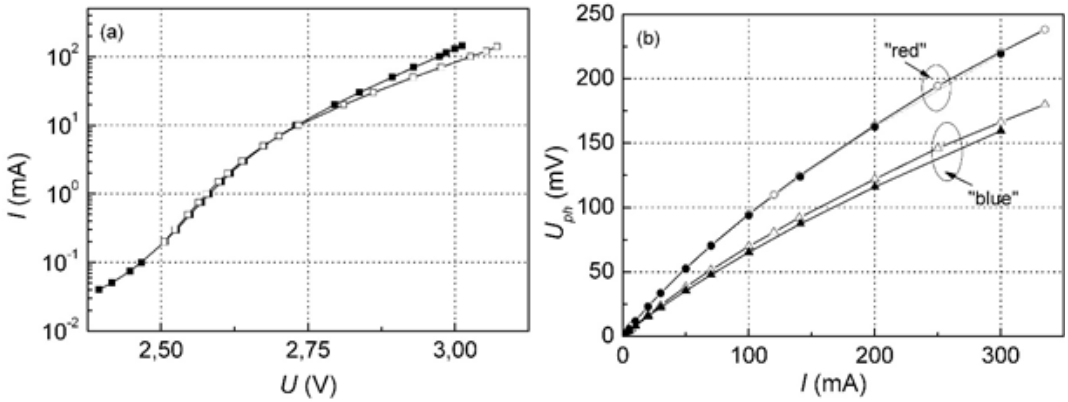

Fig. 4.31. Current-voltage (a) and output light power vs. current (b) characteristics of investigated LED (open symbols – results are for initial sample, solid symbols – results after 1344 h aging; "red" is for the light output power measurements by RSR photodetector, "blue" – for the measurements by BSR photodetector).

In Fig. 4.31, there are presented typical IV and LI characteristics of investigated devices. It is seen that changes of these operation characteristics during aging are small. After 1344 h aging the light intensity measured by RSR photodiode is neglible and the one measured by BSR photodiode decreased by a 5%. It is found that spectra type of optical and electrical noise of the investigated LEDs did not change during 1344 h aging (Fig. 4.32). But $1/f^{\alpha}$ - type noise intensity changed: the electrical noise intensity decreased about half

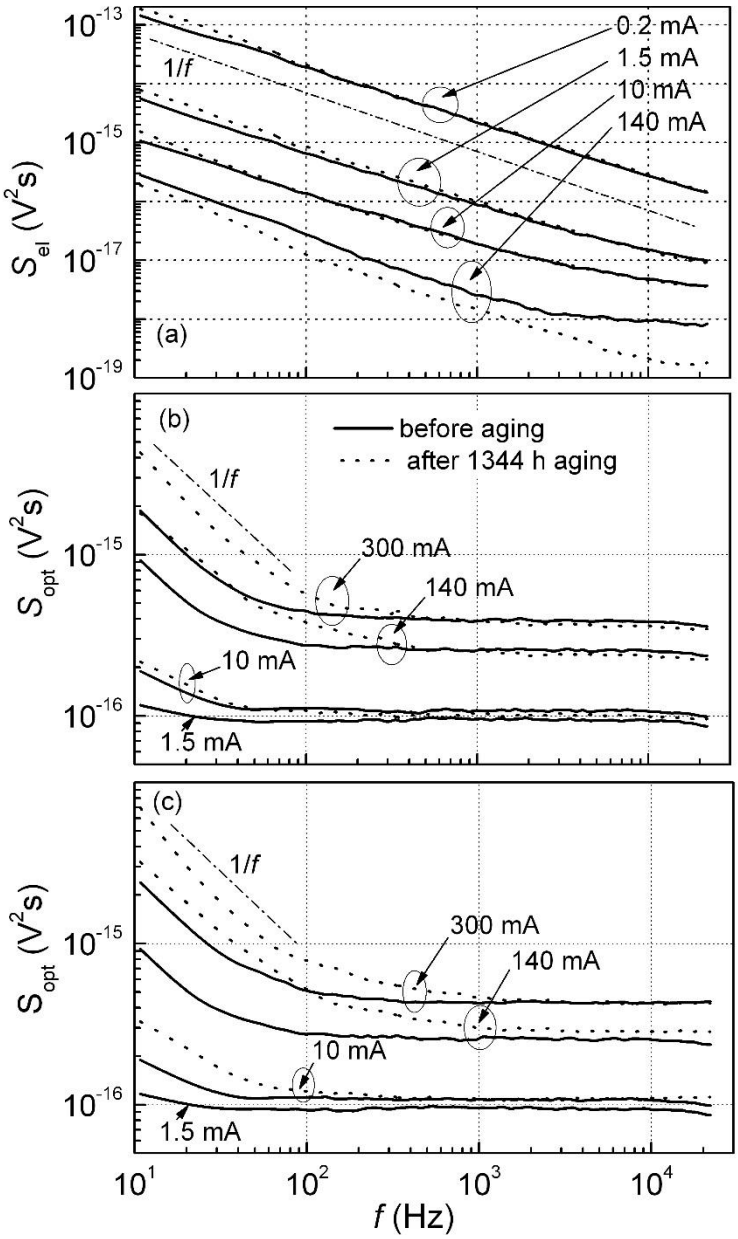

Fig. 4.32. Electrical (a) and optical ((b) - measurement by BSR photodetector, (c) - measurement by RSR photodetector) noise spectra at different forward current before aging (solid line) and after 1344 h aging (dotted line).

an order of magnitude at larger current (>100 mA) region over all investigated frequencies (graphs (a) in Fig. 4.32 and 4.33), $1/f^{\alpha}$ -type optical noise intensity after aging increased about 0.5 – 1 order of magnitude at larger current (>10 mA), while shot noise level did not change during aging (graphs (b) and (c) in Fig. 4.32 and 4.33). Decrease of electrical noise level indicate that some defects in peripheral areas of the LED (that influence current flow through the device)

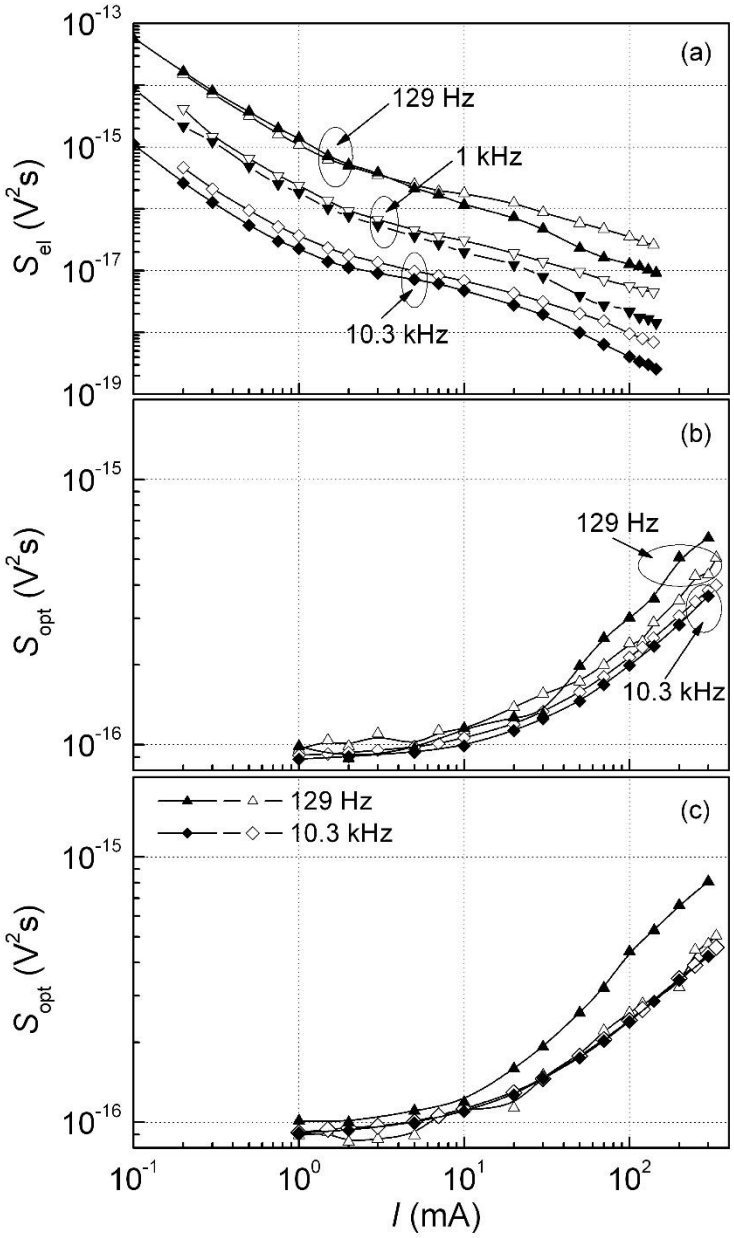

Fig. 4.33. Electrical (a) and optical ((b) - measurements by BSR photodetector, (c) - measurements by RSR photodetector) noise spectral density dependencies on current at different frequencies before aging (open symbols) and after 1344 h aging (solid symbols).

has disapeared during short time aging. However areas related with light emission (active region and phosphor layer) have degraded during aging: optical $1/f^{\alpha}$-type noise level has increased. Averaged over all investigated frequency range (10 Hz – 20 kHz) cross-correlation factor between electrical and optical fluctuations is small ((3-4) %; graph (a) in Fig. 4.34).

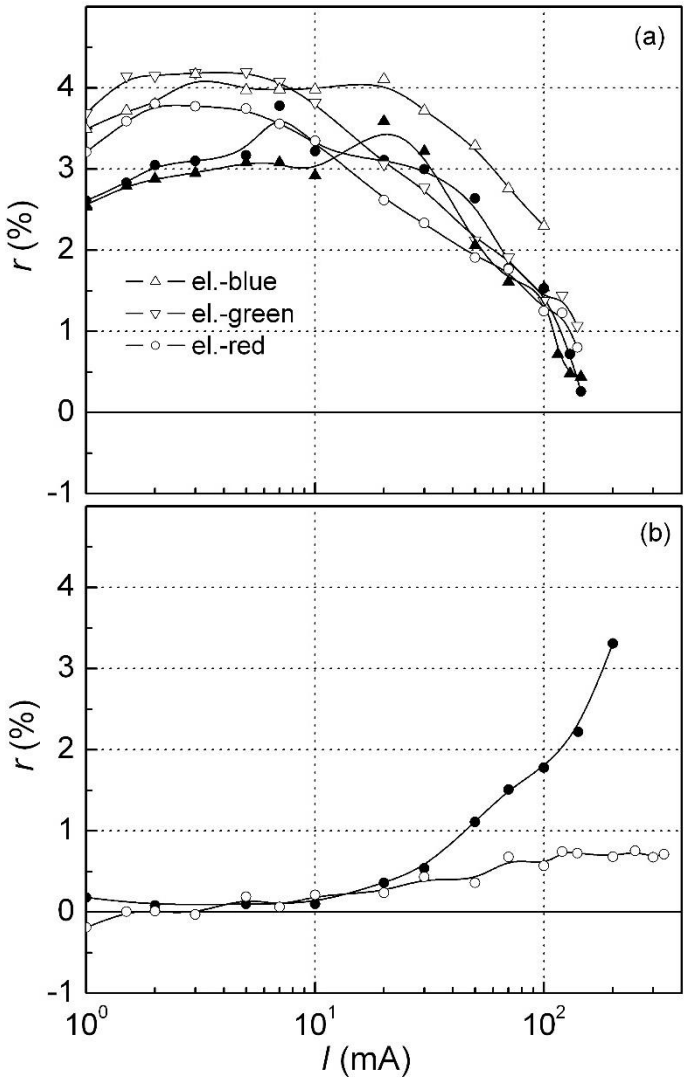

Fig. 4.34. Cross-correlation factor over 10 Hz – 20 kHz frequency range dependencies on current before aging (open symbols) and after 1344 h aging (solid symbols): (a) between electrical and optical signals measured by BSR (el.-blue), GSR (el.-green) or RSR (el.-red) photodetectors; (b) between two optical signals measured by BSR and RSR photodetectors.

After 1344 h accelerated aging cross-correlation between optical and electrical fluctuations decreased due to the decrease of the electrical noise intensity. Averaged cross-correlation factor between blue and red light intensities is low due to small $1/f^{\alpha}$ -type noise components: before aging its value is below 1 % (graph (b) in Fig. 4.34). After aging cross-correlation between two optical signals increases, what is caused by the increase of $1/f^{\alpha}$ -type optical

noise components during aging, and it increases with forward current increasing (graph (b) in Fig. 4.34).

Changes of cross-correlation between electrical and optical fluctuations after accelerated aging are negligible in investigated frequency bands (graphs (a) and (b) in Fig. 4.35). But increase of cross-correlation between fluctuations of blue and red light intensities is noticeable: after aging: in (10-20) Hz band it increased from 50 % to 80 % at 100 mA, in (80-160) Hz band increase also is obvious (graph (c) in Fig. 4.35). This increase of cross-correlation after aging is caused by the increase of $1/f^{\alpha}$ -type optical noise intensity. Partial ((30-50) %) cross-correlation between electrical and optical fluctuations at low frequencies ((10-20) Hz) shows that not all injected current flows through the active region of the LED: part of it flows through the peripheral areas and does not participate in the light emission. The fact that cross-correlation factor between electrical and optical fluctuations during accelerated aging (graphs (a) and (b) in Fig. 4.35) shows small changes despite of $1/f^{\alpha}$ -type optical noise increase can be explained by the decrease of the electrical flicker noise.

Similar values of cross-correlation factor between electrical and blue light intensity fluctuations and between electrical and red light intensity fluctuations, and also the high cross-correlation factor between blue and red light intensity fluctuations shows that phosphor layer does not have weighty impact to the $1/f^{\alpha}$ -type optical fluctuations observed in investigated LEDs – origin of this noise should be in the active region.

Noise characteristics of high power nitride-based white LEDs have been investigated during accelerated aging experiment. Electrical fluctuation of investigated LEDs has $1/f^{\alpha}$ -type spectrum, and during aging the electrical noise intensity decreased about half an order of magnitude at larger currents (>100 mA). It is shown that at low frequencies optical fluctuations are partly correlated with electrical noise. Origin of the $1/f^{\alpha}$ -type noise in investigated

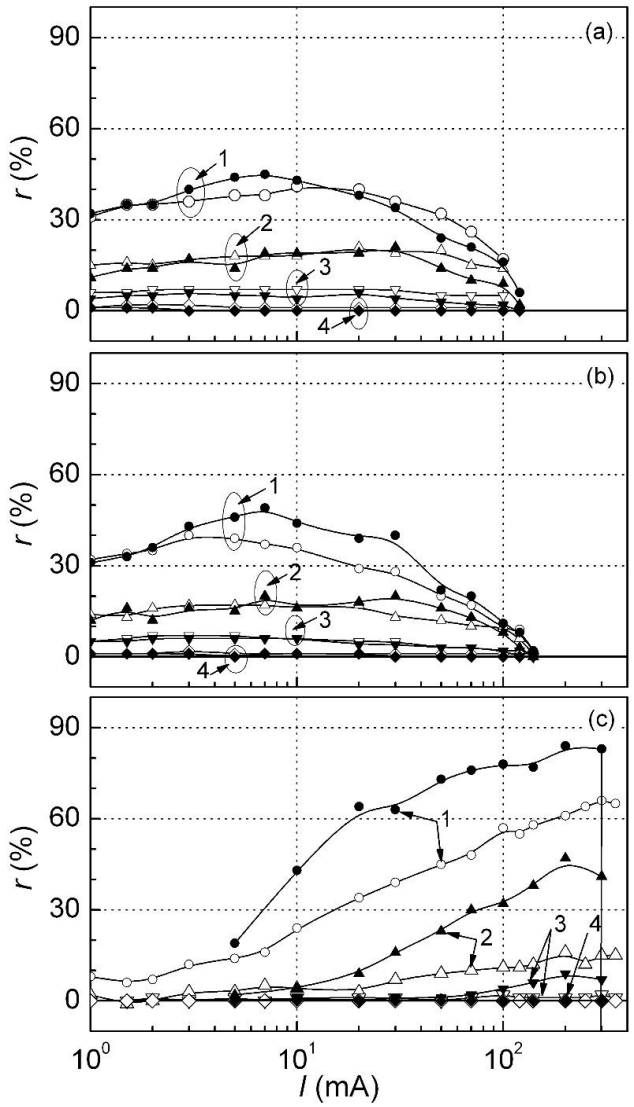

Fig. 4.35. Cross-correlation factor in one-octave frequency bands (1 – [10 – 20] Hz, 2 – [80 – 160] Hz, 3 – [0.64 – 1.28] kHz, 4 – [10.24 – 20.48] kHz) dependencies on current before aging (open symbols) and after 1344 h aging (solid symbols): (a) between electrical and optical signal measured by BSR photodetector, (b) - between electrical and optical signal measured by RSR photodetector; (c) between two optical signals measured by BSR and RSR photodetectors.

devices is generation and recombination and carrier capture processes in defects formed centers.

Analysis of cross-correlation between electrical and optical and between blue and red light intensity fluctuations shows that during aging degradation foremost occurs in light emitting area of the LED. This can be caused by the

high intensity light emitted during accelerated aging at maximum permissible forward current that leads to the considerable device heating and defects migration and formation. It also was found that during aging some ordering of peripheral areas occur that causes the decrease of low-frequency electrical noise level.

4.2.4 InGaN-based LEDs degradation processe comparison with AlInGaP-based one

High power (1 W) blue LEDs radiating at 470 nm based on InGaN and red LED radiating at 625 nm fabricated from AlInGaP have been investigated [O4, P4, C10]. Optical, electrical and noise characteristics have been carried out at room temperature for initial samples and during their aging. Aging was performed at maximum permissible forward current (350 mA) at room temperature.

Fluctuations of investigated initial LEDs both for nitride-based and phosphide-based at low frequencies are mainly characterized by $1/f^{\alpha}$ -type electrical and optical noises (Fig. 4.36 and Fig. 4.37).

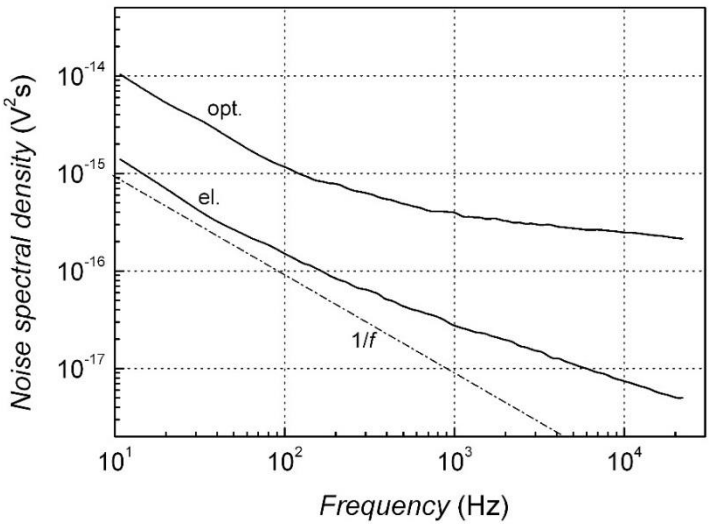

Fig. 4.36. Electrical (el.) and optical (opt.) noise spectra of blue LEDs before aging at 10 mA forward current.

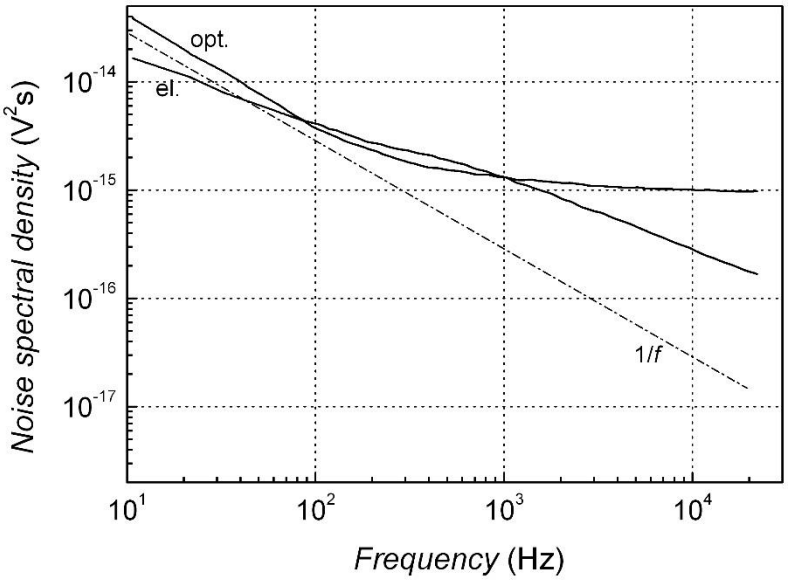

Fig. 4.37. Electrical (el.) and optical (opt.) noise spectra of red LEDs before aging at 10 mA forward current.

Current-voltage (IV) and light output power vs. current (LI) characteristics of investigated nitride-based blue LEDs are presented in Fig. 4.38 and Fig. 4.39, respectively. IV characteristic of not aged device is typical for LEDs (Fig. 4.38): the non-ideality factor *n* of the IV characteristic is about 2.4 in the current range from 0.1 mA to 10 mA. Such IV characteristic indicates that current flow through the device is mainly caused by the

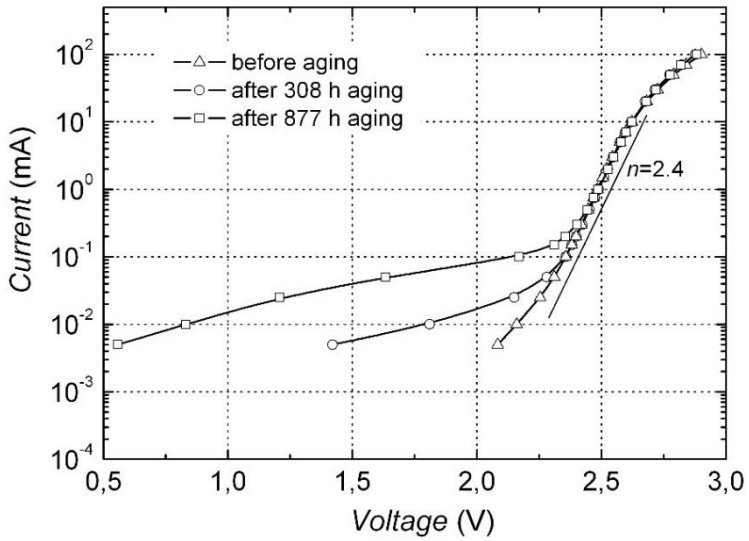

Fig. 4.38. Typical current-voltage characteristics of blue LED before, after 308 h and 877 h aging.

generation and recombination processes and at low current region (below 0.1 mA) its flow is not even through the whole device cross-section – influence of defects formed current flow channels shows up. Current deviation from exponential law at currents above 10 mA is due to series resistance of LED. During aging IV characteristic of investigated LEDs strongly changes (Fig. 4.38): at low current region (below 0.1 mA) influence of separate narrow defect formed current flow channels heavily increases. Existence of such defects also leads to the large leakage current out of the LED active region: at currents, where light radiation operation takes place ((0.1-1) mA), light output power decreases ~50 % after aging (Fig. 4.39). These leakage currents do not have influence to the LED operation at larger current region: in the current

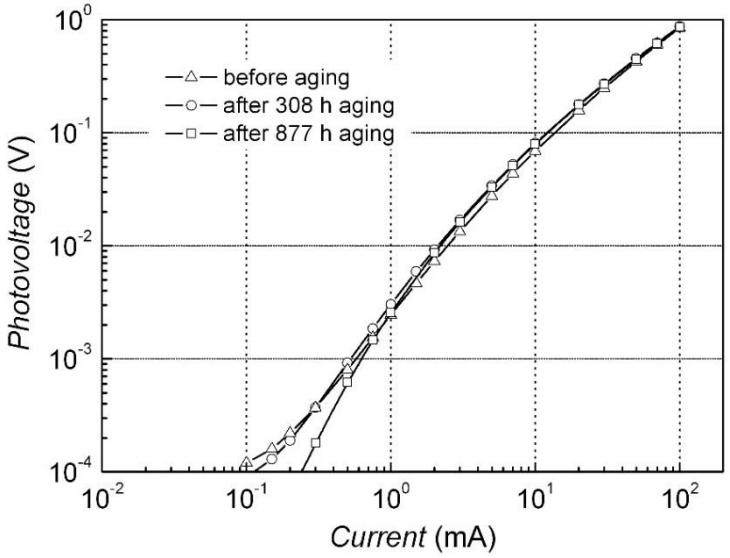

Fig. 4.39. Typical light output power vs. current characteristics of blue LED before, after 308 h and 877 h aging.

range from 1 mA to 10 mA light output power increases about 24% after short time aging and stays stable during further aging; at currents above 10 mA there is no marked change of output power observed.

$1/f^{\alpha}$-type electrical and optical noise (that dominates at frequencies lower than 1 kHz) intensity of the investigated blue LEDs increases gradually with aging time increasing at all investigated current region (Fig. 4.40 and Fig. 4.41): electrical noise spectral density after 877 h aging is 2-3 orders of magnitude

larger comparing to the results before aging, optical noise spectral density increases 1-2 orders of magnitude during the same aging. As stated above, $1/f^{\alpha}$ -type noise is caused by the generation and recombination through defects formed GR centers. Therefore, increase of $1/f^{\alpha}$ -type noise intensity indicates that number of defects increases in the device. Shot noise (caused by random photons emission) in optical fluctuations stayed stable during the aging experiment (curves at 15.1 kHz in graph (b) in Fig. 4.40).

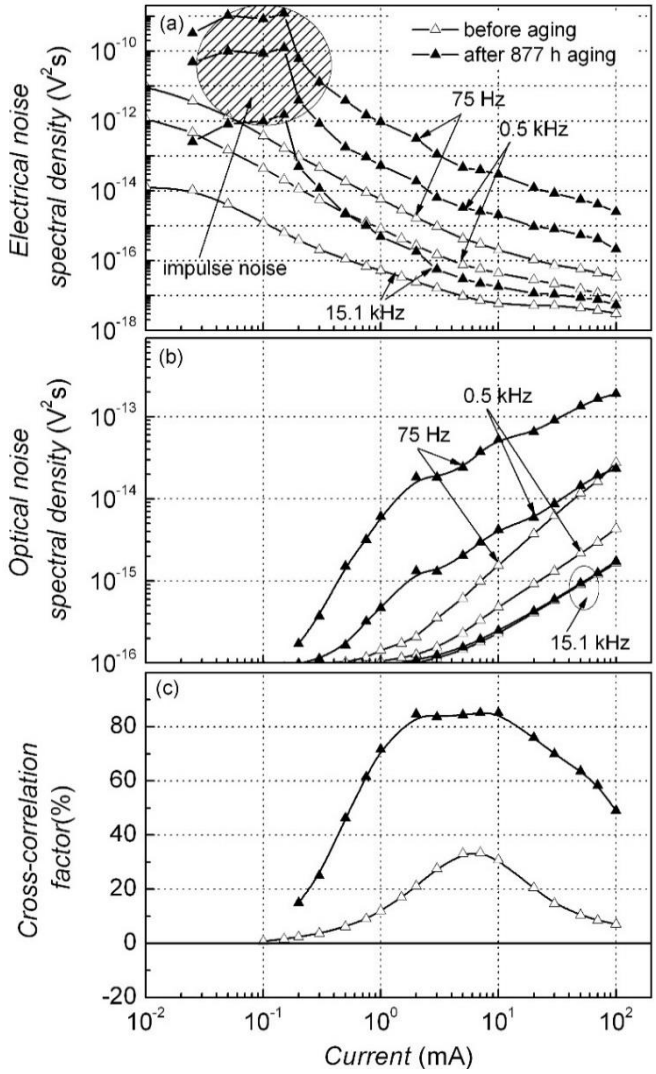

Fig. 4.40. Blue LED electrical (a) and optical (b) noise spectral densities at different frequencies and cross-correlation factor (c) (frequency range from 10 Hz to 20 kHz) dependencies on current before (open symbols) and after 877 h (solid symbols) aging.

Observed cross-correlation factor between optical and electrical fluctuations is positive, its value increases with $1/f^{\alpha}$-type optical noise intensity increase (graph (c) in Fig. 4.40). Cross-correlation factor dependency on frequency (insets in Fig. 4.41) also show that strongly correlated are noise components at low frequencies (where $1/f^{\alpha}$-type noise dominates (Fig. 4.41)). And at higher frequencies, where optical shot noise prevails $1/f^{\alpha}$ fluctuations, cross-correlation factor is low (Fig. 4.41).

Noise characteristic changes during aging show that investigated blue LED degradation is caused by defect number increase in the structure. As there is positive cross-correlation between optical and electrical fluctuations (that strongly increases during aging (graph (c) in Fig. 4.40)), these defects modulate current flow through the active region, therefore, modulate emitted photon number (i. e. output light power). Additionally, after 877 h aging impulse type electrical noise appeared at low current ((0.03-0.2) mA) region in particular sample operation (lined area in graph (a) in Fig. 4.40). This noise manifests as series of short impulses. We suppose that investigated LED degradation during accelerated aging leads to the macrodefects appearance. At low forward current major part of the current flows through the channel formed by the defect, and the system operation is governed by the current modulation determined by the defect. As forward current increases current starts to flow through the whole cross-section of the device and influence of the single defect becomes void. Appearance of such defects is also a reason of lower light output power after aging in current region from 0.1 mA to 1 mA (Fig. 4.39) as it causes leakage current out of the active region. At such low currents ((0.03-0.2) mA) investigated LEDs do not light and optical noise level is below measurement system own noise level (that is 10^{-16} V^2s). Therefore electrical noise measurement results have shown that noise characteristics due to their sensitivity can give additional valuable information on processes in LEDs, when optical characteristics do not show anything.

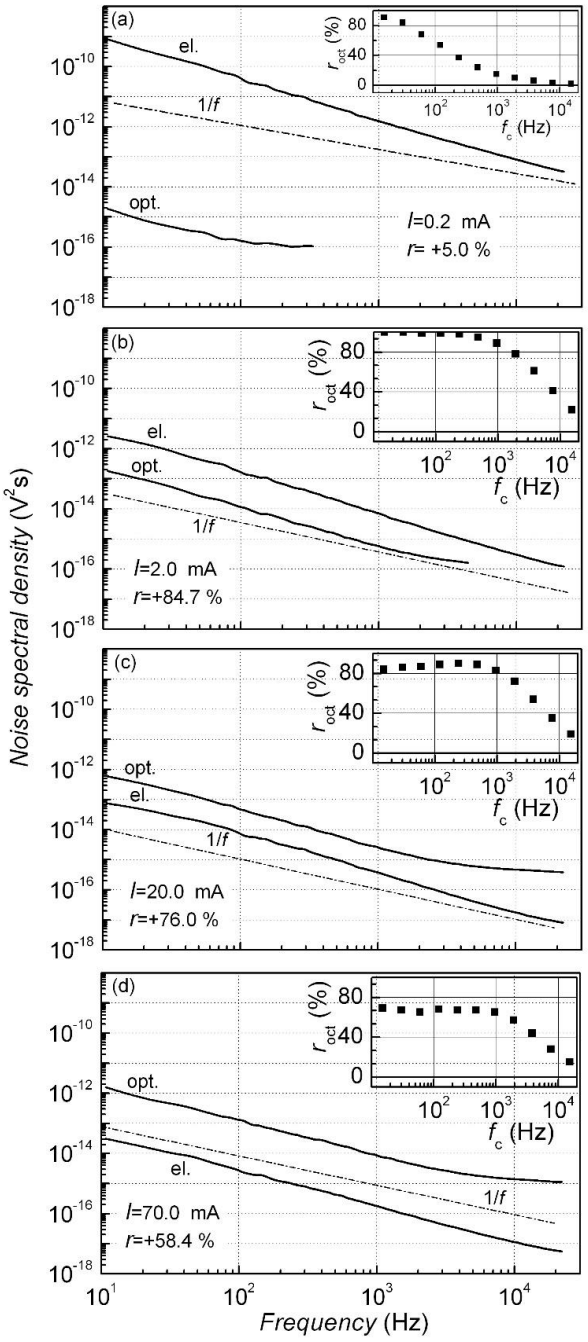

Fig. 4.41. Blue LED Optical (opt.) and electrical (el.) noise spectra at different currents (I) after 877 h aging (r is averaged cross-correlation factor in frequency range from 10 Hz to 20 kHz), and cross-correlation factor between optical and electrical fluctuations in one-octave frequency band r_{oct} dependency on central frequency f_c of octave filter (in insets).

Current-voltage (IV) and light output power vs. current (LI) characteristics before and after aging of AlInGaP red LEDs are presented in Fig. 4.42 and Fig. 4.43, respectively. The non-ideality factor n of the IV

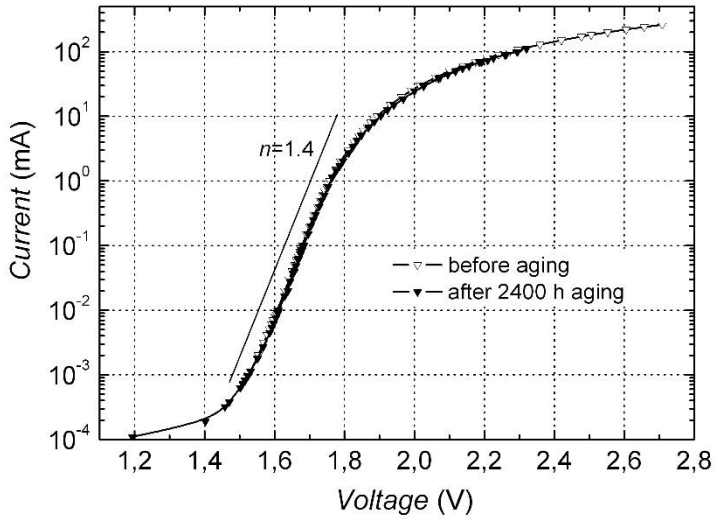

Fig. 4.42. Typical current-voltage characteristics of red LED before and after 2400 h aging.

characteristic is about 1.4, what shows on large contribution to the current of diffusion component in these samples. At currents lower than 0.3 μA IV characteristic is determined by current flow through the channels formed by defects, but not through the whole device cross-section. There are no changes of investigated LED IV characteristics during aging (Fig. 4.42). Also, at operation currents larger than 1 mA the LI characteristic has no changes during

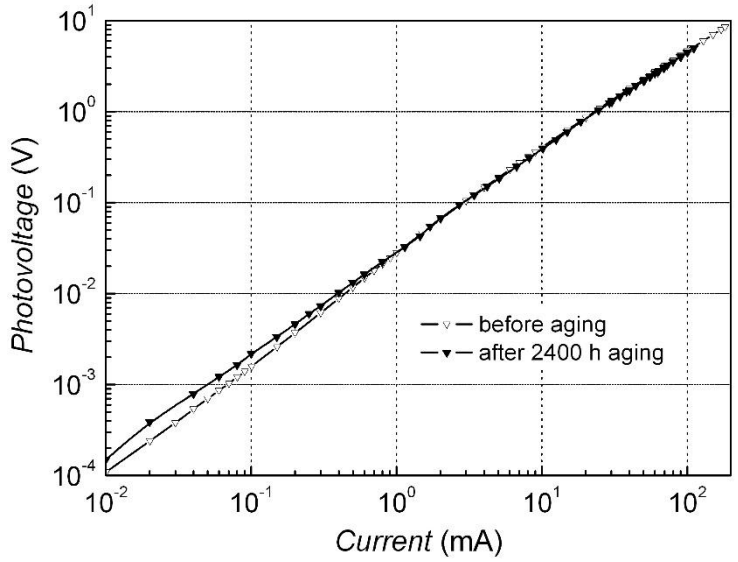

Fig. 4.43. Typical light output power vs. current characteristics of red LED before and after 2400 h aging.

aging (Fig. 4.43). At smaller currents (< 0.1 mA) the light output power of investigated LEDs increases about 40 % after 2400 h of aging.

Investigated red LEDs before aging demonstrate quite intensive electrical noise at current region from 1 mA to 100 mA (graph (a) in Fig. 4.44) that is slightly negatively (cross-correlation value is les 10 %) correlated with optical fluctuations (graph (c) in Fig. 4.44). Thus, it weakly influences the light-emitting process in the device active region: major part of the injected carriers recombines non-radiatively outside the active region; there are defects in lateral layers of LED structure, not in the active region, that mainly cause the electrical noise characteristics.

Noise characteristics of investigated LEDs have shown small changes during almost 2000 h of aging: electrical noise intensity during this time of aging only at small currents (< 0.2 mA) slightly decreased, the low-frequency (at 75 Hz) optical noise level for investigated LEDs after 2000 h aging at medium operation currents from 3 mA to 20 mA decreases about 1.5-2 times. However after approximately 2400 h aging by 350 mA current some of investigated red LEDs began to demonstrate unstable operation. Optical and electrical noise intensity started to increase rapidly with forward current at current larger 20 mA (Fig. 4.44). Also positive cross-correlation factor between optical and electrical fluctuations appeared (graph (c) in Fig. 4.44). Large electrical and optical noise intensity increase is related only with $1/f^{\alpha}$-type noise part (Fig. 4.45). In current range from 25 mA to 100 mA the noise level is very unstable (Fig. 4.44, lined region): there were no repeatable noise measurement results by increasing and decreasing the current. Though after 2400 h aging the average light output power in this current range was approximately the same as before aging (Fig. 4.43).

Optical and electrical noise spectra after 2400 h aging at small currents (< 20 mA) are similar to that before aging (graph (a) in Fig. 4.45): electrical noise spectrum is $1/f^{\alpha}$ -type, optical noise spectra contain $1/f^{\alpha}$ -type (where α is close to 1) and shot noise components, and cross-correlation factor over

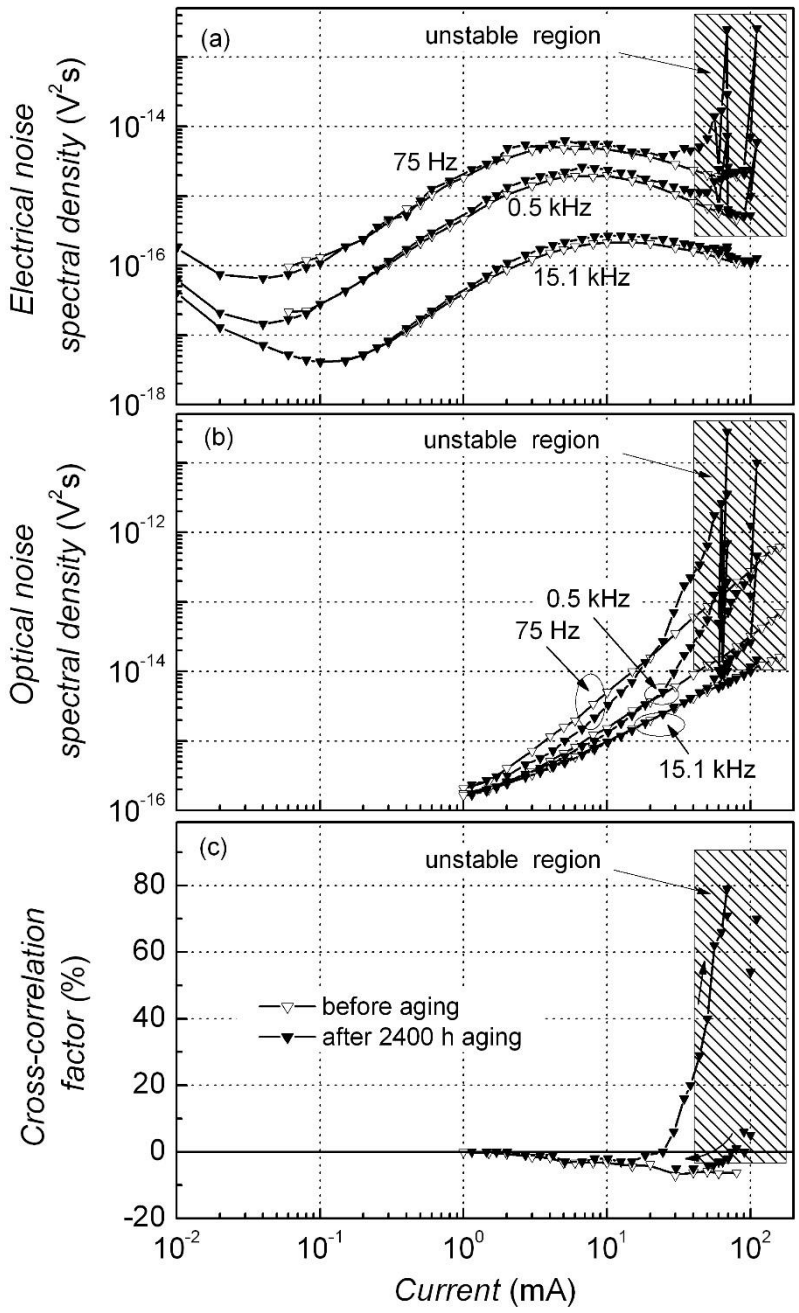

Fig. 4.44. Red LED electrical (a) and optical (b) noise spectral density at three different frequencies (75 Hz, 0.5 kHz, and 15.1 kHz) and cross-correlation factor (c) (frequency range from 10 Hz to 20 kHz) dependencies on current before and after 2400 h aging.

measured frequency band and in every one-octave frequency band is small. At larger currents level of electrical and optical fluctuations, and positive cross-correlation factor at low frequencies (<1 kHz) extremely increase (graphs (b) and (c) in Fig. 4.45), but these intensive electrical and optical noises with $1/f^{\alpha}$

-type spectra (where α is close to 2) are unstable: they are different when current is increased or decreased. As shown in inset of Fig. 4.45 (graph (c)) these electrical and optical fluctuations with $1/f^{2}$ -type spectrum are strongly correlated. Such not repeating LED operation indicates that during long-time aging in device structure there appear unstable defects. Large cross-correlation between optical and electrical noises shows that these defects are present in the

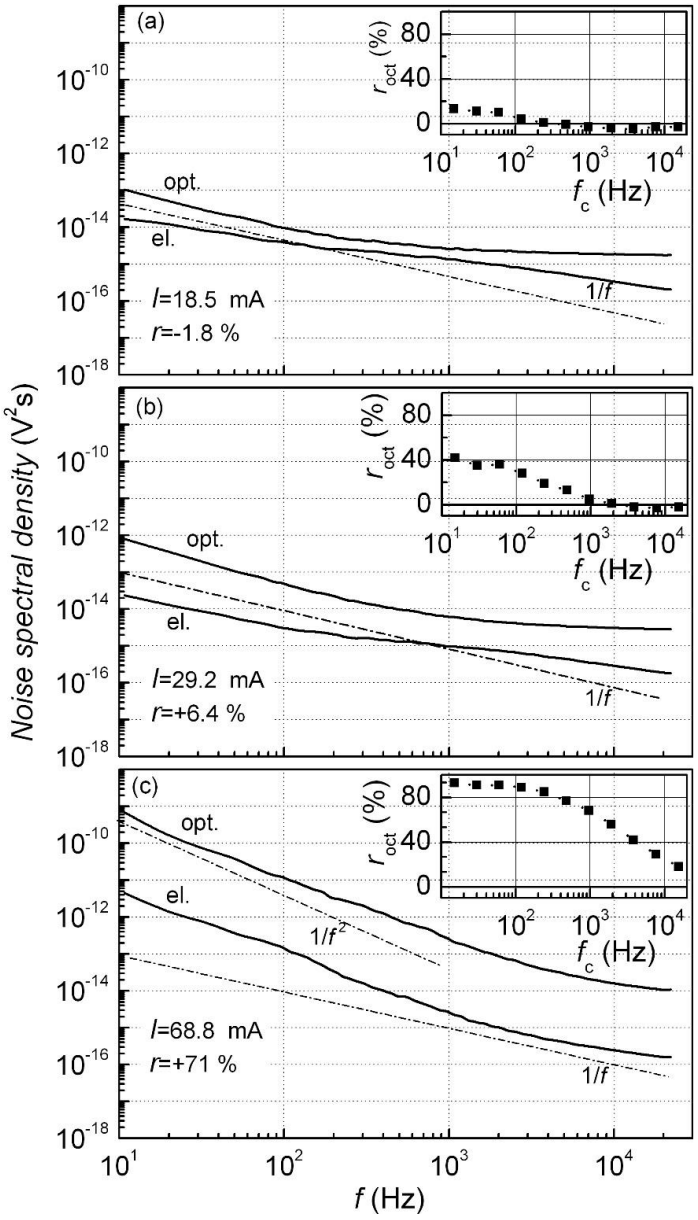

Fig. 4.45. RED LED Optical (opt.) and electrical (el.) noise spectra at different currents (I) after 2400 h aging, and cross-correlation factor between optical and electrical fluctuations in one-octave frequency band r_{oct} dependency on central frequency f_c of octave filter (in insets).

LED active region or on its interface. Observed optical and electrical noise spectra type is characteristic for generation–recombination processes in recombination centers with large relaxation time. These defects act as non-radiative recombination centers that modulate charge carrier number in the active region and, therefore, emitted photon number. So, some of investigated red LEDs after 2400 h aging at maximum permissible forward current (350 mA) at room temperature became unstable due to unstable defects appearing in the active region or its interface, that act as recombination centers and increases non-radiative recombination.

A comprehensive investigation of phosphide-based red and nitride-based blue LEDs characteristic changes during aging has been carried out. Large $1/f^{\alpha}$ electrical noise level indicates that in the LED structure there are or appears during aging many defects and imperfections, what leads to the more rapid degradation. But cross-correlation factor between optical and electrical fluctuations analyses has shown that large level of electrical fluctuations is not necessarily related with defectiveness of the LED active region, it could be related with the charge carrier recombination and capture processes in defects outside the active region, and weakly influences the emitted light. Nevertheless, these defects can lead to the large leakage current out of the active region and, therefore, lower light output power.

Investigated LEDs degradation is caused by the unstable defects appearance in the active region or on its interface. Presence of such defects reflects in the noise characteristics as additional high intensity impulse electrical noise or intensive strongly correlated optical and electrical fluctuations with $1/f^{\alpha}$ -type spectrum that is characteristic for generation and recombination processes. These defects cause large leakage current, act as non-radiative recombination centers and modulate charge carrier number in the active region, also, emitted photon number. This LED degradation mechanism is common for both phosphide-based and nitride-based investigated diodes, notwithstanding presence of the defects manifests at different LED operation conditions.

Investigation results have shown that noise characteristic measurement is more sensitive indicator to the LEDs degradation: noticeable changes in noise characteristics can be observed earlier and manifest stronger than they appear in static (light output power vs. current) LEDs characteristics. Thus, investigation of electrical and optical noises and their cross-correlation for LEDs reveals the physical processes that take place in device structure and material, and gives valuable information for improving device design and technological process, allows device lifetime prediction.

4.2.5 Summary

There was investigated white light emitting diode degradation during long term accelerated aging. It was noticed, that after short term aging, characteristics of investigated LED has improved, as nonstable defects in the active layer has moved into more stable positions. While aging further, there was observed stable LED operation for a while. After ~4000 hours of accelerated ageing LED characteristics start to degrade more rapidly and noise level increases. After 8000 hours of aging output power has decreased by about 30% of its original value before aging. Blue component of optical spectrum after aging has decreased by two times due to increased absorption of blue light in phosphor layer.

To clarify the phosphor layer degradation after accelerated aging the white light emitting LED noise characteristics were investigating using photodiode matrice with different sensitivities corresponding blue light spectrum from active layer and broadband yellow light spectrum from phosphor layer. Comparing noise characteristics of sample before and after aging, there was found that electrical noise has decreased after aging, while optical has increased. Decrease of electrical noise was caused by disappearance of some defects in the active or peripherial layer. Optical noise increase shows, that either active or phosphor layer has degraded. Slightly changed cross-correlation between electrical and optical fluctuations, and significantly increased one between

optical blue and optical red fluctuations proves, that after aging active layer has degraded.

Degradation during accelerated aging was investigated of light emitting diodes composed of different materials. There was shown that some samples of different materials have higher noise levels after aging, but in general the degradation of nitride based and phosphide based LEDs after accelerated aging are similar.

4.3 Detailed analysis of noise characteristics of LEDs

Electrical and optical noise measurements were done by converting analog voltage fluctuations over the time into digital signal and performing further data processing e.g. spectrum and cros corelation calculations. As measurements were done on time base, cross-correlation factor calculations used total electrical and optical fluctuations including own system noise, including correlated and uncorrelated LED noise components, system own noise. Electrical and optical noise with different type spectrum do not correlate. Such cross-correlation factor measurements provides collective view of relationship between electrical and optical noise sources. Also total measured cross-correlation factor value is smaller than the actual one of electrical and optical $1/f$ noise. There is explained how to reevaluate cross-correlaton factor of $1/f$ noise by calculating dispersions of different spectrum type components using measured noise spectra. Such spectrum and cross-corelation factor decomposition allows to clarify which noise sources has the largest influence, and predict where it comes from [P4, P6].

4.3.1 Evaluation of cross-correlation factor

Power spectral densities of electrical and optical fluctuations of light-emitting diodes (LEDs) at low frequencies can be presented as a sum of independent spectral components of $1/f$, $1/f^{\alpha}$, Lorentzian type (for the most intensive components of recombination processes with recombination time τ) and shot noise:

$$S_{\text{el sum}}(f) = \frac{A_{\text{el}1/f}}{f} + \frac{A_{\text{el}1/f^{\alpha}}}{f^{\alpha}} + \frac{A_{\text{el}\,gr}\tau}{1+(2\pi f\tau)^2} + S_{\text{el shot}}; \qquad (4.3.1)$$

$$S_{\text{ph sum}}(f) = \frac{A_{\text{ph}1/f}}{f} + \frac{A_{\text{ph}1/f^{\alpha}}}{f^{\alpha}} + \frac{A_{\text{ph}\,gr}\tau}{1+(2\pi f\tau)^2} + S_{\text{ph shot}}; \qquad (4.3.2)$$

here the quantities A_j define the intensities of noise components. A number of spectral components depend on complexity of spectrum. Such presentation is very useful for further analysis of noise properties because it means that noise sources with $1/f$, $1/f^{\alpha}$ and Lorentzian type spectra are statistically independent. So, according to the obtained spectrum measurement results decomposition into spectral components of the total electrical and optical noise sources can be expressed respectively in the following way:

$$u_{\text{el total}}(t) = u_{\text{el}1/f}(t) + u_{\text{el}1/f^{\alpha}}(t) + u_{\text{el gr}}(t) + u_{\text{el sh}}(t) + u_{\text{el syst}}(t); \qquad (4.3.3)$$

$$u_{\text{ph total}}(t) = u_{\text{ph}1/f}(t) + u_{\text{ph}1/f^{\alpha}}(t) + u_{\text{ph gr}}(t) + u_{\text{ph sh}}(t) + u_{\text{ph syst}}(t); \qquad (4.3.4)$$

where $u_{\text{el}1/f}(t)$ and $u_{\text{ph}1/f}(t)$ are respectively the electrical and optical fluctuation components with $1/f$ type spectrum; $u_{\text{el}1/f^{\alpha}}(t)$ and $u_{\text{ph}1/f^{\alpha}}(t)$ are respectively the electrical and optical fluctuation components with $1/f^{\alpha}$ type spectrum; $u_{\text{el gr}}(t)$ and $u_{\text{ph gr}}(t)$ are respectively the electrical and optical fluctuation components with Lorentzian type spectrum; $u_{\text{el sh}}(t)$ and $u_{\text{ph sh}}(t)$ are respectively the electrical and optical fluctuation components with shot noise spectrum; $u_{\text{el syst}}(t)$ and $u_{\text{ph syst}}(t)$ are respectively the own noise components of electrical and optical noise of measurement systems. According to expressions (4.3.3) and (4.3.4) the electrical and optical fluctuation variances can be defined as:

$$\sigma^2_{\text{el total}} = \sigma^2_{\text{el}1/f} + \sigma^2_{\text{el}1/f^{\alpha}} + \sigma^2_{\text{el gr}} + \sigma^2_{\text{el sh}} + \sigma^2_{\text{el syst}}; \qquad (4.3.5)$$

$$\sigma^2_{\text{ph total}} = \sigma^2_{\text{ph}1/f} + \sigma^2_{\text{ph}1/f^{\alpha}} + \sigma^2_{\text{ph gr}} + \sigma^2_{\text{ph sh}} + \sigma^2_{\text{ph syst}}; \qquad (4.3.6)$$

where every variance component in frequency range from f_1 to f_2 can be determined from the noise spectral components:

$$\sigma_j^2 = \int_{f_1}^{f_2} S_j(f)\mathrm{d}f; \qquad (4.3.7)$$

For the further estimation of cross-correlation coefficient in the one-octave frequency band ($f_2 = 2f_1$) it is useful to estimate the variances of electrical and optical noise components with various spectra in this frequency band [P5]:

$$\sigma_{1/f\,\mathrm{oct}}^2(f_c) = \int_{f_1}^{f_2} \frac{A_{1/f}}{f}\mathrm{d}f = A_{1/f}\ln(f_2/f_1) = A_{1/f}\ln 2; \qquad (4.3.8)$$

$$\sigma_{1/f^\alpha\,\mathrm{oct}}^2(f_c) = \int_{f_1}^{f_2} \frac{A_{1/f^\alpha}}{f^\alpha}\mathrm{d}f = (3/4)^{\alpha-1}\cdot\frac{2^{\alpha-1}-1}{\alpha-1}\cdot\frac{A_{1/f^\alpha}}{f_c^{\alpha\text{-}1}}; \qquad (4.3.9)$$

here $\alpha \neq 1$;

$$\sigma_{\mathrm{groct}}^2(f_c) = \int_{f_1}^{f_2} \frac{A_{\mathrm{gr}}\tau}{1+(2\pi f\tau)^2}\mathrm{d}f = \frac{A_{\mathrm{gr}}}{2\pi}[\arctan(8\pi\tau f_c/3) - \arctan(4\pi\tau f_c/3)]; \qquad (4.3.10)$$

$$\sigma_{\mathrm{shotoct}}^2(f_c) = \int_{f_1}^{f_2} S_{\mathrm{shot}}\mathrm{d}f = \frac{2}{3}S_{\mathrm{shot}}f_c; \qquad (4.3.11)$$

here f_c is the central frequency of the one-octave frequency band filter.

During experiment the cross-correlation coefficient was measured using the following expression:

$$r = <u_{\mathrm{el\,total}}(t)\cdot u_{\mathrm{ph\,total}}(t)> / (\sigma_{\mathrm{el\,total}}^2\cdot\sigma_{\mathrm{ph\,total}}^2)^{1/2}; \qquad (4.3.12)$$

where brackets <…> means averaging both on time and on number of realizations, and $\sigma_{\mathrm{el\,total}}^2 = <u_{\mathrm{el\,total}}^2(t)>$, $\sigma_{\mathrm{ph\,total}}^2 = <u_{\mathrm{ph\,total}}^2(t)>$ are the total variances of electrical and optical fluctuations.

For simpler interpretation of cross-correlation coefficient results the cross-correlation function ($<u_{\mathrm{el\,total}}(t)\cdot u_{\mathrm{ph\,total}}(t)>$) can be presented in the following way:

$$<u_{\mathrm{el\,total}}(t)\cdot u_{\mathrm{ph\,total}}(t)> = \sum_{j=1}^{3} <u_{\mathrm{el}\,j}(t)\cdot u_{\mathrm{ph}\,j}(t)>; \qquad (4.3.13)$$

where index $j = 1$ describes the cross-correlation function for $1/f$ type fluctuations, $j = 2$ – for $1/f^\alpha$ and $j = 3$ – for Lorentzian type fluctuations; here

we also accounted that shot, thermal and measurement system noise components are uncorrelated. It is well known that cross-correlation function reflects the linear relation between two random processes, thus every component of low-frequency optical fluctuations can be expressed as:

$$u_{\mathrm{ph}\,j}(t) = a_j u_{\mathrm{el}\,j}(t); \tag{4.3.14}$$

where a_j is the coefficient of proportionality; on the other hand, the quantity a_j reflects the modulation coefficient by which LED current fluctuations modulate the emitted light flow. Thus, the cross-correlation function between optical and electrical noise components and optical noise variance, respectively, can be described as:

$$r_j(t,t) = <u_{\mathrm{ph}\,j}(t) \cdot u_{\mathrm{el}\,j}(t)> = a_j <u_{\mathrm{el}\,j}(t) \cdot u_{\mathrm{el}\,j}(t)> = a_j \sigma^2_{\mathrm{el}\,j}; \tag{4.3.15}$$

$$\sigma^2_{\mathrm{ph}\,j} = a_j^2 \sigma^2_{\mathrm{el}\,j}; \tag{4.3.16}$$

From Eqs. (4.3.15) and (4.3.16) we have, that

$$a_j = (\sigma^2_{\mathrm{ph}\,j} / \sigma^2_{\mathrm{el}\,j})^{1/2}; \tag{4.3.17}$$

and

$$r_j(t,t) = \pm(\sigma^2_{\mathrm{ph}\,j} \cdot \sigma^2_{\mathrm{el}\,j})^{1/2}; \tag{4.3.18}$$

The sign of the cross-correlation function is determined by the sign of quantity a_j. We also accounted that in common case not all low-frequency electrical fluctuations (for example, with $1/f$ type, or $1/f^{\alpha}$ type, or with Lorentzian type spectrum) can be completely correlated with optical fluctuations: contact or electrical noises in passive layers of LED do not cause the emitted light intensity fluctuations, e.g., every spectral component of low-frequency electrical noise can be presented as a sum of correlated and uncorrelated parts:

$$S_{\mathrm{el}\,j}(f) = S_{\mathrm{el}\,j\,\mathrm{cor}}(f) + S_{\mathrm{el}\,j\,\mathrm{uncor}}(f) = d_j S_{\mathrm{el}\,j}(f) + (1-d_j) S_{\mathrm{el}\,j}(f); \tag{4.3.19}$$

here quantity d_j shows what part of spectral component $S_{\mathrm{el}\,j}(f)$ of electrical noise is related with emitted light intensity fluctuations. So, the cross-correlation

coefficient (4.3.12), including Eqs. (4.3.13), and (4.3.17)-(4.3.19), can be expressed as:

$$r = [\sum_{j=1}^{3} (d_j \sigma_{j\,\mathrm{el}}^2 \cdot \sigma_{j\,\mathrm{ph}}^2)^{1/2}] / (\sigma_{\mathrm{el\ total}}^2 \cdot \sigma_{\mathrm{ph\ total}}^2)^{1/2}; \qquad (4.3.20)$$

For frequency range from 10 Hz to 20 kHz, and respectively, for every one-octave frequency band:

$$r_{\mathrm{oct}} = [\sum_{j=1}^{3} (d_j \sigma_{j\,\mathrm{el\,oct}}^2 \cdot \sigma_{j\,\mathrm{ph\,oct}}^2)^{1/2}] / (\sigma_{\mathrm{el\ total\,oct}}^2 \cdot \sigma_{\mathrm{ph\ total\,oct}}^2)^{1/2}; \qquad (4.3.21)$$

The presented technique enables to determine the cross-correlation factor dependency on frequency and to estimate what part of cross-correlation factor is produced by the low frequency fluctuations with 1/*f*, and Lorentzian type spectra.

4.3.2 Detailed analysis of cross-correlation of investigated LEDs

Detailed analysis of explained principles was applied to the blue light emitting diode noise measurement results. Measured optical and electrical noise spectrums were aproximated using equations 4.3.1 and 4.3.2. Spectrum decomposition of electrical and optical fluctuations at 100 mA forward current is provided in Fig. 4.46. Measurement results are displayed as a dots and solid lines are results of approximation. In optical spectrum there dominates 1/*f* and $1/f^{1.5}$ at low frequencies and shoot noise overcomes above 600 Hz. In electrical noise spectrum in adition to these components there is generation and recombination noise component just bellow shot noise level.

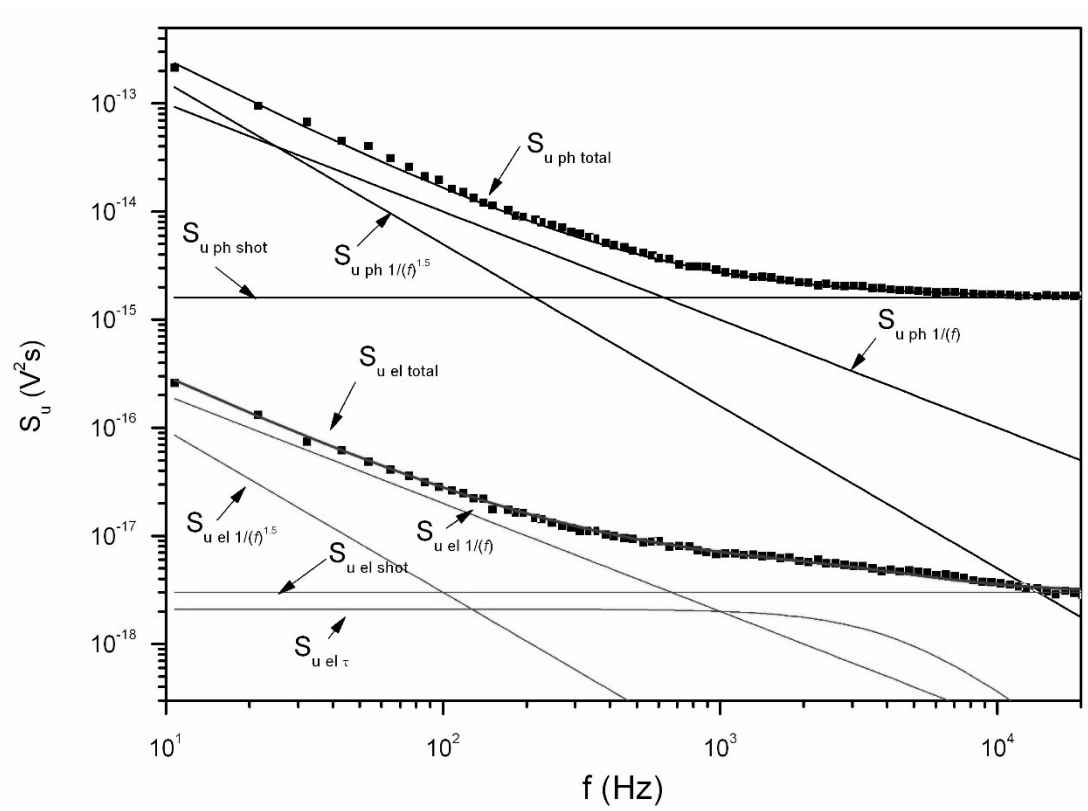

Fig. 4.46. Decomposition of electrical and optical spectrum of LED noise into the noise components (dots - measured results; solid line – approximations; forward current 100 mA).

Measured electrical and optical noise specta at different forward current are displayed in Fig. 4.47. There we can see that for the electrical noise spectrum generation and recombination component has noticable influence at 20 mA and higher forward currents. While at lower forward current $1/f$ and $1/f^{1,5}$ dominates within all measured frequency range. Optical spectrum type do not change within all meassured current range: at low frequencies dominates $1/f$ and $1/f^{1,5}$ and shot noise overcomes at higher frequencies.

Measured cross-correlation factor value is high at low frequencies and starts to decrease with increasing octave center frequency (Fig. 4.48). This shows, that dominating noise components at low frequency are highly correlated. Cross-correlation factor decreases with increasing octave center frequency can be explained by fact, that optical shot noise dominates at higher frequencies and measured cross-correlation factor takes all the correlated and

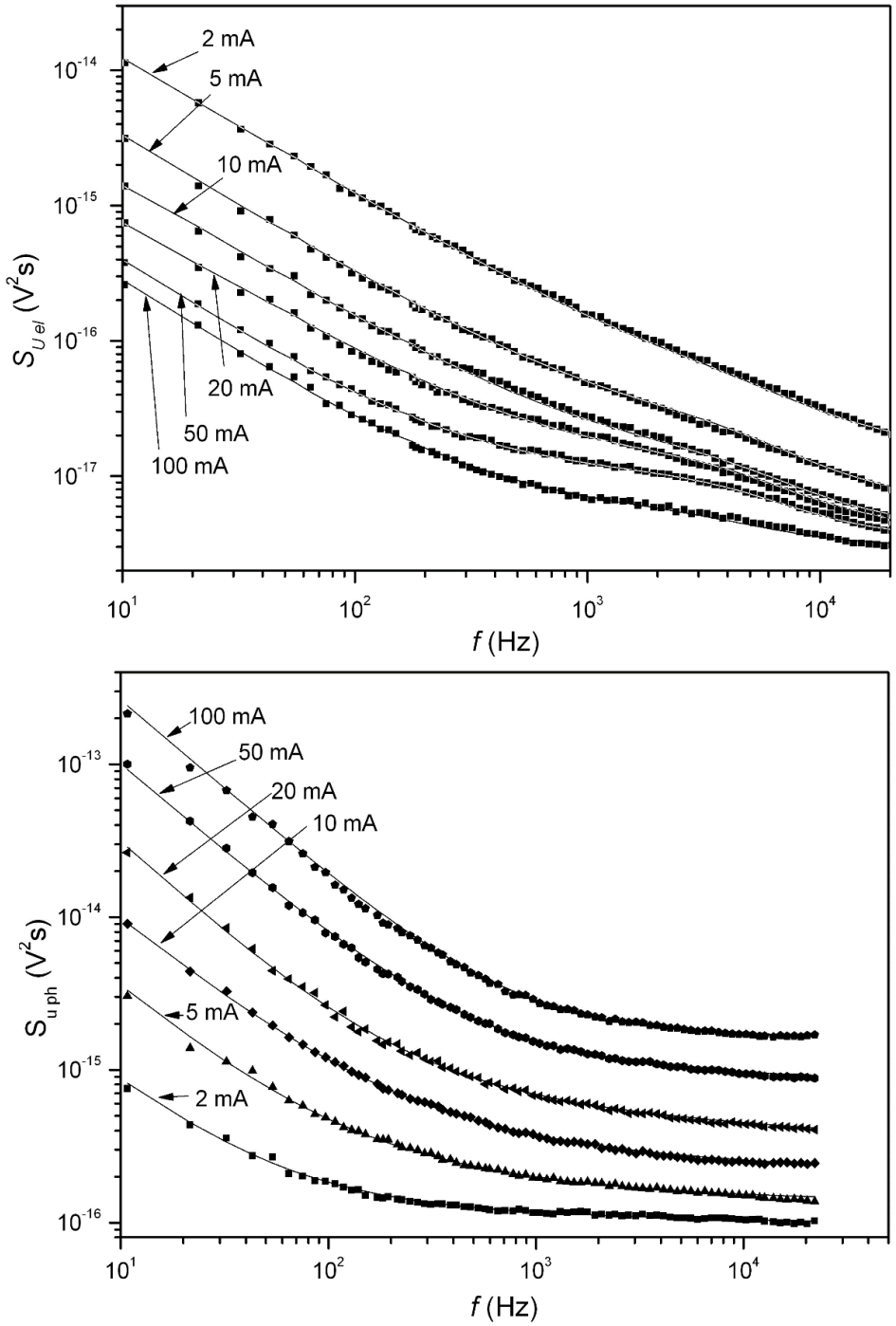

Fig. 4.47. Electrical (on top) and optical (at bottom) spectrum at different forward currents (dots are measured results; solid lines – approximations).

uncorrelated noise components into account. For more detailed investigations cross-correlation factor can be recalculated by removing not correlated noise components. To do so it is necessary to calculate appropriate dispersions of noise components by using equations (4.3.8) – (4.3.11). As electrical

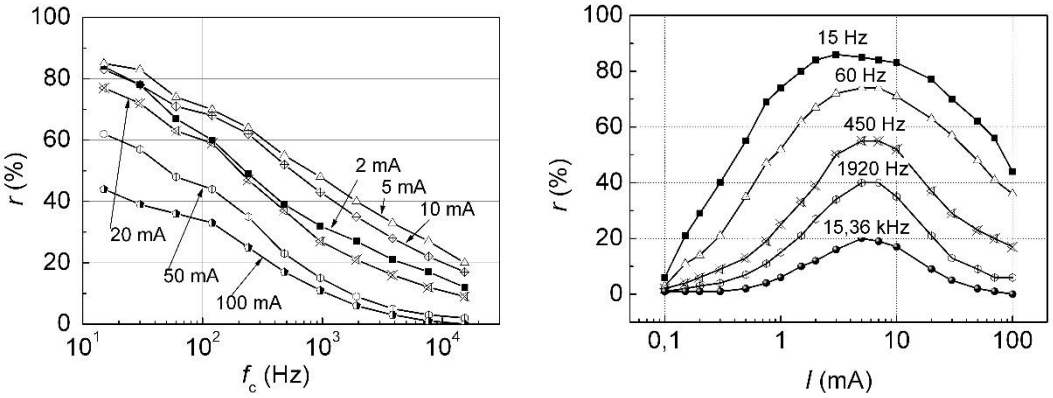

Fig. 4.48. Measured cross-correlation factor dependency on center frequency of octave (on the left), and forward current (on the right).

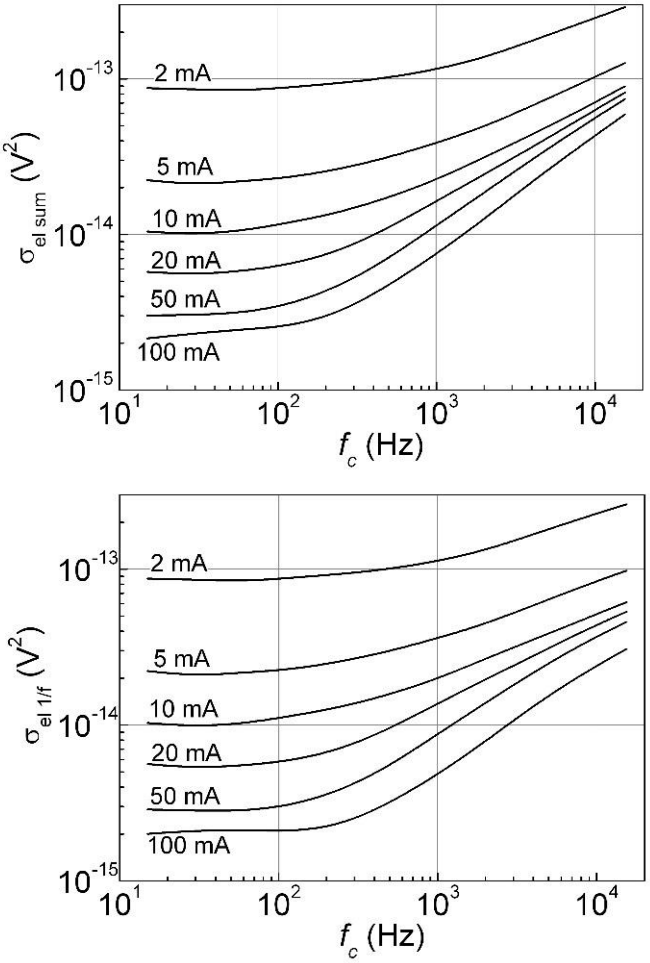

Fig. 4.49. Electrical noise variance dependency on central frequency of octave filter at different DC current: total on the top and 1/*f* in the bottom.

noise spectrum is dominant by 1/*f*, $1/f^{1,5}$ and generation and recombination

components, total dispersion and flicker noise component dispersions are very similar (Fig. 4.49). Because of removed shot noise component there is slightly decrease in dispersion at higher frequencies and higher current range. As optical spectrum has dominant shot noise component at higher frequencies, differences between total dispersion and flicker noise component dispersion are noticeable especially in higher frequencies (Fig. 4.50). Having flicker dispersions of electrical and optical noise components, the cross-correlation factor can be recalculated by using equation (4.3.21). Calculation results are displayed in Fig. 4.51. Increase of cross-correlation factor especially at higher frequencies is

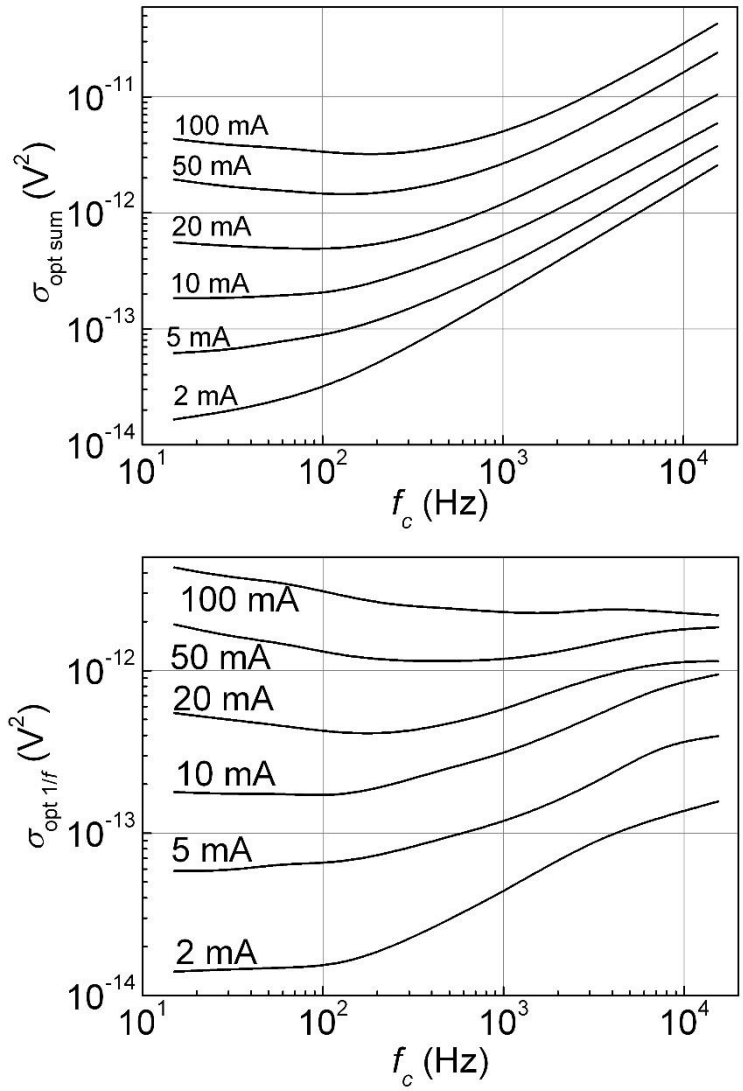

Fig. 4.50. Optical noise variance dependency on central frequency of octave filter at different DC current: total on the top and 1/*f* in the bottom.

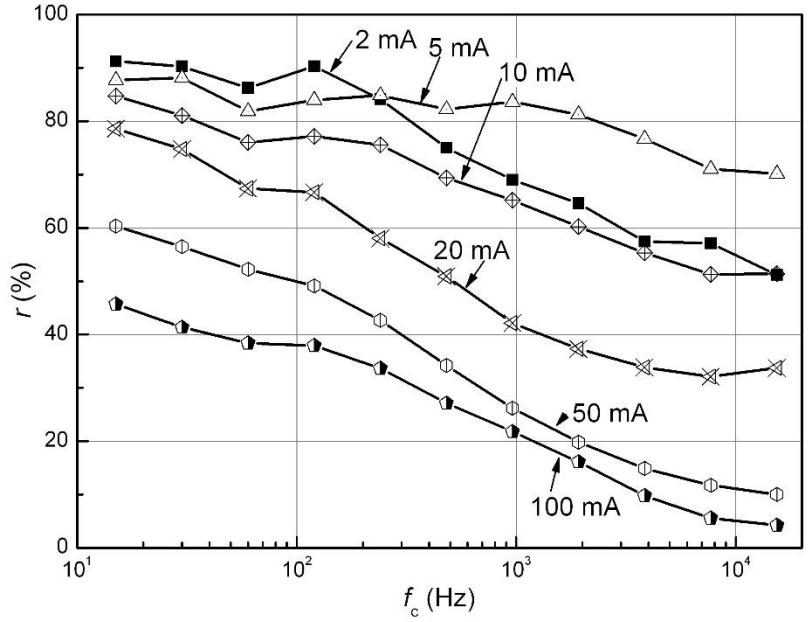

Fig. 4.51. Cross-correlation factor in one-octave frequency band dependence on central frequency of octave filter at different d. c. currents. Dots are measured results; solid lines are calculation data by Eq. (4.3.21).

noticeable. Not 100% cross-correlation factor between 1/*f* electrical and optical noise components shows, that not all the noise is completely correlated. This means, what not all electrical 1/*f* noise component generates optical fluctuations, i.e. part of electrical noise origin is in peripheria and not in the active layer. As only the same type of spectrum components of electrical and optical noise fluctuations can be correlated, there cross-correlation factor of each spectrum component can be calculated. Cross-correlation factor in one octave frequency bands dependency on the center frequency of octave filter and contribution of 1/*f*, $1/f^{1.5}$ and Lorentzian type fluctuations are shown in Fig. 4.52. The quantities d_j were determined by comparing measured results with the one calculated using equation (4.3.21). There we can see, that at low frequencies dominates both 1/*f* and $1/f^{1.5}$ while at higher frequencies only 1/*f* prevails. Lorentzian type noise spectrum component is noticeable in the electrical spectrum (Fig. 4.46) at higher frequencies, but it is weakly correlated with the same type of optical noise component (Cross-correlation factor is close to 0 in Fig. 4.52 and d_3=0.03). $1/f^{1.5}$ type noise is completely correlated (d_2= 1) – the source of this type of noise is

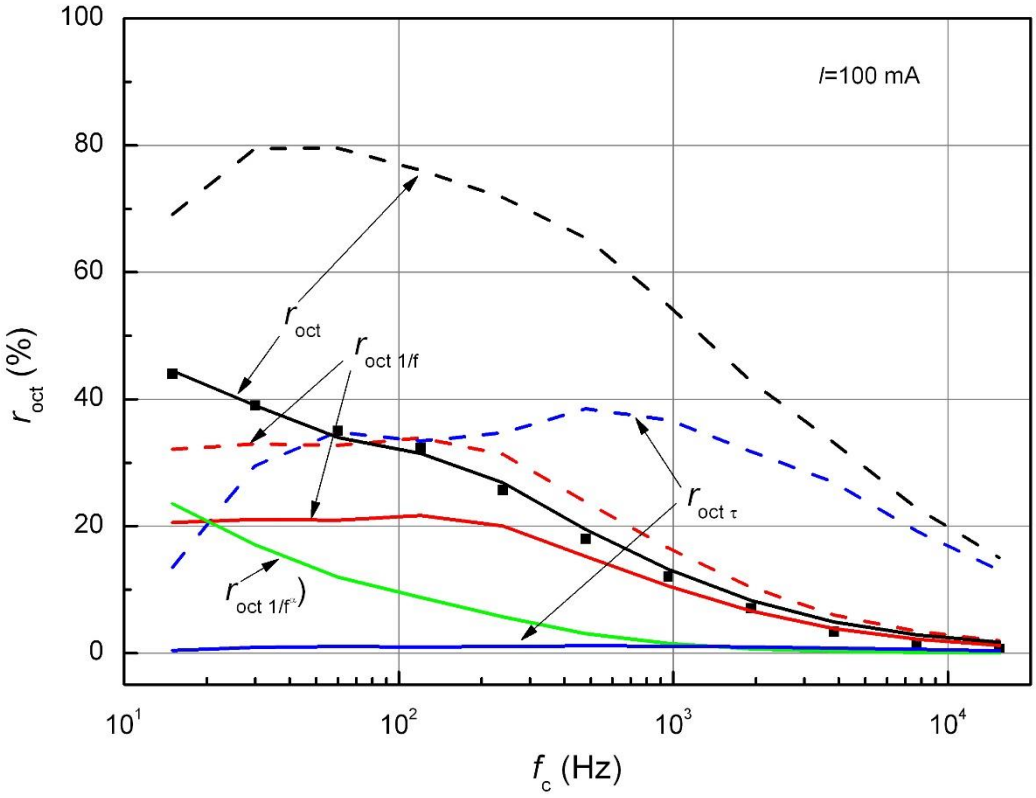

Fig. 4.52. Cross-correlation factor in one-octave frequency band dependence on central frequency of octave filter at I=100 mA. Dots are measured results; black solid line is calculation data by Eq. (4.3.21) with d_1= 0.64, d_2= 1, d_3=0.03; color solid lines are contribution to cross-correlation factor of $1/f$, $1/f^{1,5}$, and Lorentzian type fluctuations; dashed lines present the case as if $1/f$, $1/f^{1,5}$, and Lorentzian type electrical and optical fluctuations were completely correlated (d_1= 1, d_3= 1).

in active layer of the LED. At higher frequencies cross-correlation decreases due to large contribution of uncorrelated shot noise components.

4.3.3 Summary

The technique that enables decomposition of experimentally measured noise spectra into the separate noise component of different spectrum type was explained in detail. Such spectrum decomposition allows calculating the variances of different type spectrum components. There was also explained the method for reevaluation of measured cross-correlation factor by considering only the spectrum components which could be correlated. In addition to

separating flicker noise spectrum from not correlated shot and system noise spectrum, it allows to investigate the cross-correlation of different low frequency noise spectrum components (1/*f*, $1/f^{\alpha}$ and Lorentzian type components).

The above explained technique for the blue light emitting InGaN LED was applied. Measured electrical and optical noise spectra were successfully approximated by 1/*f*, $1/f^{1.5}$, Lorentzian type and shot noise components. Cross-correlation factor was approximated with different flicker noise components by using appropriate quantity d_j values to reach measured cross-correlation factor. Such approximation allowed to presume which low frequency components are the most correlated. Although Lorentzian type noise spectrum component is noticeable in the electrical spectrum at higher frequencies, but its cross-correlation with the same type of optical noise component is very weak: d_3=0.03. Also, its contribution to total cross-correlation factor is close to 0. 1/*f* type noise has highest contribution to total cross-correlation factor. However not all 1/*f* type electrical noise is completely correlated (d_1= 0.64). $1/f^{1.5}$ type electrical and optical spectrum is completely correlated (d_2= 1).

5 Conclusions

Noise characteristics of investigated nitride-based LEDs have $1/f^{\alpha}$-type spectrum transforming into shot noise at higher frequencies for optical noise. Noise characteristics of nitride-based LEDs and phosphide-based LEDs are comparable.

Cross-correlation factor close to 100% between two optical noises from opposite sides of the conical reflector proved, that optical fluctuations measured with two different photodiodes are from the same source, i.e. from the active layer and not from the lenses.

Separately investigated blue light from the active layer and broadband yellow from the phosphor one confirmed that phosphor layer does not influence the noise characteristics of white light emitting LED.

LED noise characteristics are similar to the ones of LD at stable operation range. Because of resonator of LD at specific current and temperature conditions mode hopping effect appears folowed by unstable noise characteristics and optical spectrum caused by generation and recombination processes in defects in the active layer.

After short term aging, characteristics of investigated white LED has improved, and was observed stable LED operation for a while. After ~4000 hours LED characteristics start to degrade more rapidly and noise level increases. After 8000 hours of aging output power has decreased by about 30%.

Optical noise increase of white light emitting LED shows, that either active or phosphor layer has degraded. Slightly changed cross-correlation between electrical and optical fluctuations, and significantly increased one between optical blue and optical red fluctuations proves, that after aging active layer has degraded.

Some samples of different materials have higher noise levels after aging, but in general the degradation of nitride based and phosphide based LEDs after accelerated aging are similar.

Measured electrical and optical noise spectra of blue light emitting InGaN LED were successfully approximated by $1/f$, $1/f^{1.5}$, Lorentzian type and shot noise components. Although Lorentzian type noise spectrum component is noticeable in the electrical spectrum at higher frequencies, but its cross-correlation with the same type of optical noise component is very weak: d_3=0.03. Also its contribution to total cross-correlation factor is close to 0. $1/f$ type noise has highest contribution to total cross-correlation factor. However not all $1/f$ type electrical noise is completely correlated (d_1= 0.64). $1/f^{1.5}$ type electrical and optical spectrum is completely correlated (d_2= 1).

Reference list

[1] E. F. Schubert, *Light-Emitting Diodes* (Cambridge University Press, 2nd edition, 2006). 978-0521865388

[2] http://www.cree.com/About-Cree/History-and-Milestones. Retrieved 2015-09-14.

[3] S. Nakamura, T.Mukai, M. Senoh, Candela-Class High-Brightness InGaN/AlGaN Double-Heterostructure Blue-Light-Emitting-Diodes. Appl. Phys. Lett. 64 (13): 1687 - 1689. (1994), http://dx.doi.org/10.1063/1.111832

[4] T. Mukai, Recent Progress in Group-III Nitride Light-Emitting Diodes, IEEE J. Selected topics in Quant. Electron. 8(2), 264-270 (2002), https://doi.org/10.1109/2944.999179

[5] Y. Arakawa, Progress in GaN-based quantum dots for optoelectronics applications, IEEE J. Selected Topics in Quant. Electron. 8(4), 823-832 (2002) https://doi.org/10.1109/JSTQE.2002.801675

[6] H. J. Round, A note on carborundum, Electrical World 19, 309 (1907)

[7] R. M. Potter, J. M. Blank, A. Addamiano, Silicon carbide light emitting diodes, J. Appl. Phys. 40 2253 (1969), http://dx.doi.org/10.1063/1.1657967

[8] R. N. Hall , G. E. Fenner, J. D. Kingsley, T. J. Soltys, R. O. Carlson, Coherent light emission from GaAs junction, Phys. Rev. Lett. 9, 366 (1962), http://dx.doi.org/10.1103/PhysRevLett.9.366

[9] N. Holonyak, S. F. Bevacqua, Coherent (visible) light emission from $Ga(As_{1-x}P_x)$ junctions, Appl.Phys Lett. 1, 82 (1962), http://dx.doi.org/10.1063/1.1753706

[10] C. J. Nuese, J. J. Tietjen, J. J. Gannon, H. F. Gossenberger, Optimization of electroluminescent efficiencies for vapor-grown GaAsP diodes, J. Electrochem. Soc., Vol. 116, pp. 248-253, (1969), doi: 10.1149/1.2411807

[11] N. Holonyak, C. J. Neuse, M. D. Sirkis, G. E. Stillman, Effect of donor impurities on the direct-indirect transition in Ga(AsP), Appl. Phys. Lett. 8, 83, (1966), http://dx.doi.org/10.1063/1.1754498

[12] M. R. Krames, H. Amano, J. J. Brown, P. L. Heremans, Introduction to the issue on high-efficiency light-emitting diodes, Special issue of IEEE Journal. Selected Topics in Quantum Electronics 8, 185-188, (2002), http://dx.doi.org/10.1109/2944.999171

[13] I. Vurgaftman, J. R. Meyer, Band parameters for III-V compound semiconductors and their alloys, J. Appl. Phys., vol. 89, 5815–5875, (2001), http://dx.doi.org/10.1063/1.1368156

[14] M. R. Krames, O. B. Shchekin, R. Mueller-Mach, G. O. Mueller, L. Zhou, G. Harbers, G. Craford, Status and Future of High-Power Light-Emitting Diodes for Solid-State Lighting, Journal of Display Technology, VOL. 3, NO. 2, (2007), http://dx.doi.org/10.1109/JDT.2007.895339

[15] S. Chichibu, T. Azuhata, T. Sota, S. Nakamura, Spontaneous emission of localized excitons in InGaN single and multi-quantum well structures, Appl. Phys. Lett. 69(27), 4188-4190 (1996), http://dx.doi.org/10.1063/1.116981

[16] S. Nakamura, G.Fasol, The blue laser diode, GaN Based Light Emitters and Lasers (Springer, Berlin, 1997), http://dx.doi.org/10.1007/978-3-662-03462-0

[17] M. K. Kwon, J. Y. Kim, I. K. Park, K. S. Kim, G. Y. Jung, S. J. Park, J. W. Kim, Y. C. Kim, Enhanced emission efficiency of GaN/InGaN multiple quantum well light-emitting diode with an embedded photonic crystal, Appl. Phys. Lett. 92(25), 251110, (2008), http://dx.doi.org/10.1063/1.2948851

[18] H. Gao, F. Yan, Y. Zhang, J. Li, Y. Zeng, G. Wang, Enhancement of the light output power of InGaN/GaN light-emitting diodes grown on pyramidal patterned sapphire substrates in the micro- and nanoscale, J. Appl. Phys. 103 (1), 014314. (2008), http://dx.doi.org/10.1063/1.2830981

[19] Y. J. Lee, H. C. Kuo, T. C. Lu, S. C. Wang, K. W. Ng, K. M. Lau, Z. P. Yang, S. P. Chang, and S. Y. Lin, Study of GaN-Based Light-Emitting Diodes Grown on Chemical Wet-Etching-Patterned Sapphire Substrate With V-Shaped Pits Roughening Surfaces, J. Lightwave Technol. 26(11), 1455–1463. (2008), http://dx.doi.org/10.1109/JLT.2008.922151

[20] E. H. Park, J. Jang, S. Gupta, I. Ferguson, C. H. Kim, S. K. Jeon, J. S. Park, Air-voids embedded high efficiency InGaN-light emitting diode, Appl. Phys. Lett. 93(19), 191103, (2008), http://dx.doi.org/10.1063/1.2998596

[21] J. W. Lee, C. Sone, Y. Park, S. N. Lee, J. H. Ryou, R. D. Dupuis, C. H. Hong, H. Kim, High efficiency GaN-based light-emitting diodes fabricated on dielectric mask-embedded structures, Appl. Phys. Lett. 95(1), 011108, (2009), http://dx.doi.org/10.1063/1.3166868

[22] S. Chhajed, Y. Xi, Y.-L. Li, Th. Gessman, E. F. Schubert, Influence of junction temperature on chromaticity and color rendering properties of trichromatic white light sources based on light emitting diodes, J. Appl. Phys. 97 054506, (2005), http://dx.doi.org/10.1063/1.1852073

[23] D. Corell, H. Ou, C. Dam-Hansen, P. Petersen, D. Friis, Light Emitting Diodes as an alternative ambient illumination source in photolithography environment, Optics Express, 17(20):17293{17302, (2009), http://dx.doi.org/10.1364/OE.17.017293

[24] M. Fontoynont, L. Piqueras, Innovative lighting for Mona Lisa. Annex 45 Energy Efficient Electric Lighting for Buildings, 2:1 - 3, (2005).

[25] J. P. Miras, L. G. Novakosky, M. Fontoynont, Illumination of Mona Lisa - new lighting solutions. Light and Engineering, 5:28-33, (2005)

[26] R. Mueller-Mach, G. O. Mueller, M. R. Krames, T. Trottier, High-Power Phosphor-Converted Light-Emitting Diodes Based on III-Nitrides, IEEE Journal on Selected Topics in Quantum Electronics, vol. 8, no. 2, pp. 339–345, (2002), http://dx.doi.org/10.1109/2944.999189

[27] M. Meneghini, M. Dal Lago, L. Rodighiero, N. Trivellin, E. Zanoni, G. Meneghesso, Reliability issues in GaN-based light-emitting diodes:

effect of dc and PWM stress, Microelectron Reliab 52:1621–6 (2012), https://doi.org/10.1016/j.microrel.2011.10.012.

[28] A. Žukauskas, *Puslaidininkiniai šviestukai,* Progretus, Vilnius, 2008)

[29] Reliability and Lifetime of LEDs Application Note, OSRAM Opto Semiconductors (2008), http://www.osram-os.com/Graphics/XPic5/00165201_0.pdf/Reliability%20and%20Lifetime%20of%20LEDs.pdf

[30] L. Liu, J. Yang, G. Wang, The investigation of LED's reliability through highly accelerated stress testing methods, IEEE proc. conf. electronic materials and packaging (EMAP), 1–3 (2012), https://doi.org/10.1109/EMAP.2012.6507888.

[31] E. Jung, M.S. Kim, H. Kim, Analysis of contributing factors for determining the reliability characteristics of GaN-based white light-emitting diodes with dual degradation kinetics, IEEE Trans Electron Dev, 60:186–91 (2013), https://doi.org/10.1109/TED.2012.2226039.

[32] T. Sutharssan, C. Bailey, S. Stoyanov, A comparison study of the prognostics approaches to light-emitting diodes under accelerated aging, IEEE proc. conf. thermal, mechanical and multi-physics simulation and experiments in microelectronics and microsystems (EuroSimE); 1-6 (2012), https://doi.org/10.1109/ESimE.2012.6191783.

[33] L. A. Escobar, W. Q. Meeker, A Review of Accelerated Test Models, Statistical Science, Vol. 21, No. 4, 552–577, (2006), http://dx.doi.org/10.1214/088342306000000321.

[34] M. H. Chang, D. Das, P.V. Varde, M. Pecht, Light emitting diodes reliability review, Microelectronics Reliability 52, 762–782, (2012), http://dx.doi.org/10.1016/j.microrel.2011.07.063

[35] S. Koh, W. van Driel, G.Q. Zhang, Degradation of epoxy lens materials in LED systems, Thermal, Mechanical and Multi-Physics Simulation and Experiments in Microelectronics and Microsystems (EuroSimE), 12th International Conference, (2011), http://dx.doi.org/10.1109/ESIME.2011.5765850

[36] E. Nogueira, M. Vázquez, N. Núñez, Evaluation of AlGaInP LEDs reliability based on accelerated tests, Microelectronics Reliability Vol. 49 (9–11), 1240–1243, (2009), http://dx.doi.org/10.1016/j.microrel.2009.06.031

[37] C. H. Seager, S. M. Myers, A. F. Wright, D. D. Koleske, A. A. Allerman, Drift, diffusion, and trapping of hydrogen in p type GaN, J. Appl. Phys., vol. 92, no. 12, pp. 7246–7252, (2002), http://dx.doi.org/10.1063/1.1520719

[38] M. Meneghini, L.-R. Trevisanello, R. Penzo, M. Benedetti, U. Zehnder, U. Strauss, G. Meneghesso, E. Zanoni, Reversible degradation of GaN LEDs related to passivation, Reliability physics symposium, 2007. proceedings. 45th annual. ieee international, pp. 457–461, (2007), http://dx.doi.org/10.1109/RELPHY.2007.369933

[39] F. Rossi, M. Pavesi, M. Meneghini, G. Salviati, M. Manfredi, G. Meneghesso, A. Castaldini, A. Cavallini, L. R. U. Strauss, U. Zehnder, E. Zanoni, Influence of short term low current dc aging on the electrical and optical properties of AlGaN blue Light-Emitting Diodes, J. Appl. Phys., vol. 99, pp. 053 104–1–053104–7, (2006), http://dx.doi.org/10.1063/1.2178856

[40] M. Meneghini, M. Dal Lago, N. Trivellin, G. Meneghesso, E. Zanoni, Degradation mechanisms of high power LEDs for lighting applications: an overview, IEEE Trans Ind Appl. 99:1–8 (2013), https://doi.org/10.1109/TIA.2013.2268049.

[41] S. Tomiya, T. Hino, S. Goto, M. Takeya, M. Ikeda, Dislocation related issues in the degradation of GaN-based laser diodes, IEEE Journal of Selected Topics in Quantum Electronics, vol. 10, no. 6, pp. 1277–1286, (2004), http://dx.doi.org/10.1109/JSTQE.2004.837735

[42] D.A. Vanderwater, I.-H. Tan, G.E. Hofler, D.C. DeFevere, F.A. Kish, High-brightness AlGaInP light emitting diodes, Proceedings of the IEEE, Vol. 85, Issue 11, Pages 1752-1764, (1997), http://dx.doi.org/10.1109/5.649654

[43] P.N. Grillot, M.R. Krames, Hanmin Zhao, Seng Hup Teoh, Sixty Thousand Hour Light Output Reliability of AlGaInP LEDs, IEEE Transactions on Device and Material Reliability, Vol. 6, No.4, 564-574, (2006), http://dx.doi.org/10.1109/TDMR.2006.887416

[44] M. Sawant, A. Christou, A Bayes Approach And Criticality Analysis For Reliability Prediction Of AlGaInP Light Emitting Diodes, Reliability Of Compound Semiconductors Workshop (ROCS 2012), Boston, Mass. (2012)

[45] Mitsuo Fukuda, *Reliability & Degradation of Semiconductor Lasers & LEDs*, Artech House 1991), 978-0890064658

[46] M. Koike, N. Shibata, H. Kato, Y. Takahashi, Development of high efficiency GaN-based multiquantum-well light-emitting diodes and their applications, IEEE J. Selected Topics in Quant. Electron. 8(2), 271-277, (2002), http://dx.doi.org/10.1109/2944.999180

[47] A. Usui, H. Sunakawa, A. Sakai, A. A. Yamaguchi, Thick GaN epitaxial growth with low dislocation density by hydride vapor phase epitaxy, Jpn. J. Appl. Phys. 36(7B), L899-L902 (1997), http://dx.doi.org/10.1143/JJAP.36.L899

[48] H. Kim, S.-J. Park, H. Hwang, Design and fabrication of highly efficient GaN-based light-emitting diodes, IEEE Trans. on Electron Dev. 49(10), 1715-1722 (2002), http://dx.doi.org/10.1109/TED.2002.802625

[49] H. Amano, N. Sawaki, I. Akasaki, Y. Toyoda, Metalorganic vapor phase epitaxial growth of a high quality GaN film using an AlN buffer layer, Appl. Pyhs. Lett., vol. 48, pp. 353–355, (1986), http://dx.doi.org/10.1063/1.96549

[50] S. C. Jain, M. Willander, J. Narayan, R. V. Overstraeteten, III-nitrides: Growth, characterization, and properties," J. Appl. Phys., vol. 87, no. 3, pp. 965–1006, (2000), http://dx.doi.org/10.1063/1.371971

[51] H. Nyquist, Thermal Agitation of Electric Charge in Conductors," Phys Rev 32, 110-113, (1928), http://dx.doi.org/10.1103/PhysRev.32.110

[52] V. Palenskis, *Fliuktuacijos elektroninėse sistemose*, (Vilnius 1998),

[53] L. K. J. Vandamme, Noise as a Diagnostic Tool for Quality and Reliability of Electronic Devices", IEEE Transactions on Electron Devices, Vol. 41. No 11, (1994), http://dx.doi.org/10.1109/16.333839

[54] S. L. Rumyantsev, S. Sawyer, M. S. Shur, N. Pala, Y. Bilenko, J. P. Zhang, X. Hu, A. Lunev, J. Deng, R. Gaska, Low-frequency noise of GaN-based ultraviolet light-emitting diodes, J. Appl. Phys. 97, 123107 (2005), http://dx.doi.org/10.1063/1.1928310

[55] S. Bychikhin, L. K. J. Vandamme, J. Kuzmik, G. Meneghesso, S. Levada, E. Zanoni, D. Pogany, Accelerated aging of GaN light emitting diodes studied by 1/f and RTS noise, Noise and Fluctuations: 18th Int. Conf. on Noise and Fluctuations, 709-712 (2005), http://dx.doi.org/10.1063/1.2036849

[56] Brian K. Jones, Low-Frequency Noise spectroscopy, IEEE Transactions on Electronic Devices, Vol 41, No. 11. (1994), http://dx.doi.org/10.1109/16.333840

[57] B. K. Jones, Electrical noise as a reliability indicator in electronic devices and components, IEE Proc.-Circuits Devices Syst., Vol 149, No. 1, (2002), http://dx.doi.org/10.1049/ip-cds:20020331

[58] S. Sawyer, S.L. Rumyantsev, N. Pala, M.S. Shur, Y. Bilenko, J.P. Zhang, X. Hu, A. Lunev, J. Deng, R. Gaska, Optical and current noise of GaN based light emitting diodes, IEEE Proc Semicond Dev Res Symp 2005:89–90, https://doi.org/10.1109/ISDRS.2005.1595992.

[59] S. Bychikhin, D. Pogany, L.K.J Vandamme, G. Meneghesso, E. Zanoni, Low-frequency noise sources in as-prepared and aged GaN-based light-emitting diodes, J Appl Phys 97:123714 (2005), http://dx.doi.org/10.1063/1.1942628.

[60] S. Sawyer, S.L. Rumyantsev, M.S. Shur, N. Pala, Y. Bilenko, J.P. Zhang, X. Hu, A. Lunev, J. Deng, R. Gaska, Current and optical noise of GaN/AlGaN light emitting diodes. J Appl Phys 100:034504 (2006), http://dx.doi.org/10.1063/1.2204355.

[61] M. Meneghini, Analysis of the physical processes that limit the reliability of GaN-based optoelectronic devices, Doctoral thesis (2008), http://paduaresearch.cab.unipd.it/353/1/fdi.pdf

[62] L. R. Trevisanello, Analysis of the Temperature impact on Reliability of GaN-based Light Emitting Diodes, Doctoral thesis (2008), http://paduaresearch.cab.unipd.it/1327/1/thesis.pdf

[63] M. Vazquez, N. Nunez, E. Nogueira, A. Borreguero, Degradation of AlInGaP red LEDs under drive current and temperature accelerated life tests, Microelectronics Reliability Vol. 50, Issues 9–11, (2010), 1559–1562, http://dx.doi.org/10.1016/j.microrel.2010.07.057

[64] H. Kim, H. Yang, C. Huh, S. W. Kim, S. J. Park, H. Hwang, Electromigration-induced failure of GaN multiquantum well light emitting diode, Electron. Lett. 36(10) 908-910 (2000), https://doi.org/10.1049/el:20000657

[65] J. Berntgen, T. Lieske, B. Scineller, M. Deufel, M. Heuken, H. Jeurgensen, K. Heime, Influence of thermal stress on I-V characteristics and low frequency noise of AlGaInP UHB-LEDs, Proc. Of 10th Intern. Conf. on Indium Phosphide and Related Materials 741-744 (1998), http://dx.doi.org/10.1109/ICIPRM.1998.712752

[66] M. A. Naby, Degradation characterization of AlGaInP LEDs using I-V and low frequency noise measurements, Proc of 11th Int. Conf. on Microelectronics 43-46 (1999), http://dx.doi.org/10.1109/ICM.2000.884801

[67] J. Conti, M. Strutt, Optical fluctuations of light-emitting diodes, IEEE J. Quant. Electron. 8(10), 815-818 (1972), https://doi.org/10.1109/JQE.1972.1076867.

[68] V. Palenskis, Flicker noise problem, Lith. Phys. J. 30(1) 107-152, (1990)

[69] Keysight Technologies, The Parametric Measurement Handbook Application Note 24-25 (2014)

[70] J.-S. Lee, J. Lee, S. Kim, H. Jeon, GaN Light-Emitting Diode with Deep-Angled Mesa Sidewalls for Enhanced Light Emission in the Surface-

Normal Direction, IEEE Trans. Electron. Dev. 55, 523 (2008), https://doi.org/10.1109/TED.2007.913004

[71] D. Ursutiu, B. K. Jones, Low-frequency noise used as a lifetime test of LEDs, Semicond. Sci. Technol. 11(8), 1133-1136 (1996), https://doi.org/10.1088/0268-1242/11/8/002

[72] S. L. Rumyantsev, S. Sawyera, N. Palaa, M. S. Shura, Yu. Bilenkob, J. P. Zhang, X. Hub,A. Lunev, J. Deng, R. Gaska, Low frequency noise of light emitting diodes, Noise in Devices and Circuits III, Proc. of SPIE Vol. 5844 (SPIE, Bellingham, WA, 2005), http://dx.doi.org/10.1117/12.608559.

[73] Z. Li, P. T. Lai, H. W. Choi, A reliability study on green InGaN-GaN light emitting diodes, IEEE Photon. Technol. Lett. 21 (2009) 1429–1431, http://hdl.handle.net/10722/73854.

[74] M. Akbulut, C. H. Chen, M. Hargis, A. M. Weiner, M. R. Melloch, J. M. Woodall, Digital communications using 890-nm surface-emitting light-emitting diodes above 1 Gbit/s, Proc. of Conf. on Lasers and Electro-Optics (CLEO 2000) 509-510 (2000), https://doi.org/10.1109/CLEO.2000.907321.

[75] D. Zhu, J. Xu, A. N. Noemaun, J. K. Kim, E. F. Schubert, M. H. Crawford, D. D. Koleske, The origin of the high diode-ideality factors in GaInN/GaN multiple quantum well light-emitting diodes, Appl. Phys. Lett. 94, 081113 (2009), http://dx.doi.org/10.1063/1.3089687.